Development of High Resolution Simulations of the Atmospheric Environment Using the MASS Model

Final Contract Report for NAS5-30145

Prepared By:

Michael L. Kaplan, John W. Zack and
V. Mohan Karyampudi

MESO Inc.
28 Research Drive
Hampton, Virginia
23666-1325

Prepared For:

Goddard Laboratory for Atmospheres
NASA Goddard Space Flight Center
Greenbelt, Maryland
20771

30 November 1989

Table of Contents

List of Tables

List of Figures

Executive Summary

Numerical simulations were performed with the MASS 4.0 numerical weather prediction model in an effort to recreate the atmospheric environment over the Kennedy Space Center just before, during, and after the Shuttle Challenger disaster at 1639 GMT 28 January 1986. The results of these simulations clearly indicate that the vertical wind shear rapidly increased during the two hour period between 1500 and 1700 GMT 28 January 1986. MASS 4.0 was initialized at 1200 GMT 28 January with conventional synoptic scale stratospheric and tropospheric data and integrated with nested grid mesh intervals of 58, 14.5, and 7.25 km (true at 90 ° north latitude). The dynamical processes responsible for the increasing vertical wind shear as simulated by the 7 km version of MASS can be seen depicted in the schematic diagram of parcel trajectories accompanying the summary. The model indicates that between 1500 and 1700 GMT air parcels in the lower stratosphere (at approximately 13 km, or 175 mb) were entering a zone of confluence (converging air) between the deep cold trough moving eastward off the southeast coast of the United States and the deep warm ridge over the southwestern Atlantic Ocean region. As air parcels moving east-northeastward, which already exhibit significant inertia, are "caught" in this subtropical jet stream, they encounter very weak westward-directed values of the pressure gradient force just west of the Kennedy Space Center which enables them to accelerate to velocities in excess of 60 ms^{-1} by 1645 GMT within a narrow layer of the lower stratosphere. As can be seen in the schematic, the parcels are initially subgeostrophic to the southwest of the Kennedy Space Center and are subsequently accelerated to near geostrophic equilibrium by the coriolis force as they pass over the Kennedy Space Center. Just 1-2 km below this layer, i.e., near 225 mb or approximately 11.0 km, air parcels which originate 5 hours earlier over northwestern Florida, which have much less inertia and therefore much weaker coriolis force, drift eastward in this layer above the polar front jet stream and below the subtropical jet stream, just west of the Kennedy Space Center. These lower level parcels have much less inertia and then encounter a pressure gradient force which (unlike that at 13 km) further decelerates them over the region of east-central Florida resulting in a strong vertical wind shear over the Kennedy Space Center of approximately 20 ms^{-1} in 1.6 km or 1.3 x 10^{-2} s^{-1}. This shear reaches peak values at approximately 1645 GMT

resulting in calculated Richardson numbers of about 1.0 which indicate the possibility of shear-induced turbulence over the Kennedy Space Center.

It is interesting to note that while the 7 km simulations did not produce significantly stronger shears than the 58 km simulation, the zone of maximum shear was better concentrated in space by this 7 km simulation and this meso-beta scale simulation produced very realistic looking fields which exhibited no numerically-induced noise. Also, comparisons between the NASA/Goddard version of MASS employed in Uccellini, et. al. (1986) and these MASS 4.0 simulations indicated that MASS 4.0 verified much more accurately against the 1647 GMT rawinsonde launched at the Kennedy Space Center than did GMASS.

The analysis of the simulations over Florida suggested that the quality of the simulations might be improved by the incorporation of a high resolution planetary boundary layer scheme into the GMASS model. The implementation of a Blackadar high resolution PBL scheme into the GMASS model was completed under task 6 of this contract. A comparison of the Blackadar PBL with the original mixed layer PBL representation on one test case indicated that the high resolution scheme significantly improved the quality of the simulated structure within the PBL. Further tests will be required to determine the full extent of this improvement.

These modeling results dramatically indicate that the meso-beta scale version of MASS 4.0 can provide critical information concerning vertical wind shear prior to launch and landing. This numerical model can provide comprehensive high resolution data over significant spatial regions and time periods thus aiding decision makers at the Kennedy Space Center in evaluating the potential for turbulence or other weather-related hazards.

1. Introduction

In the aftermath of the Shuttle Challenger tragedy a number of questions were posed concerning the possible role of shear-induced turbulence on the vehicle's performance. In an effort to understand the synoptic scale structure of the atmosphere during the accident, Uccellini et al. (1986) performed a detailed analysis of the atmospheric conditions prior to and after the ill-fated launch of the Challenger employing radiosonde, jimsphere, and satellite data. Since these data sets were largely bereft of spatially and temporally useful mesoscale information, a mesoscale numerical weather prediction model was used to "dynamically interpolate" between observations and observational periods to produce the most comprehensive data set of winds, temperatures, and pressures possible for use in the analysis of the atmospheric conditions during the period of the accident. The study to be discussed in this report, represents a logical extension of the modeling technology applied by Uccellini et al. (1986). The goal of this project was to employ more comprehensive initial data sets and a higher resolution and an improved numerical model to enhance our understanding of the atmospheric vertical wind shear and static stability over the Kennedy Space Center immediately before, during, and after the Challenger accident, and to improve our knowledge of the dynamical processes responsible for creating these shear and stability profiles. In sections 2 through 5 of this report we will describe the work performed under Tasks 1 through 5 of contract NAS5-30145. These sections will present a detailed comparisons of high resolution simulations from the Mesoscale Atmospheric Simulation System (MASS) numerical model (Kaplan et al., 1982) with observations and simulation results from the NASA/Goddard version of the MASS model (GMASS) published in Uccellini et al. (1986) in an effort to determine the mesoscale atmospheric environment which existed during the launch of the Shuttle Challenger and the dynamical processes responsible for this environment.

During the analysis of the high resolution simulations of the atmospheric environment over Florida, scientists at MESO, Inc. and at NASA/GSFC jointly found that the simulations lacked sufficient detail in the planetary boundary layer (PBL) structure. They concluded that the simulations could be further improved if a high resolution PBL model could be included within the MASS model. Therefore, NASA/Goddard added the implementation and testing of this new PBL scheme to the orginal

statement of work as Task 6.

The work performed under Task 6 prepresents a logical extension of the study reported by Mcqueen and Koch (1988). They performed numerous experiments with the 2-D GMASS model which contained a mixed-layer type PBL model (Wong et al, 1983). They initialized the 2-D GMASS model with analytical initial conditions from the Hoskins-Bretherton (1972) frontal model. They showed some deficiencies in the simulation of the PBL structure which are inherent within mixed-layer type PBL models. The purpose of the Task 6 work was not only to include a high resolution PBL model (Blackadar, 1979; Zhang and Anthes, 1983), hereafter referred to as the Blackadar PBL, into the 2-D and 3-D GMASS models but to compare simulations produced by each of the two types of PBL models. The results of this work are presented in section 6.

2. Florida Simulation Experiment Overview

The numerical weather prediction model employed for these simulations was MASS version 4.0 (Karyampudi et al., 1988) described in detail in Table 1. This model version represents a significant improvement over the Goddard version of MASS 4.0 employed in the simulations published by Uccellini et al. (1986). The most significant improvement for this case study is the modification of the time marching scheme employed, i.e., the change from the Euler - backward technique (Kaplan et al., 1982) to the Adams-Bashforth and forward-backward schemes in this new split-explicit version of the model (Mesinger, 1977). This new formulation reduces the temporal damping which permits more of the fine scale adjustments to be simulated by the model during the integration of the primitive equations.

In an effort to achieve a higher degree of understanding of the wind shear and static stability conditions which existed around 1630 UTC 28 January 1986, which is 9 minutes before the Challenger accident, a 32-layer version of MASS was employed in a series of nested grid simulation experiments. Figures 1a, 1b, and 1c depict the horizontal matrices over which MASS 4.0 was integrated. These represent grid mesh lengths of 58 (Grid A), 14.5 (Grid B), and 7.25 km (Grid C) true at 90 ° north latitude. Grids B and C were centered approximately 200 km upstream (west) from the Kennedy Space Center because of the strong westerly wind component throughout most of the troposphere. The lateral boundary conditions for grid A were derived from the NWS LFM II model while the lateral

boundary conditions for grids B and C were derived from the next coarser mesh MASS simulation fields. The lateral boundary conditions were applied as specified by Kreitzberg and Perkey (1976) . The 12 hour simulation performed over grid A was initialized at 1200 UTC while the 5 and 1.5 hour nested grid simulations performed over grids B and C were initialized at 1300 and 1530 UTC, respectively.

The initial data was derived from an analysis of temperature, moisture, and winds from the National Meteorological Center's (NMC's) Regional Area Forecast System (RAFS). These data were vertically interpolated to 25-mb layers and then updated with the standard operational radiosonde data base using a Cressman (1958) analysis procedure. The initial fields were then enhanced with an isentropic analysis over the contiguous United States using a procedure that has been shown to yield more-reliable simulations of jet streaks and their attendant circulation patterns (Peterson et al., 1985). These initial data sets were further supplemented by the addition of 8 ship reports over the southwestern part of the North Atlantic Oceanic Region between 65 °and 85 ° west longitudes and 25 °and 45 ° north latitude.

The sounding data set used for 28 January 1200 UTC was obtained from the GALE data center. It contained temperature, dew point, wind direction, wind speed and height at 10 mb intervals from the surface to 100 mb. All available soundings from the United States, Canada, Mexico and the Virgin Islands were included in the data set. One supplemental class sounding (ILM) was used to enrich the data set along the east coast. In addition, 7 new soundings were constructed in the Atlantic Ocean between 78 ° and 64 ° W longitude and 27 ° and 40 ° N latitude to provide better ocean coverage. The surface data for these 7 soundings were obtained from actual ship reports. Temperature and wind data were obtained at the mandatory levels using RAFS data and NMC analyses, respectively.

Furthermore, the following changes were unique to this data set:

1) There was a modification to the interpolation program removing any extrapolations.

2) The sea-surface temperature analysis used a combination of observed and climatological SST's.

3) The sea-surface temperature analysis program was modified slightly.

4) The theta insert was blended with RAFS data on the edge of the domain.

5) The wind speeds were strengthened at station 72208 at upper

levels to be consistent with surrounding stations.

6) Station 78367 was removed from the analysis.

7) The variational adjustment of temperature was done after the isentropic data was inserted.

Output from the numerical model included horizontal depictions on pressure surfaces, vertical cross sections, vertical soundings at the Kennedy Space Center, and backward trajectories ending at the Kennedy Space Center for all 3 simulations.

3. Basic Intercomparisons Among GMASS, Nested MASS 4.0, and the Cape Canaveral Florida (XMR) 1647 UTC Rawinsonde

Prior to determining what dynamical processes were occurring during the Challenger accident, we will first evaluate the quality of the MASS 4.0 simulations. In Table 2 we compare the MASS 4.0 58 and 7.25 km simulations to the published GMASS simulation and the 1647 UTC Cape Canaveral (XMR), Florida rawinsonde. This comparison is limited to the upper troposphere and lower stratosphere where the region of large vertical shears are to be studied. Two fundamental conclusions can be drawn from this table. First, that the MASS 4.0 simulations produce a fine scale vertical wind shear structure within the upper troposphere and lower stratosphere which is noticeably different from the GMASS simulations. Second, the MASS 4.0 winds appear to verify considerably better than GMASS when both are compared to the rawinsonde released at 1647 UTC at XMR. It is apparent from this table that both MASS 4.0 simulations produce larger magnitude vertical wind shear and produce this wind shear at a higher level than the GMASS does when 25 mb deep increments of data are compared. The largest vertical wind shear simulated by MASS 4.0 between 250 and 150 mb being 11 ms^{-1} over 25 mb or approximately 1.3 x 10^{-2} s^{-1} . This shear occurs between 200 and 175 mb. The largest shear generated by GMASS was 8 ms^{-1} over the 225-200 mb layer or approximately 1.0 x 10^{-2} s^{-1}. The corroborative observations are sketchy since there are relatively large vertical gaps in the rawinsonde data, particularly near 175 and 250 mb as is depicted in

Table 3. These data indicate that the 52 ms^{-1} peak velocity at 1645 UTC for GMASS at 200 mb is not correct with an 8 ms^{-1} error at this level. The observations indicate that the winds near 150 mb are stronger, i.e. , 50 ms^{-1} as opposed to the GMASS value of 45 ms^{-1}. This could indicate the possibility of a wind maximum in nature between 200 and 150 mb which is, of course difficult to rigorously verify since rawinsonde observations exist only at 202, 159, and 152 mb. This inferred upward shift in the maximum wind velocity values and, hence, vertical shear as diagnosed from the rawinsonde is clearly evident in the MASS 4.0 simulations. Note, in particular, the 7.25 km simulations which has a maximum total wind velocity of 57 ms^{-1} just below 175 mb near 180 mb by 1630 UTC. This jet maximum can be seen in the MASS 7.25 km soundings depicted in Figure 2. The maximum vertical shear produced by MASS 4.0 lies within the 215 to 180 mb layer. In contrast, GMASS produces two maxima of shear one above and one below this layer. The charts in Figure 3 indicate that the MASS 4.0 shear zone is deeper, higher, and slightly stronger. The MASS 4.0 Richardson number plots (Figure 3), therefore, depict a deeper and higher region of low Ri values which suggests a possible zone of shear-induced turbulence at about the 12 km level.

It is beyond the scope of this limited study to determine why MASS 4.0 apparently outperforms GMASS in the upper troposphere and lower stratosphere. The fundamental model differences include improved horizontal resolution and a less diffusive time marching scheme in MASS 4.0. However, the difference in the initial state could also be very important since GMASS was not initialized with ship reports and supplemental soundings in the oceanic region from 65 °to 85 ° west longitude and 25 °to 45 ° north latitude.

The vertical shift in maximum wind shear simulated by MASS 4.0 and generally corroborated by the XMR 1647 UTC rawinsonde demonstrates that the subtropical jet may not have been decreasing in strength over XMR at the time of the Challenger accident. As a matter of fact, the MASS 4.0 7.25 km simulated 57 ms^{-1} wind maximum over XMR occurs at 1630 UTC near the 180 mb level which should be compared to the GMASS simulated maximum of 52 ms^{-1} at the same level between 1530 and 1545 UTC. This jet maximum is occurring in space and time directly above a region of decelerating flow near 225 mb which is well above and displaced in space form the polar front jet maximum . Hence, the shear

layer which develops by 1630 UTC over XMR is the result of complex interactions between jet streaks involving subtle nonlinear processes. In the next 2 sections of this report the dynamical processes responsible for the creation of this shear layer will be addressed.

4. MASS 4.0 Simulation of the Large Vertical Wind Shear over XMR within the Lower Stratosphere

Figure 4 depicts south to north spatial cross sections of total wind velocity for the 58 and 7.25 km simulations performed with MASS 4.0. The cross section depicting 58 km simulation results extends from western Cuba to Myrtle Beach, South Carolina for the period from 1300-1620 UTC on 28 January 1986. It is quite apparent from these cross sections (Figures 4c-4f) that, above 200 mb the wind velocity maximum over Fort Myers (FMY) in Florida at 1400 UTC rather abruptly shifts northeastward to be centered approximately 100 km north-northeast of Daytona Beach (DAB) during the 1500-1620 UTC time period. This shift is into a region where there is very little curvature in the height field in the lower stratosphere. This region exhibits a highly confluent structure in the mass field with a large south to north height gradient where the low height values associated with the polar air mass encounter the resistance of the deep high pressure ridge over the subtropical Atlantic Ocean. The geometry of the height field suggests that this abrupt shift in position and increase in velocity of the subtropical jet stream is largely the result of the confluence of relatively high velocity air parcels into a region where there is a local reduction in the magnitude of the westward directed pressure gradient force in the 200-150 mb layer. This confluent structure is quite apparent from Uccellini's depiction of TOMS ozone data between 1545 and 1730 UTC. This mass field can be inferred from the south to north cross sections of the tangential component of the geostrophic wind velocity (m s^{-1}) depicted in Figure 5 as well as the 175 mb height field depicted in Figures 6a-g. It is evident from Figure 5 that the east to west pressure gradient force is nearly zero by 1530 UTC above XMR in the lower stratosphere due to the lack of curvature in the height field (Figures 6a-g). With virtually no pressure gradient force to retard parcels entering the confluent zone under the influence of the coriolis force, this region near DAB is clearly a candidate for strong geostrophic adjustment with the u wind component accelerating significantly above the tropopause. It is interesting to note that in Figure 4, the north-south cross section of wind

velocity generated by GMASS indicates a splitting of the lower stratospheric wind velocity maximum into 2 lobes during the 1600 to 1700 UTC time period. In the GMASS simulation a maximum forms near 190 mb just north of XMR by 1700 UTC. GMASS was not able to produce as strong a "signal" of the eastward acceleration of the u wind component just north of XMR as is MASS 4.0. This was evidently due to an unknown combination of the data enhancements used for the MASS 4.0 initialization and the less diffusive time-differencing scheme used in MASS 4.0.

From a synoptic scale perspective, the relaxation of the pressure gradient force within the lower stratosphere is the result of the juxtaposition of the tropospheric pool of cold air streaming off the southeastern coast of the United States and the deep subtropical ridge over the southwestern Atlantic Ocean region. Adding an additional level of complexity to this scenario is the fact that this perturbed layer of mass within the lower stratosphere is directly above a relatively shallow layer between 250 and 225 mb in which inertial advective adjustments are acting to locally decelerate the meridional (v) wind component above XMR. Figures 7 through 9 depict the wind velocity in this layer near and just west of XMR from a variety of perspectives. Figure 7 indicates that a distinct minimum in the v wind component develops just above the 250 mb level over the region between Orlando (ORL) and DAB by 1615 UTC. The minimum is more distinct in the 7.25 km simulation than in the 58 km simulation. This can be seen by comparing figures 7f (58 km) and 7i (7.25 km). The value of the simulated v wind component drops in the 7.25 km simulation to 1 ms^{-1} by 1615 UTC directly underneath the region where the 200 mb to 175 mb u wind component is accelerating to values in excess of 50 ms^{-1}. This minimum is the direct result of the advection of low values of positive v component eastward across north central Florida into the layer below the accelerating u wind component. This fact is supported by the west to east cross sections of normal wind component which depict the large zonal gradient of the meridional wind component to the west of XMR by 1530 UTC (Figure 7h). Back trajectories arriving at XMR at 225 mb pass through this region at this time and arrive with nearly 0 ms^{-1} v component values (Figure 8b). Such a small value of the v wind component inhibits the acceleration of the u wind component *at this level (225 mb)* because the coriolis force is so small. The magnitude of the local decrease in the v wind component at 225 mb over east central Florida is nearly 6 ms^{-1} hr^{-1} for more than 3 hours. This v component

minimum is verifiable from the 1647 UTC XMR rawinsonde data listed in Table 3. The data indicates a 269 ° wind direction at 222 mb and therefore no significant meridional component . Hence, the MASS 4.0 simulation reveals the development of a vertically superimposed wind maximum and wind minimum caused by inertial advective processes near 225 mb and geostrophic adjustment processes near 175 mb over XMR by 1630 UTC. This is the region where the vertical shear is maximized and Richardson numbers minimized between 1630 and 1700 UTC.

5. Nonlinear Jet Streak Interaction

The two processes which produce the vertical shear described in the previous section of this report are nonlinearly coupled through a deep multi-stage sequence of adjustments . These adjustments are part of definable circulations which occur on both sides of the tropopause boundary.

The first stage in the coupling of the subtropical and polar front streak involves the development of a region of significant confluence and mass flux convergence by 1530 UTC below the tropopause to the west and northwest of GNV. Over this area at 225 mb the eastward advection of air parcels with little meridional kinetic energy interfaces with the increasing northwesterly flow along the leading edge of the polar front jet streak. Within this zone near GNV increasing values of mass flux convergence between 250 and 200 mb result in a zone of significant sinking motion near 225 mb. This process is depicted in Figure 8a which shows the rapid eastward turn of an air parcel at 238 mb just west of GNV at 1500 UTC and its 9 mb "plunge" to 247 mb by 1540 UTC near GNV. This upper tropospheric convergence zone is directly above the velocity convergence between 400 and 300 mb associated with also the leading edge of the polar front jet stream propagating southeastwards towards the Gulf Coast States.

This deep layer of mass flux convergence establishes stage 2 of the interaction between the jet streaks. Figure 11 indicates that there is a distinct mesoscale region of mean sea level pressure rises which builds directly over GNV during the period between 1500 and 1630 UTC. This region, in both the model and in the real world, is the locus of maximum mean sea level pressure rises during this period. The model indicates a 3

mb rise in 90 minutes near GNV. This rise is a result of the mass flux convergence occurring over a deep layer of the troposphere and hence, is dependent upon the proper phasing between the advection of low values of v component from the west and significant negative values of v from the north.

Stage 3 commences between 1500 and 1630 UTC during which the increase in mass within the boundary layer manifests itself throughout the column as 10 to 20 meter height rises in the mesoscale region surrounding GNV. This increase in surface pressure hydrostatically extends into the lower stratosphere as can be seen from the 175 mb height field depicted in Figure 6. Note, in particular, during the 1530-1600 UTC time period, the repositioning of the 12720 meter isoheight line northward over the north western side of the Florida peninsula. This is directly above the surface pressure rises west of GNV while along the northeastern side of the Florida peninsula there is little change in the position of the isoheight line. This results in the further reduction in the magnitude of the westward directed pressure gradient force beyond that already established by the synoptic scale thermal advection processes. This process produces subgeostrophic flow over and to the north of XMR at the 175 mb level. This is occurring in space and time precisely where the tangential component of the geostrophic wind (mostly the meridional component) depicted in Figure 5 reaches its lowest magnitude over XMR. Hence, parcels are accelerated eastward over XMR within the lower stratosphere.

Stages 4 and 5 result from the development of the acceleration of the subtropical jet streak in the stratosphere over XMR. Here, divergence caused by the subtropical jet streak acts in opposition to the mass flux convergence forced by the southeastwards propagating polar front jet. This results in weaker low-level pressure rises over north central Florida. This in turn, reduces the hydrostatic pressures rises near GNV and diminishes the confluence and geostrophic adjustment in the stratosphere to the east near XMR.

These nonlinear interactions are associated with three distinct mesoscale circulations during the 1500 to 1630 UTC time period. We will now describe these backwards in time from 1630 to 1500 UTC. The development of the lobe of the subtropical jet streak extending from the northwest to the north-northeast of XMR near the 175 mb level results in

a vertical circulation which tends to reinforce the existing south to north height gradient within this region. Figures 12 and 13 depict horizontal plots of omegas generated by MASS 4.0 during this time period. It is indeed interesting to note that, by comparison, the lower stratospheric GMASS trajectories rise rather than sink between 1600 and 1630 UTC indicating differences in the strength of the circulations north and west of XMR as simulated by the two models. The MASS 4.0 simulation indicates that as parcels in the lower stratosphere accelerate eastward arriving at XMR at 1645 UTC they are descending and adiabatically warming while just to the north of DAB parcels are rising and cooling. This is probably an indication of the enhanced mass flux convergence above XMR in the lower stratosphere. This results in downward motion ahead (to the southeast) of the new lobe of the subtropical jet which forms just to the north of XMR. This indirect circulation above the tropopause in which parcels sink and warm over and to the south of XMR while they rise and cool to the north of XMR acts to sustain the mesoscale characteristics of the front in the lower stratosphere. The pattern of adiabatic temperature change associated with the vertical motion pattern produces height rises on the warmer side and falls on the colder side which reinforces the south to north height gradient and promotes an environment for the eastward acceleration of air parcels to the north of XMR within the lower stratosphere.

The stratospheric frontogenetical circulation is the result of a thermally direct circulation before 1600 UTC in the same region. This is evident in Figure 10 in which parcels, during the initial development of the new lobe of the subtropical jet streak are sinking on the cold side of the front over XMR and rising on the warm side north of DAB.

These stratospheric circulations are the consequence of the indirect circulation in the upper troposphere which developed northwest of GNV near 225 mb. This vertical motion pattern in Figure 13 indicates substantial sinking at 225 mb on the warm side of the convergence zone near GNV during the early part of the 1500 to 1630 UTC time period.

6. Planetary Boundary Layer Improvements.

As noted in the introduction, the analysis of the results from the simulations of the atmospheric environment in the vicinity of the Challenger explosion suggested that a high resolution PBL scheme might improve the quality of the simulations. The implementation of such a

scheme was assigned as Task 6 under NAS5-30145. The implementation and testing of the PBL scheme was partitioned into several sub-tasks under Task 6. A review of the work performed and the results obtained under each sub-task is presented in this section.

6.1 Sub-Task 1: Eady Wave Initialization of 2-D GMASS

The 2-D GMASS model including the Eady wave initialization software and the model-output plotting programs were transferred from the NASA-Goddard computer system to the NASA/Langley computer system. The software was modified so that it would correctly execute on the NASA-Langley computer system. At first, there were some discrepancies in the initial ground temperature data. However, these were quickly resolved and the NASA/Goddard and NASA/Langley versions of the model were demonstrated to produce identical results.

For example, a 24 hour benchmark simulation with the 2-D GMASS model performed on the NASA-Langley computer system produced normal and tangential wind components (Figures 14a and 14b) that were identical to the corresponding fields (Figures 15a and 15b) produced by Jeff Mcqueen at NASA/Goddard. Both of these adiabatic, inviscid GMASS runs were initialized by the analytic Eady wave solutions at 60 H-B hours (Mcqueen and Koch, 1988) and integrated to 84 H-B hours (i.e., 2100 UTC).

6.2 Sub-Task 2: Incorporation of the Blackadar PBL in 2-D GMASS

The NASA-Langley version of the 2-D GMASS model was modified to include non-uniform sigma layers. A 1-D Blackadar planetary boundary layer (PBL) parameterization (Blackadar, 1979; Zhang and Anthes, 1982) was added to the 2-D GMASS model. This version of GMASS was transferred to the NASA/Goddard computer system by Mohan Karyampudi.

Preliminary tests with the non-uniform sigma layer version of the 2-D model produced satisfactory results. Two 7 hour simulations with differential heating were performed after the simulations were initialized with the Eady wave analytical solutions at 77 H-B hours. The non-uniform sigma layer version of the model used higher resolution in the lower atmosphere than the uniform sigma layer version. Figures 16a and 16b illustrate the vertical velocity fields obtained from the non-uniform and the uniform sigma-layer versions of the model, respectively. The updraft just to the east of the heating maximum is slightly stronger and located

higher in the non-uniform sigma run. In addition, the depth of the boundary layer (not shown) is deeper in the non-uniform sigma layer simulation.

6.3 Sub-Task 3: Testing of 2-D GMASS with the Blackadar PBL

The 2-D GMASS model with the Blackadar PBL was tested on a low-level frontogenesis case. This case has previously been used by Mcqueen and Koch (1988) to test the sensitivity of the mixed-layer PBL parameterization. Several sensitivity tests were performed with the Blackadar PBL on this low-level frontogenesis case.

A seven hour simulation with differential heating was run with the Blackadar PBL scheme. The initial and boundary conditions were kept the same as those used by Mcqueen and Koch (1988) in order to compare the Blackadar PBL scheme results with those from the mixed-layer PBL parameterization. As in Mcqueen and Koch, diabatic heating was allowed after sunrise in the adiabatic, inviscid 2-D MASS integrations beginning at 77 H-B hours. However, the Blackadar PBL version of the model used a non-uniform vertical grid with higher resolution below 700 mb whereas the mixed layer version of the model utilized a uniform sigma-layer thickness.

Figure 17 shows the vertical velocity (w), potential temperature (θ), ageostrophic wind vectors (u_{ag} + w) and v-component of the wind from simulations performed with the Blackadar and mixed-layer versions of the model. The results from the Blackadar simulation were compared with the results from simulations with explicit mixing of mass and momentum in which the sensible heating rate (**Q**) was invariant with height and one with implicit mixing of mass and momentum in which **Q** was linearly decreased with height (see Mcqueen and Koch, 1988).

The vertical velocity field (Figure 17) from the Blackadar PBL version of the GMASS model shows a strong updraft with a maximum of 21 cm s^{-1} located ahead of the front near the 2 km level. This resembles the updraft simulated by the implicit mixing run. However, the explicit mixing run shows several unrealistic features in the vertical motions to the east of the front. Significant noise in the potential temperature field above the top of the PBL is also apparent in this run. On the other hand, both the Blackadar and the implicit mixing model runs show smooth profiles of potential temperature. The superiority of the Blackadar high resolution PBL scheme over the implicit as well as the explicit mixed-layer schemes is clearly

evident in the v-component of the wind field. The low-level jet, located at a level of about 1 km on the east side of the front, is well captured by the Blackadar model run. In contrast, the explicit mixed layer simulation produced no evidence of such a wind speed maximum whereas the implicit mixing simulation created a double jet maximum with one located above 2 km and the other unrealistically close to the ground. Such unreasonable wind simulations by the mixed-layer type model have previously been noted by Anthes et al (1980).

6.4 Sub-Task 4: Test of 2-D GMASS with Heat Island Case

A test of the Blackadar PBL on a heat island case was performed. In preparation for this test, homogeneous initial conditions along a 2-D cross-section across the Florida peninsula were created using Tampa rawinsonde data. However, after holding discussions with NASA/Goddard scientists it was decided that modified Eady wave solutions would be a more useful heat island test case.

The heat island case was initialized with homogeneous atmospheric conditions in which no horizontal temperature gradient was allowed in the east-west direction (Figure 18a) while the v-component of the wind was set equal to zero. The u-component of the wind was set equal to u_g which was allowed to increase with height with the westerly shear as in the frontogenesis case. Differential heating was turned on after 17 hours of adiabatic, inviscid model integration by specifying complete cloud cover on the west side of the domain and clear sky conditions on the east side of the domain. After 7 hours of heating an inland sea breeze front developed near the center of the domain with an inland sea breeze directed from the cool air to the warm air near the surface and a return flow at about 3 km (Figure 18b). On the warm side of this front, there is an updraft of 1 cm s^{-1} and a downdraft of equal magnitude on the cool side of the front (Figure 18c). These vertical velocities are slightly weaker than those found in other studies (e.g. Pielke, 1974). This might be due to a combination of several factors including (1) the large horizontal domain, (2) the presence of weak heating on the cool side of the circulation in the simulation in contrast to no heating in this area in a real sea breeze situation and (3) the initial specification of no horizontal pressure gradient in the east-west direction.

6.5 Sub-Task 5: Implementation of the Blackadar PBL in 3-D GMASS

A 1-D Blackadar PBL code was successfully implemented in the 3-D GMASS model residing on the CYBER 205 computer at NASA/Goddard. This GMASS code was modified to allow specification of non-uniform sigma layers which are essential for the Blackadar PBL to perform accurate simulations with real data cases.

Preliminary results from the 12 hour simulation of the 16-17 April 1982 case with the Blackadar version of the 3-D GMASS model (BLKMASS) were encouraging. The BLKMASS was initialized with LFM analysis data at 1200 UTC, 16 April 1982 with a grid distance of 190.5 km. A vertical distribution of 32 non-uniformly-spaced sigma layers was used. Also, no cumulus parameterization scheme was included in this run. The results from this simulation were compared with an identical run in which the mixed layer PBL (MIXMASS) parameterization replaced the Blackadar scheme. Figure 19 illustrates the 12 hour 850 mb forecasts from each of these runs and the verifying LFM analysis. In general, the simulated 850 mb fields of winds, temperature and relative humidity from the BLKMASS run are in closer agreement with the analysis of observed data than those produced by the MIXMASS run. In particular, it should be noted that the northerly winds produced by the BLKMASS run agree quite well with the LFM analysis. Stronger wind speeds behind the cold front in the BLKMASS run might have contributed to the advection of colder and drier air further southward over the Texas panhandle than in the MIXMASS run. Consequently, the front is stronger in the BLKMASS simulation than in the MIXMASS simulation. MIXMASS's inability to adequately account for the vertical wind shear in the boundary layer may be responsible for the uniform westerly winds which bring unrealistically warm and dry air over the northern Texas and southern Oklahoma region.

6.6 Sub-Task 6: Tests of the 3-D GMASS with the Blackadar PBL

LFM analysis gridded data for 3 consecutive 12 hour time periods for the AVE-SESAME I April 10-11, 1979 case were written to a magnetic tape at NASA/Langley and then transferred to the NASA/Goddard computer facility.

The first attempt to perform a 24 hour benchmark simulation of the 10-11 April case were not successful for two reasons: (1) the GMASS model memory requirements for a 128 X 96 X 20 grid size exceeded the

maximum number of large memory pages available on the Cyber 205 computer after additional arrays were added to the 3-D model to reduce the use of computer resources by storing values that had been recalculated at frequent intervals and (2) a coding error within the Blackadar PBL code was found to cause unrealistic surface temperatures over the ocean.

After these initial problems were solved, a satisfactory 24 hour simulation initialized at 1200 UTC 10 April 1979 was obtained. This simulation employed a horizontal grid increment of 58.5 km over the LFM analysis domain and 20 non-uniformly spaced sigma layers. These model grid characteristics and initial conditions were identical to those used for simulations of this case by MESO with the MASS 4.0 model. This version of the model also used the Blackadar PBL scheme but differed from GMASS in several ways. The most significant difference was MASS 4.0's use of the Adams-Bashforth time integration scheme in place of the Euler backward scheme used in GMASS. A comparison of the 12 hour simulations valid at 0000 UTC 11 April from GMASS and MESO's MASS 4.0 model are presented in Figures 20 through 24.

The surface temperature fields, in general, appear to be similar in both the GMASS and the MASS 4.0 simulations (Figures 20a and 20b). Sea surface temperatures are almost identical in both runs. However, the GMASS simulation shows a slightly cooler warm temperature anomaly along the east coast of Mexico than does MASS 4.0. Both simulations show a warm tongue over the Texas panhandle which extends into the low-levels of the atmosphere and is clearly visible at 850 mb (Figures 21a and 21b). A warm tongue extends northwestward over Mexico at 850 mb in both simulations.

The mean sea level pressure pattern (Figures 22a and 22b) is similar in both simulations except that the minimum central pressure value over Colorado in the GMASS run is higher than in the MASS 4.0 run. The central pressure value of 987 mb from the GMASS simulation is much closer to the observed value of 988 mb than the 980 mb value produced by MASS 4.0. There are several possible explanations for this discrepancy between the GMASS and MASS 4.0 simulations. The most obvious possibilities are that (1) the time integration schemes are not the same in the two versions of the model and (2) the sea level pressure reduction methods employed in the models are not the same.

Both simulations show cyclonic rotation of the winds at 850 mb (Figures 23a and 23b) with wind maxima of 25 m s^{-1} located over Texas and Oklahoma. The wind maximum over Oklahoma ahead of the front

agrees well with the observations whereas the simulated wind maximum over Texas is much stronger than the observed maximum. The simulated convective rainfall during the three hours preceding 0000 UTC 11 April has a similar patterns in both runs (Figures 24a and 24b). However, the GMASS simulation produces a larger area of precipitation over the Texas, Oklahoma and Colorado region.

7. Summary, Conclusions and Recommendations

Numerical simulation studies were performed with the MASS 4.0 numerical model for the 28 January 1986 Shuttle Challenger case. Numerical simulations employing 58, 14.5, and 7.25 km grid mesh versions of the model were performed for time periods of 12, 5, and 1.5 hours, respectively. The fundamental purpose of these simulations was to understand the mesoscale dynamical processes which produced layers of substantial vertical wind shear over the Kennedy Space Center during the period of the Challenger disaster.

The MASS 4.0 simulations indicate that the layer of maximum vertical wind shear was deeper and at a higher vertical level than previous published simulations by the GMASS model. Simulations employing MASS 4.0 verified better near the tropopause when compared against the 1647 UTC XMR rawinsonde data than did GMASS. It should be noted, however, that critical gaps in the rawinsonde data inhibited the comparisons both in space and time.

MASS 4.0 simulations indicated that two fundamental nonlinearly-coupled processes were involved in establishing the high vertical wind shear and low Richardson number zone between 210 and 180 mb. The first process involved the development of a region of confluence off the northeastern coast of Florida in which high velocity air was accelerated eastward in the region where the height field exhibited little or no westward-directed pressure gradient force. This process resulted in a new lobe of the subtropical jet stream centered to the northeast of XMR. This feature developed during the 1500 to 1630 UTC time period and was responsible for a simulated 57 ms^{-1} 180 mb wind velocity over XMR.

The second key process involved the advection of air parcels from the west over XMR by 1630 UTC which exhibit very low values of meridional kinetic energy just below (at about 210 mb) the new lobe of the subtropical jet at 180 mb but above and to the south of the polar front jet.

These 2 processes resulted in a 30 mb deep region in which vertical

wind shears approached 2 x 10^{-2} s^{-1} with Richardson numbers of approximately 1.1 centered near 12 km. These 2 processes were nonlinearly coupled through a sequence of several well-defined stages in which several mesoscale frontogenetical circulations were created and destroyed over a 1 to 3 hour time period.

The analysis of the simulations over Florida suggested that the quality of the simulations might be improved by the incorporation of a high resolution planetary boundary layer scheme into the GMASS model. The implementation of a Blackadar high resolution PBL scheme into the GMASS model was completed under task 6 of this contract. A comparison of the Blackadar PBL with the original mixed layer PBL representation on one test case indicated that the high resolution scheme significantly improved the quality of the simulated structure within the PBL. Further tests will be required to determine the full extent and scope of this improvement.

Based upon the results of this study, recommendations for additional research would include:

1) a thorough evaluation of the differences between the MASS 4.0 and the GMASS simulations of the 28 January 1986 case including model sensitivity studies to determine whether the initial data or model formulation was responsible for the differences in the simulated fields,

2) a series of 3-dimensional simulation studies with a nonhydrostatic model employing sufficient horizontal and vertical resolution (a three-dimensional grid of approximately 100 meters) to resolve the breakdown of the flow into nonhydrostatic gravity waves and their attendant turbulence when initialized from the MASS 4.0 7.25 km simulation,

3) an execution of the high resolution non-hydrostatic model to attempt to simulate the structure of the observed smoke plume produced by the Challenger; the use of the model and photographic information could be employed to infer the 3-dimensional wind structure which occurred during the time of the disaster, and

4) general studies of mesoscale nonlinear jet streak interactions with the meso-beta scale version of the MASS 4.0 including the impact of these interactions on the stratospheric-tropospheric exchange processes,

5) further sensitivity studies with the Blackadar PBL version of the GMASS 3-D model.

Acknowledgements

The authors would like to acknowledge the work of Keith Brill of General Software Corporation and Jeffry Homan of NASA/Goddard Laboratory for Atmospheres who prepared the data cube used to initialize the MASS model at 1200 UTC 28 January 1986 as well as Glen Coats of MESO, Inc. who transferred the data to the NASA Langley VPS 32 supercomputer. The authors also thank Jeff Mcqueen of STX Corporation for providing the 2-D GMASS model code and data on magnetic tapes and Mary Bousquet of MESO, Inc. for her assistance in transferring these files to the NASA/Langley computer system. The authors also acknowledge Dr. Louis Uccellini and Dr. Steven Koch of the NASA/Goddard Laboratory for Atmospheres and Dr. Jon Theon of NASA Headquarters for supporting this effort. The 28 January 1986 simulations were done on the NASA/Langley VPS 32 supercomputer. The implementation of the high resolution Blackadar PBL scheme into the 2-D and 3-D GMASS models was done on the NASA/Langley and NASA/Goddard computer systems.

References

Anthes, R. A., N.L. Seaman, T.T. Warner, 1980: Comparisons of numerical simulations of the planetary boundary layer by a mixed-layer and a multi-level model. *Mon. Wea. Rev.*, **108**, 365-376.

Blackadar, A.K., 1979: High resolution models of the planetary boundary layer. *Advances in Environmental Science and Engineering.* **Vol. 1, No. 1**, J. Pfafflin and E. Ziegler, Eds., Gordon and Breach, 50-85.

Hoskins, B. J. and F. P. Bretherton, 1972: Atmospheric frontogenesis models: Mathematical formulations and solutions. *J. Atmos. Sci.*, **29**, 11-37.

Kaplan, M. L., J. W. Zack, V. C. Wong, and J. J. Tuccillo, 1982: Initial results from a mesoscale atmospheric simulation system and comparisons with the AVE-SESAME I data set. *Mon. Wea. Rev.*, **110**, 1564-1590.

Karyampudi, V. M., J. W. Zack, M. L. Kaplan, and J. M. Cram, 1988: A split explicit time integration scheme for the MASS model. *Preprints, 8th Conference on Numerical Weather Prediction*, Baltimore, Amer. Meteor. Soc., Boston.

Kreitzberg, C. W. and D. J. Perkey, 1976: Release of potential instability: Part I. A sequential plume model within a hydrostatic primitive equation model. *J. Atmos. Sci.*, **33**, 456-475.

Mcqueen, J. T. and S. E. Koch, 1988: Experiments with the vertical mixing of heat and momentum in the two-dimensional GMASS. NASA/GSFC internal report, 23 pp.

Mesinger, F., 1977: Forward-Backward scheme, and its use in a limited area model. Contrib. *Atmos. Phys.*, **50**, 200-210.

Petersen, R. A., J. J. Tuccillo, K. F. Brill, and L. W. Uccellini, 1985: The sensitivity of a mesoscale forecast model to detailed three-dimensional isentropic initial analysis and varied vertical model resolution. *Preprints, 7th Conference on Numerical Weather Prediction*, Amer. Meteor. Soc., Montreal, 83-90.

Pielke, R.A., 1974: A comparison of three-dimensional and two-dimensional numerical predictions of sea breezes. *J. Atmos. Sci.*, **31**, 1577-1585.

Uccellini, L. W., K. F. Brill, R. A. Petersen, D. Keyser, R. Aune, P. J. Kocin, and M. des Jardins, 1986: A report on the upper-level wind conditions preceding and during the Shuttle Challenger (STS 51L) explosion. *Bull. Amer. Meteor. Soc.*, **67**, 1248-1265.

Wong, V.C., J. W. Zack, M. L. Kaplan and G.D. Coats, 1983: A nested-grid limited-area model for short-term weather forecasting. *Preprints, Sixth Conference on Numerical Weather Prediction*, Omaha, American Meteorological Society, Boston, 9-15.

Zhang, D. and R. A. Anthes, 1982: A high resolution model of the planetary boundary layer: sensitivity tests and comparisons with SESAME-79 data. *J. Appl. Meteor.*, **21** (11), 1594-1609.

TABLE 1.
Technical Specifications of MASS 4.0

Numerics
•3-D primitive equations for u, v, T, q, and p
•Terrain following σ_p vertical coordinate
•Arakawa 'A' grid on a polar stereographic map image plane
•Fourth-order accurate horizontal space differencing
•Split-explicit time integration scheme
•Fourth-order bi-harmonic diffusion operator
•Flexible specification of both horizontal and vertical grid dimensions and resolution
•One-way interactive grid nesting
•Time dependent lateral boundary conditions from NMC analyses

Initialization
•NGM analysis of 10 mandatory pressure levels as first guess
•Reanalysis using optimum interpolation objective analysis scheme with significant level and surface data
•Interpolation to finer mesh using cubic splines under tension
•Choice of pressure, sigma, or isentropic vertical analysis coordinate
•Automatic calculation of terrain, land/water distribution, and soil moisture at resolution of chosen grid domain
•Assimilation of synthetic relative humidity soundings derived from infrared satellite data
•Removal of integrated mass divergence to reduce gravity wave noise

PBL Formulation
• Choice of Blackadar high resolution PBL model with explicit entrainment by convective boundary layer plumes or mixed layer generalized similarity scheme
•Force-restore surface energy budget over land
•Surface moisture budget over land

Moisture Physics
•Grid-scale condensation based on layer supersaturation
•No liquid water: all condensate falls out of layer
•Condensate can evaporate in unsaturated layers
•Choice of Kuo-Anthes, Fritsch-Chappell, Molinari cumulus parameterization schemes
•Modifiable passive scalar equations for cloud water or chemically inert tracers (scavenging not included)

Radiation
•Radiation is considered only in the surface energy budget

TABLE 2. Simulated Versus Observed Total Velocity (m/s)

Level (P)	1640 GMT MASS 4.0 (58 km)	Error	1645 GMT MASS 4.0 (7.25 km)	Error	1645 GMT GMASS (60 km)	Error	1647 GMT XMR Rawinsonde
125	47	4	47	4	?	?	(125) 43
150	51	1	51	1	45	-5	(152) 50
175	55	?	56	?	50	?	Missing
200	46	2	45	1	52	8	(202) 44
225	38	-2	38	-2	44	4	(222) 40
250	36	?	36	?	36	?	Missing
Average Difference		2.25		2.0		5.67	

TABLE 3

Listing of the pressure (p) in mb, altitude in m, wind direction in degrees and speed in m s^{-1}, potential temperature (θ) in K, wind shear in s^{-1}, and Richardson number (Ri) for Cape Canaveral, Florida (XMR) at 1647 GMT 28 January 1986. Vertical position of polar jet (PFJ) and subtropical jet (STJ) also noted. (From Uccellini et al., 1986)

P	*Altitude*	*U*	θ	*Shear*	*Ri*	
419	7010	292 33	317.0			
				0.004	2.42	
401	7315	291 34	317.5			
				0.004	2.68	
384	7620	290 35	317.8			
				0.006	0.25	
368	7925	288 36	317.9			
				0.008	1.58	
353	8230	385 37	318.6			PFJ
				0.004	-0.38	
337	8534	284 36	318.6			
				0.004	0.42	
323	8839	285 35	318.7			
				0.008	1.27	
308	9144	288 34	319.3			
233	10973	275 36	332.7			
				0.017	1.74	
222	11278	269 40	338.0			
				0.013	0.48	
212	11582	266 43	338.9			
				0.008	3.28	
159	13411	265 50	363.1			
				0.003	27.75	
152	13716	264 50	366.9			
144	14021	264 51	369.6			STJ
				0.008	1.68	
138	14326	266 49	370.9			
				0.011	2.84	
131	14630	268 46	374.6			
				0.009	3.62	
125	14935	269 43	378.3			

A

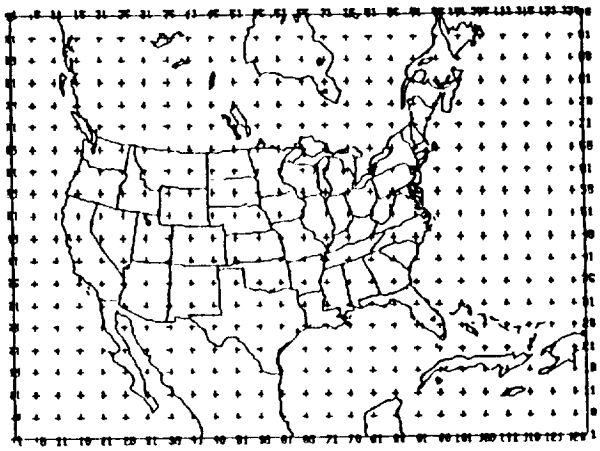

MASS 4.0 GRID A: 58.5 KM

B

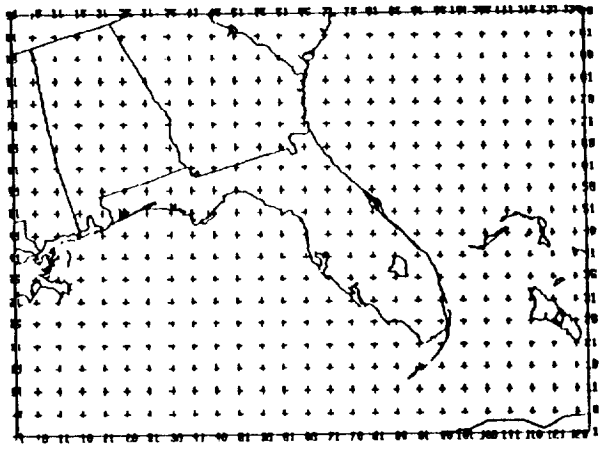

MASS 4.0 GRID B: 14.6 KM

C

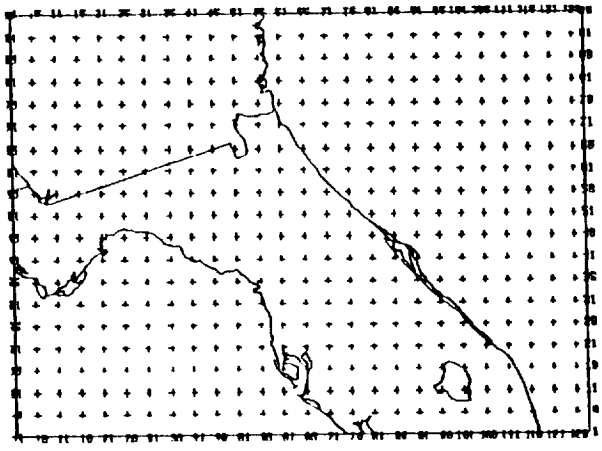

MASS 4.0 GRID C: 7.3 KM

FIGURE 1

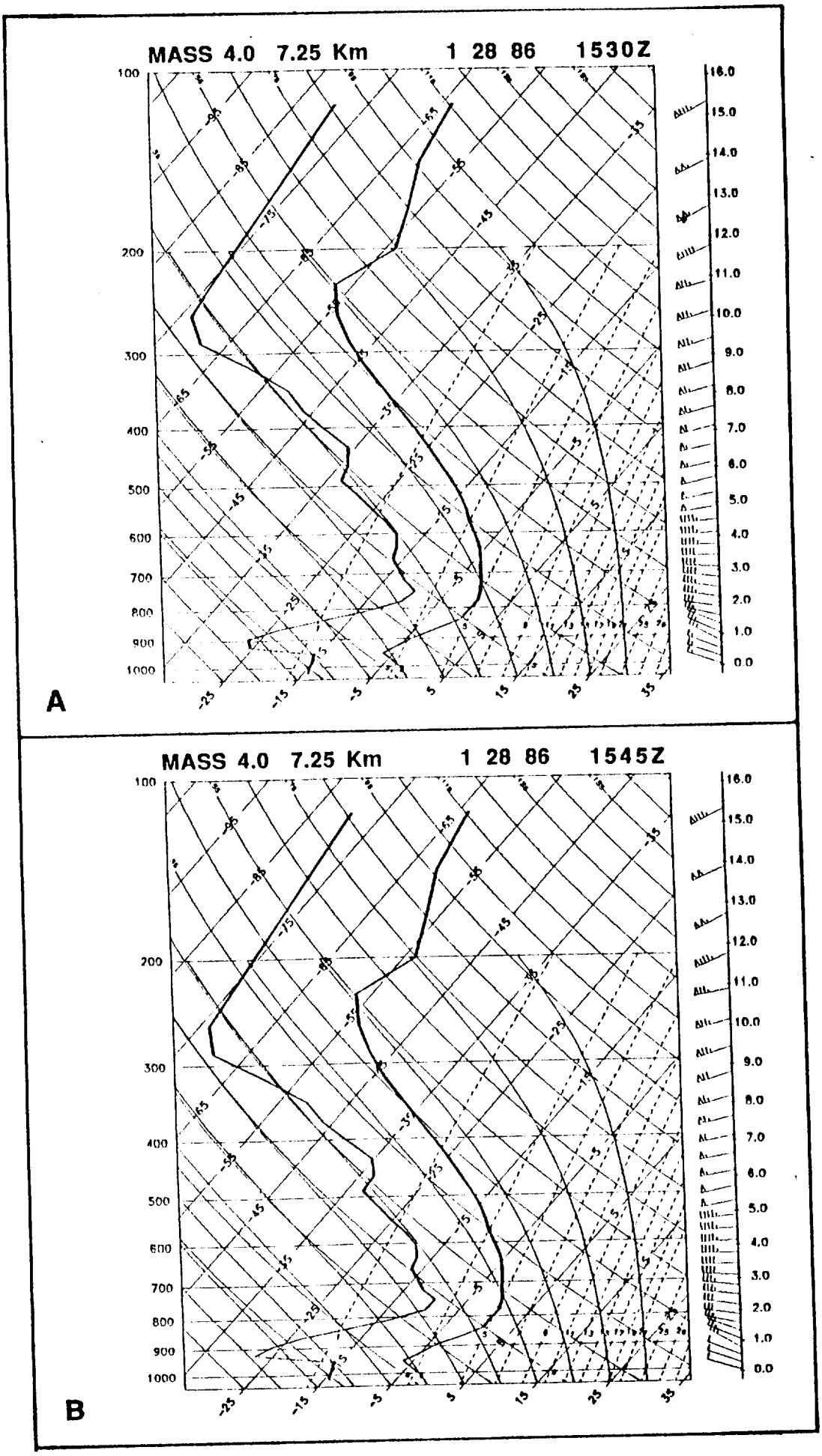

FIGURE 2

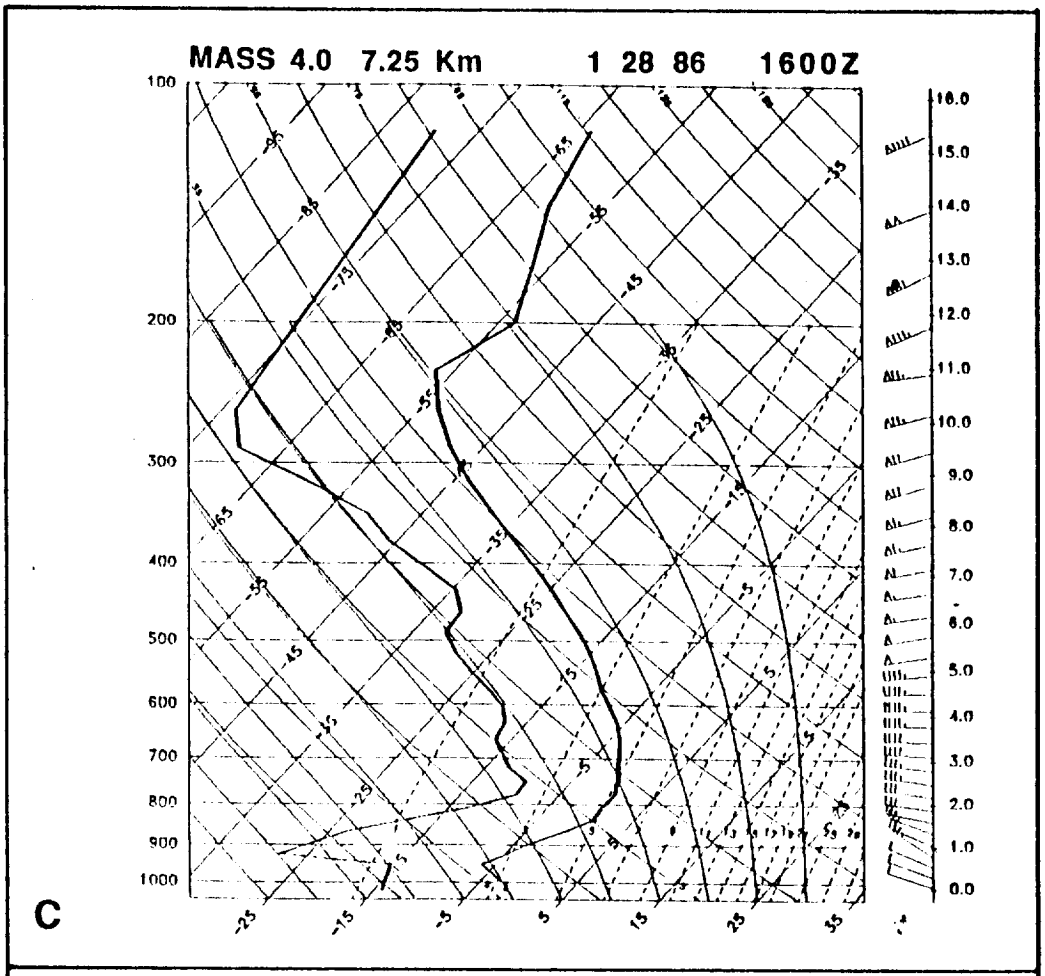

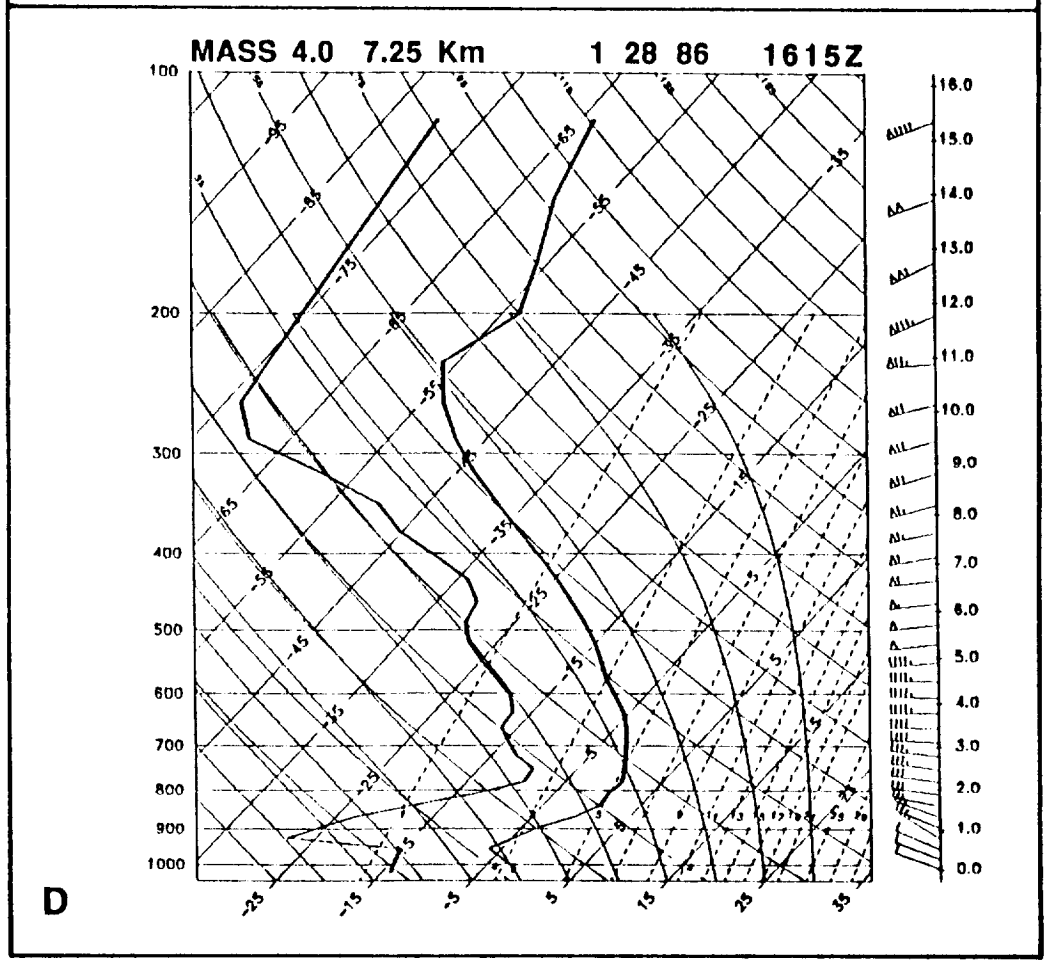

FIGURE 2 continued

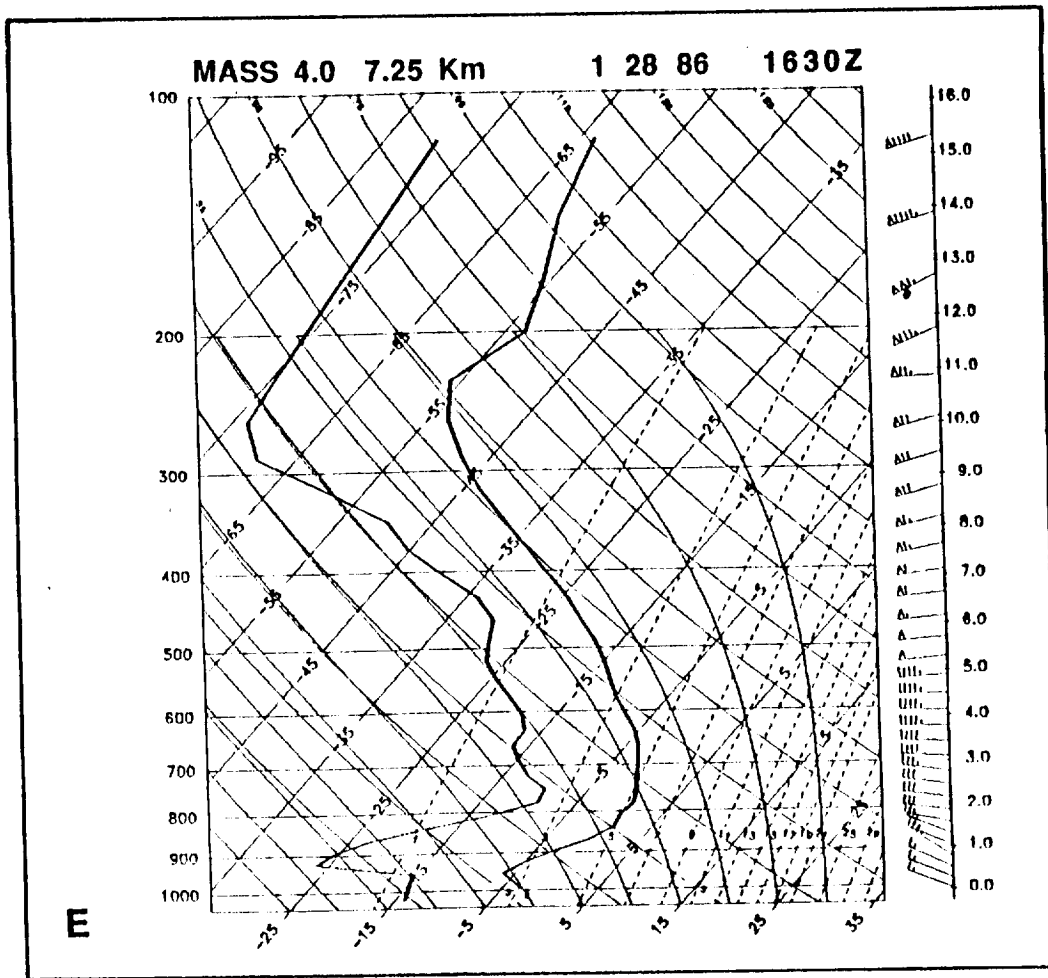

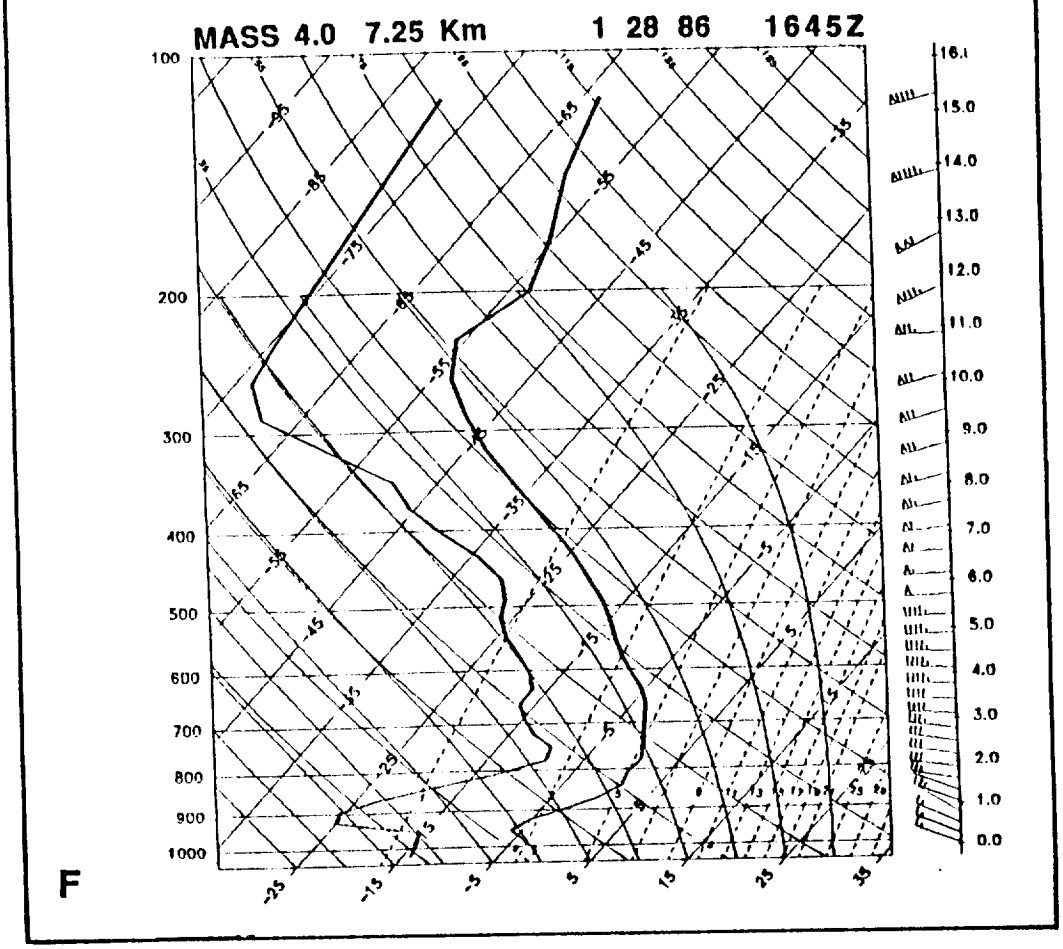

FIGURE 2 continued

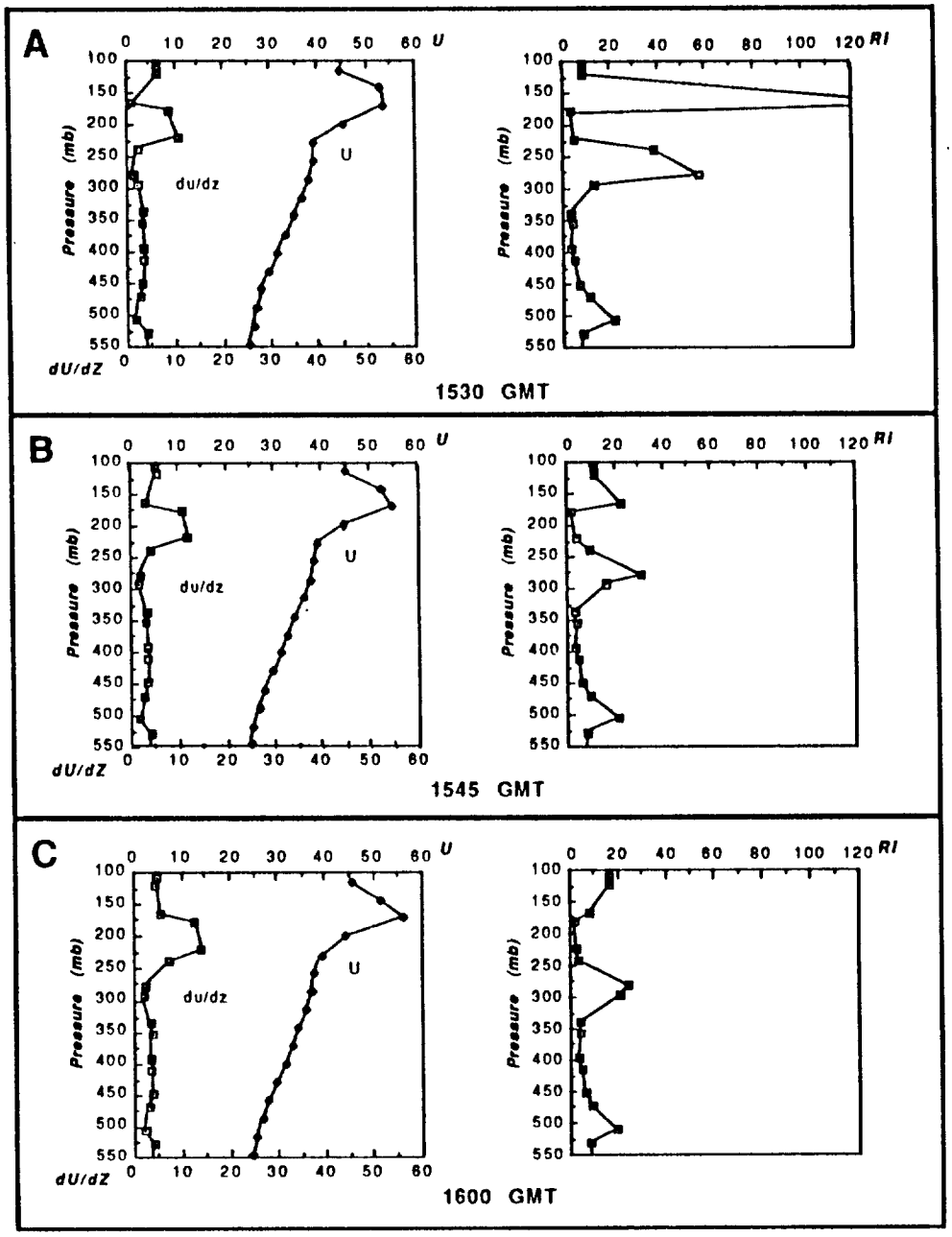

FIGURE 3

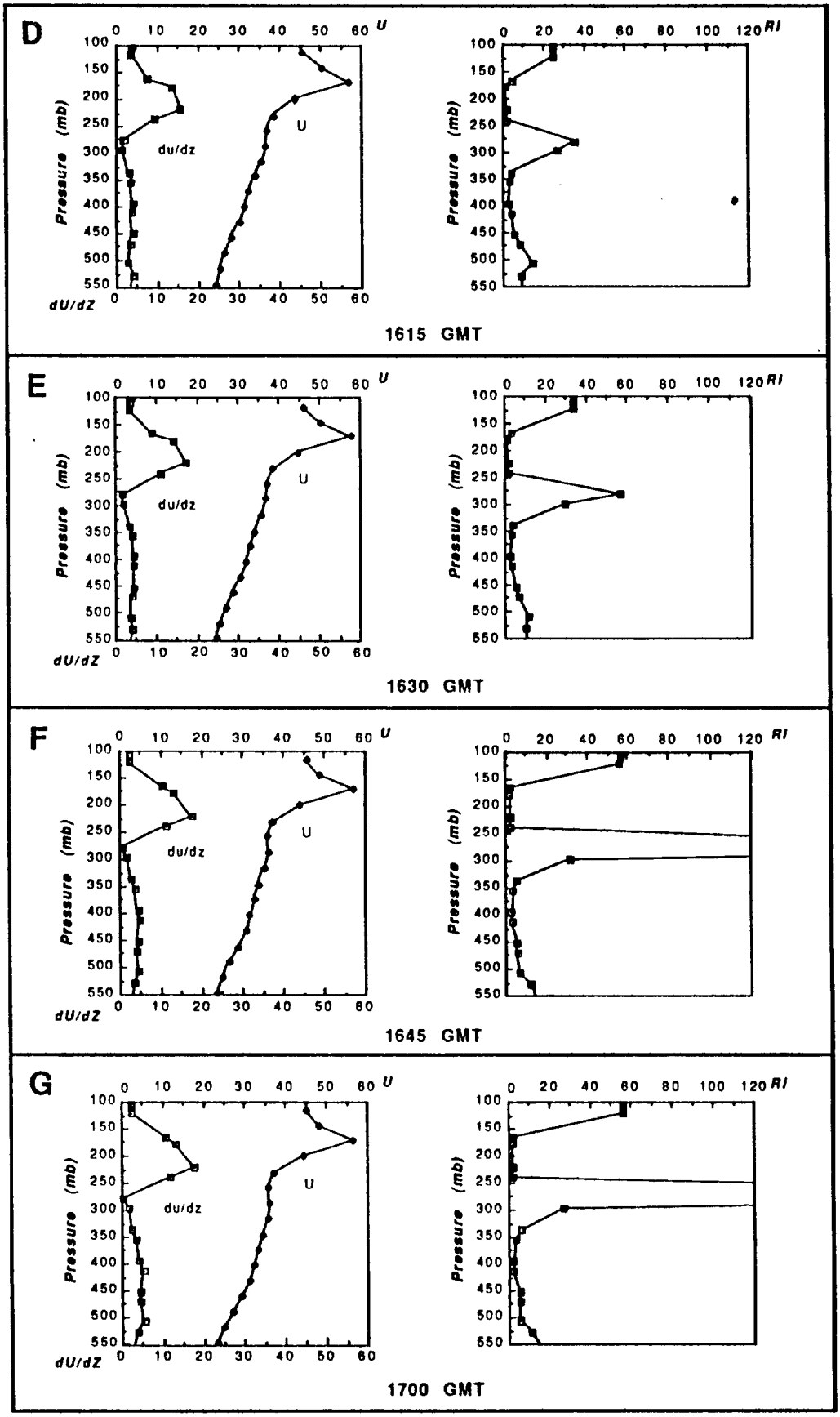

FIGURE 3 continued

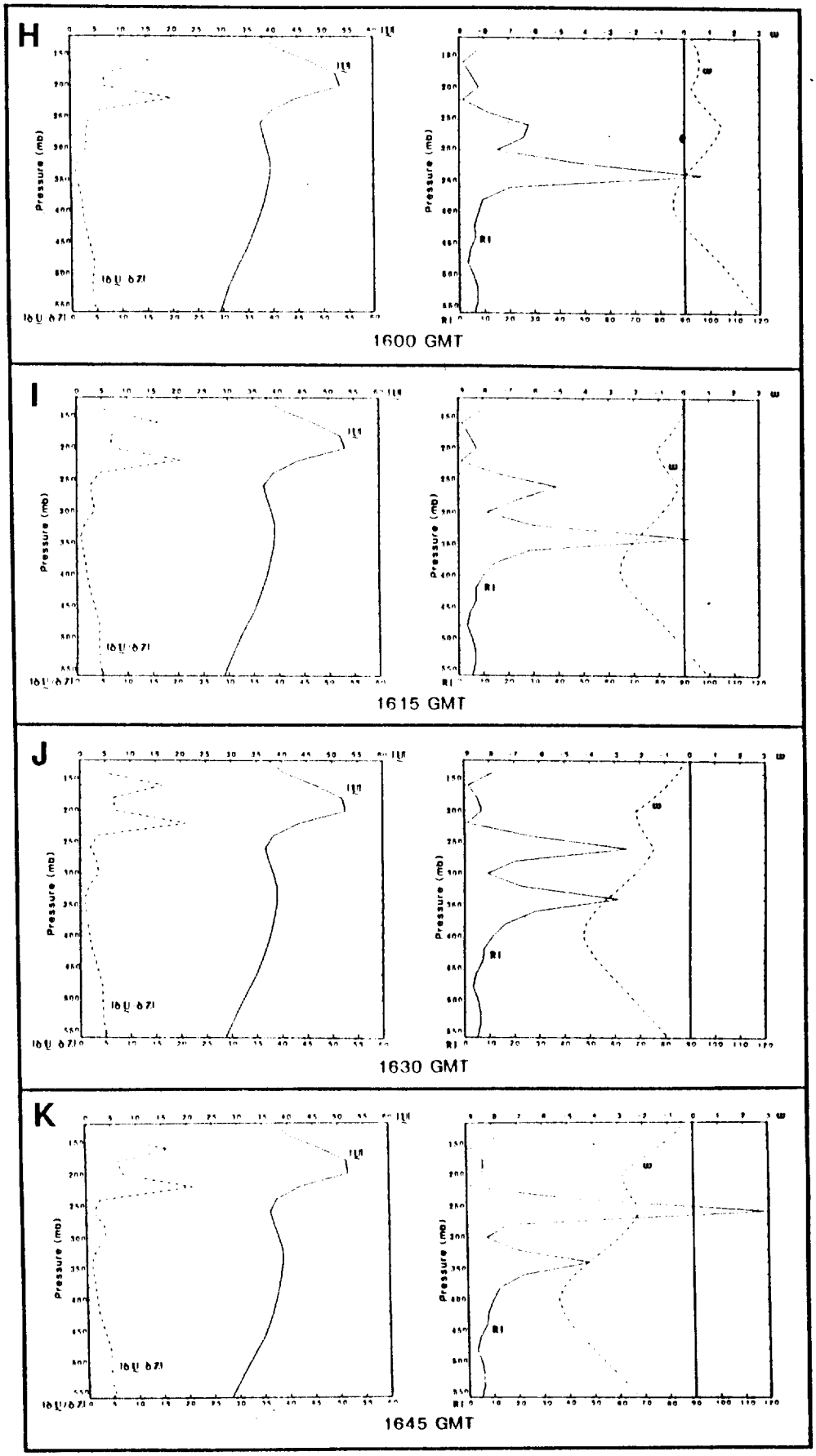

FIGURE 3 continued

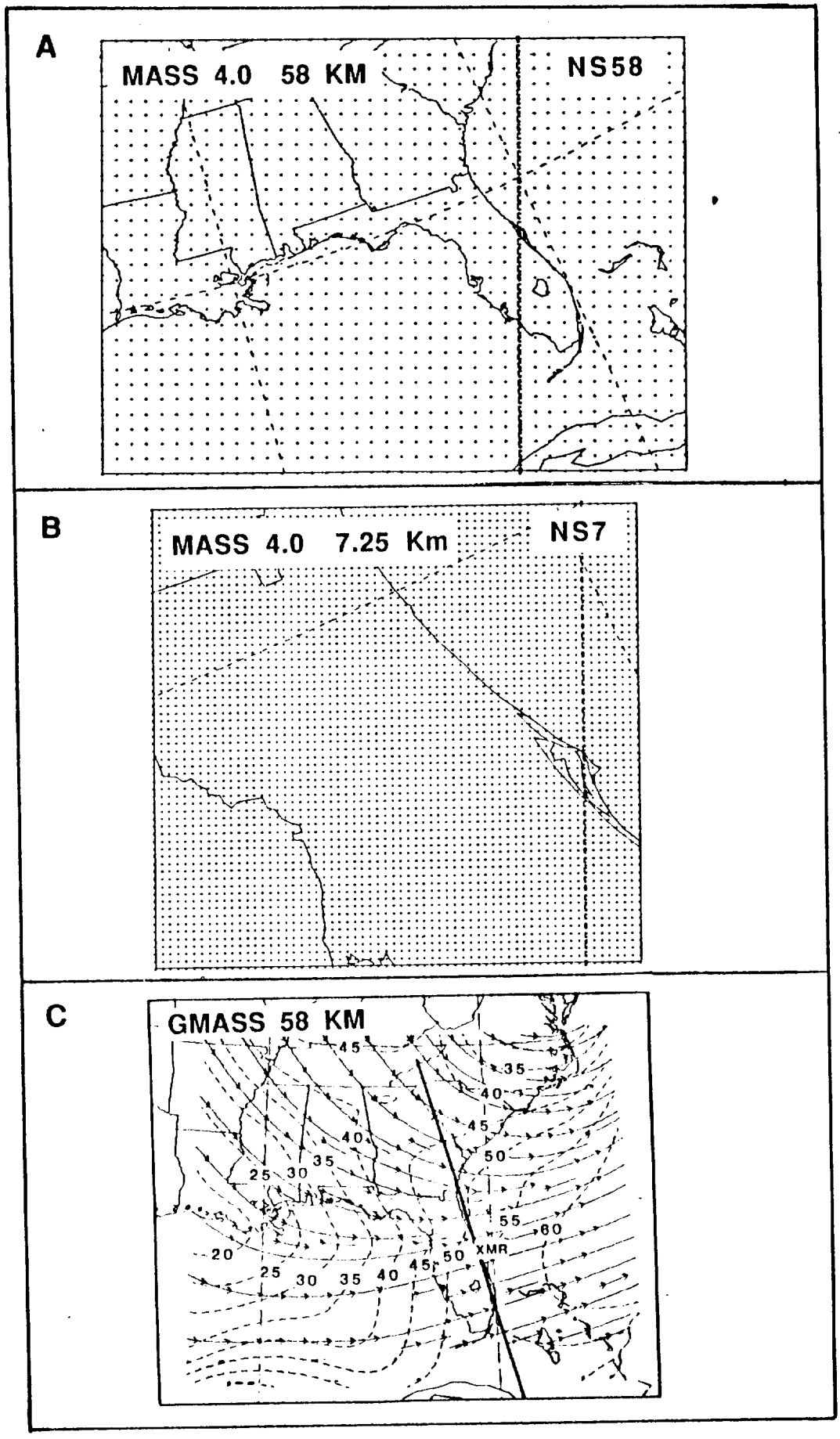
A
MASS 4.0 58 KM
NS58
B
MASS 4.0 7.25 Km
NS7
C
GMASS 58 KM
45
35
40
45
50
40
35
25 30
55
60
XMR
20
25 30 35 40 45 50

FIGURE 4

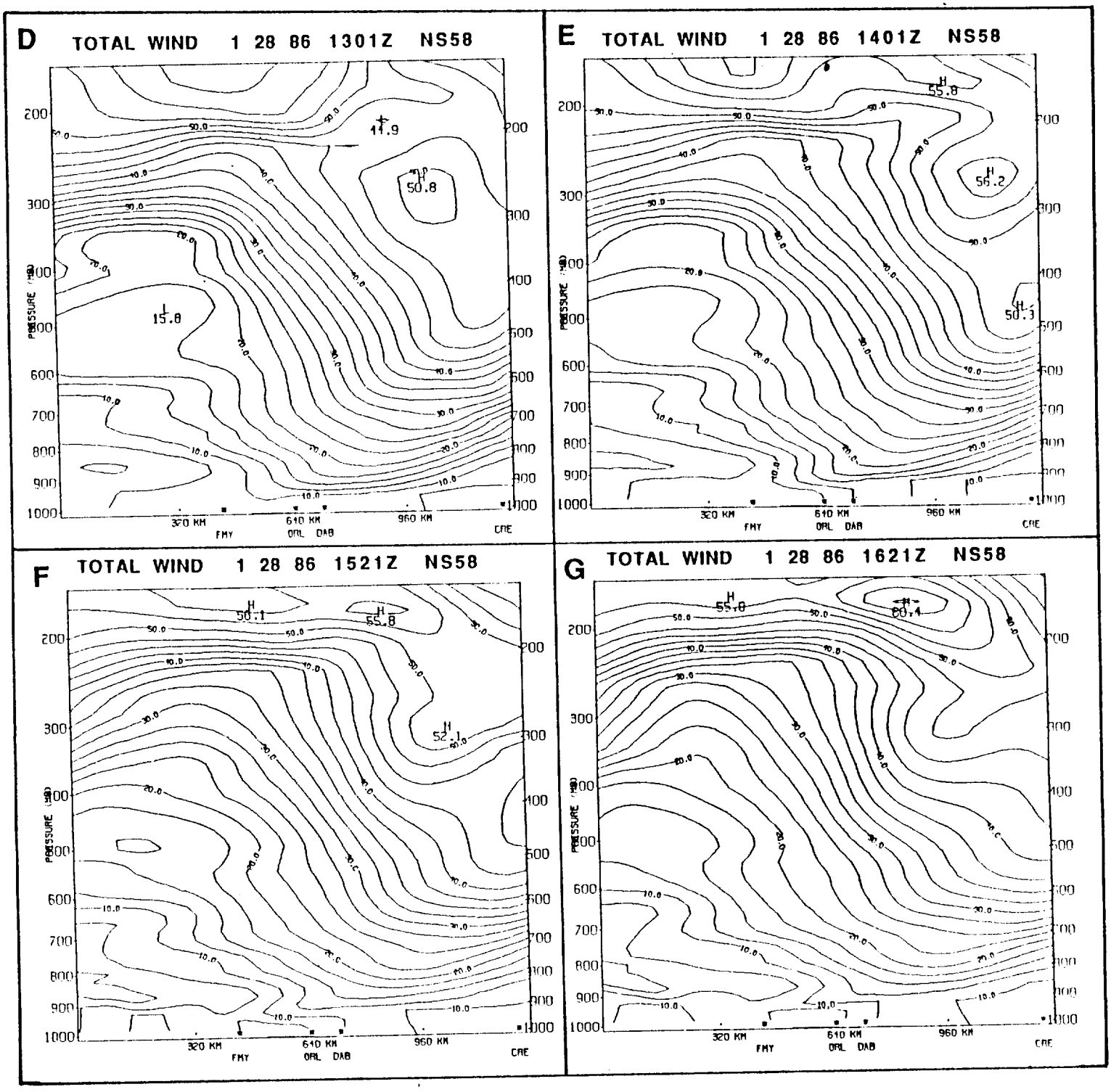

FIGURE 4 continued

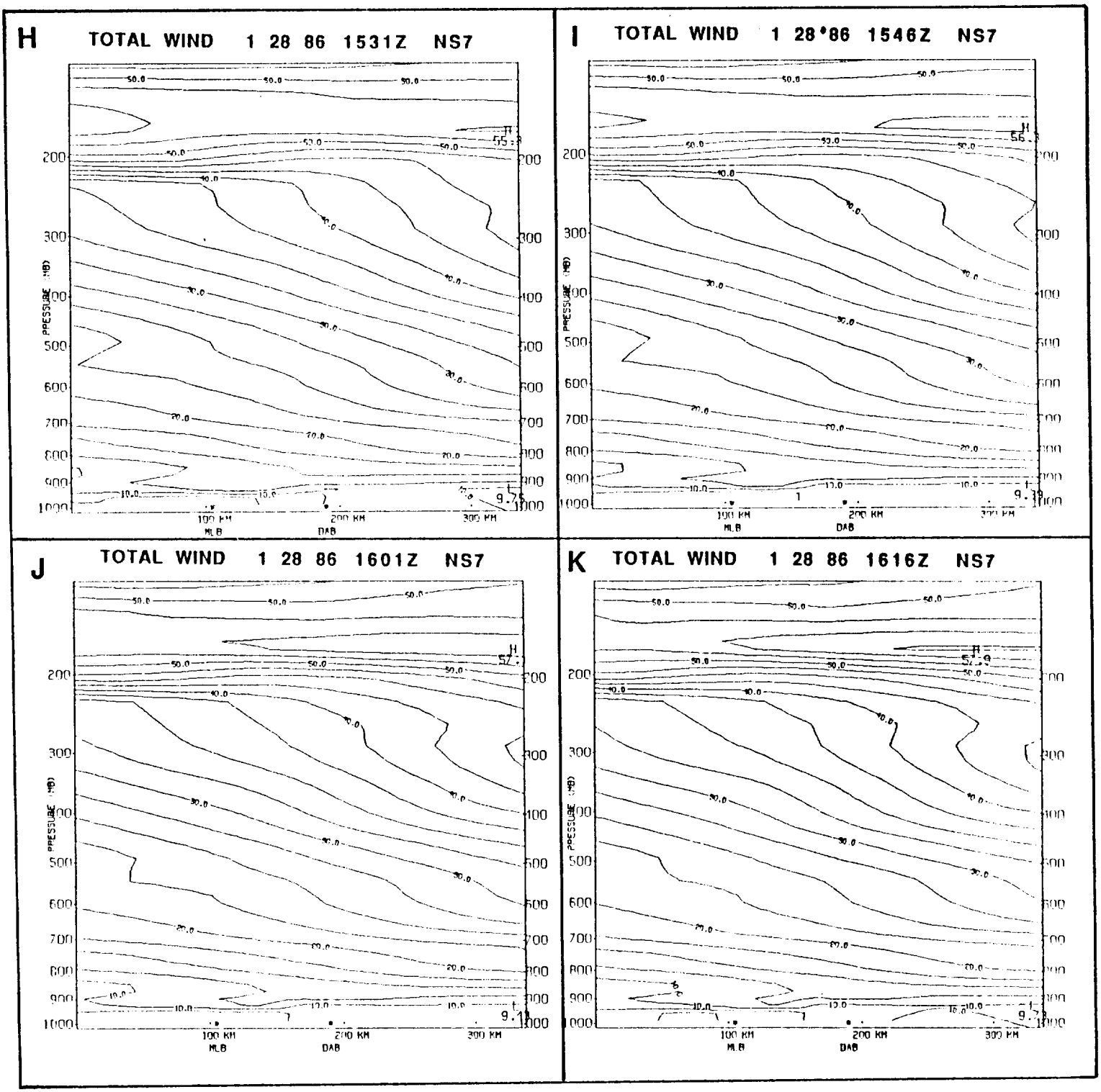

FIGURE 4 continued

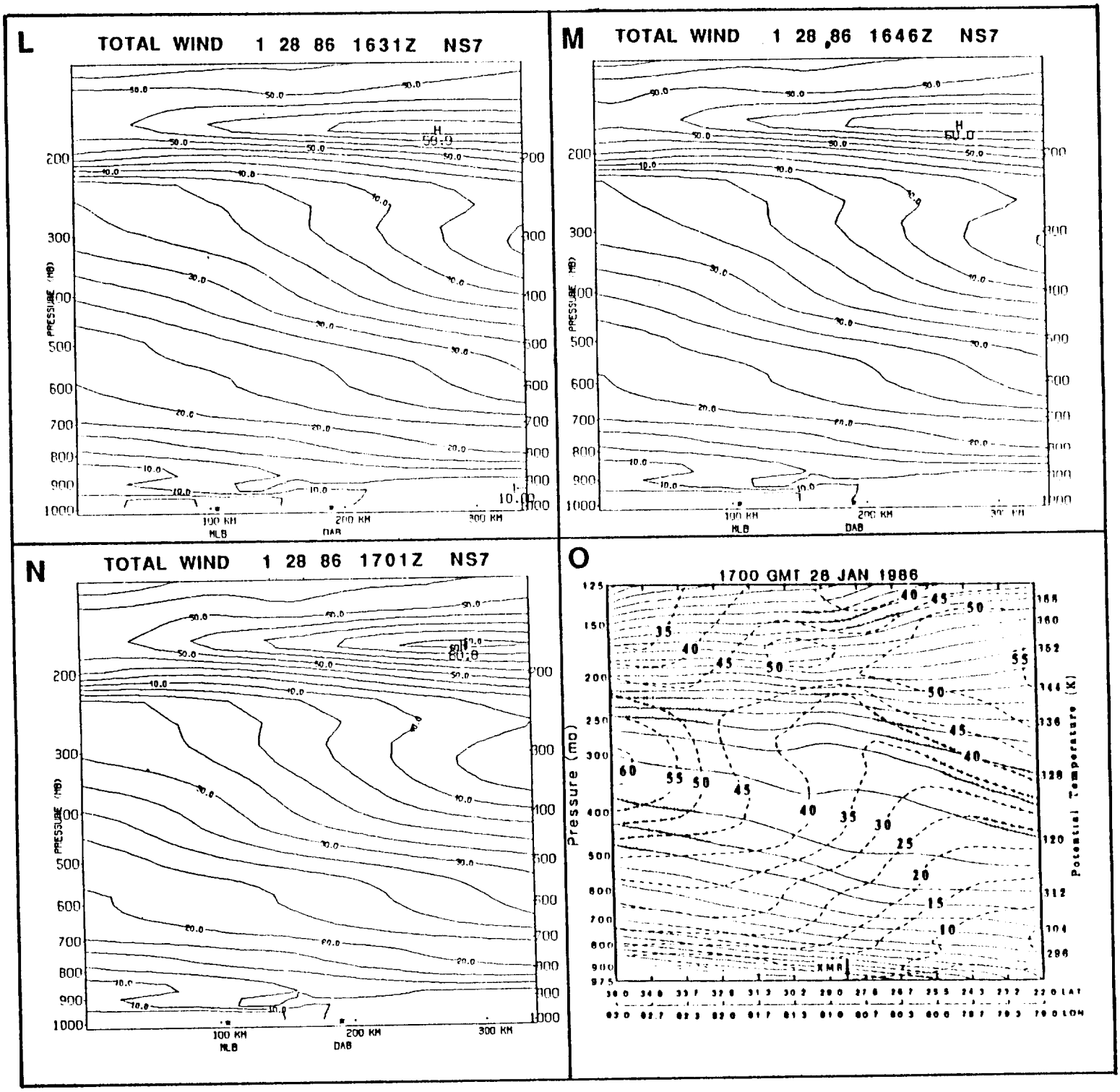

FIGURE 4 continued

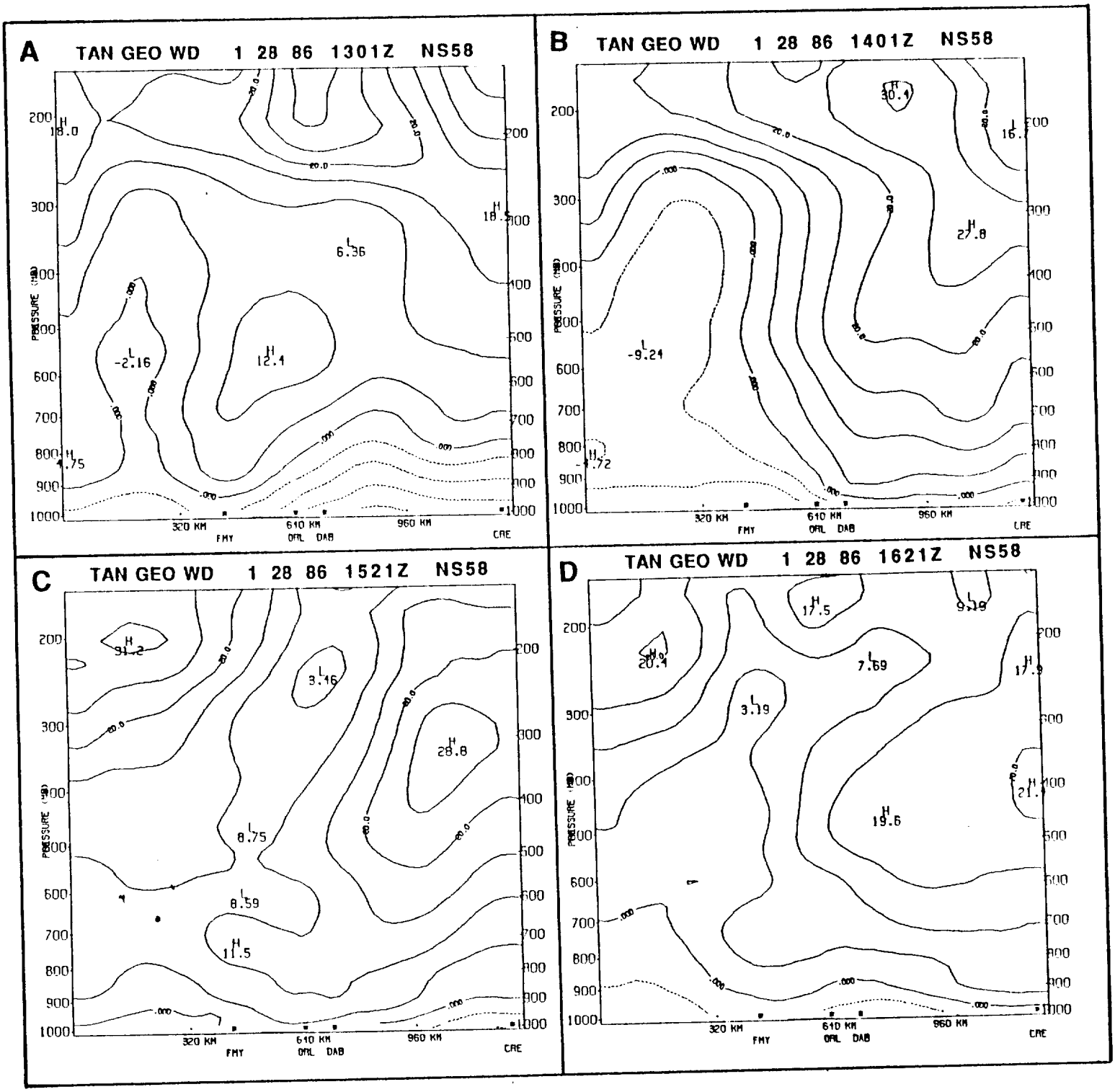
A
TAN GEO WD 1 28 86 1301Z NS58
B
TAN GEO WD 1 28 86 1401Z NS58
C
TAN GEO WD 1 28 86 1521Z NS58
D
TAN GEO WD 1 28 86 1621Z NS58
PRESSURE (MB)
320 KM
610 KM
960 KM
FMY
ORL DAB
CRE

FIGURE 5

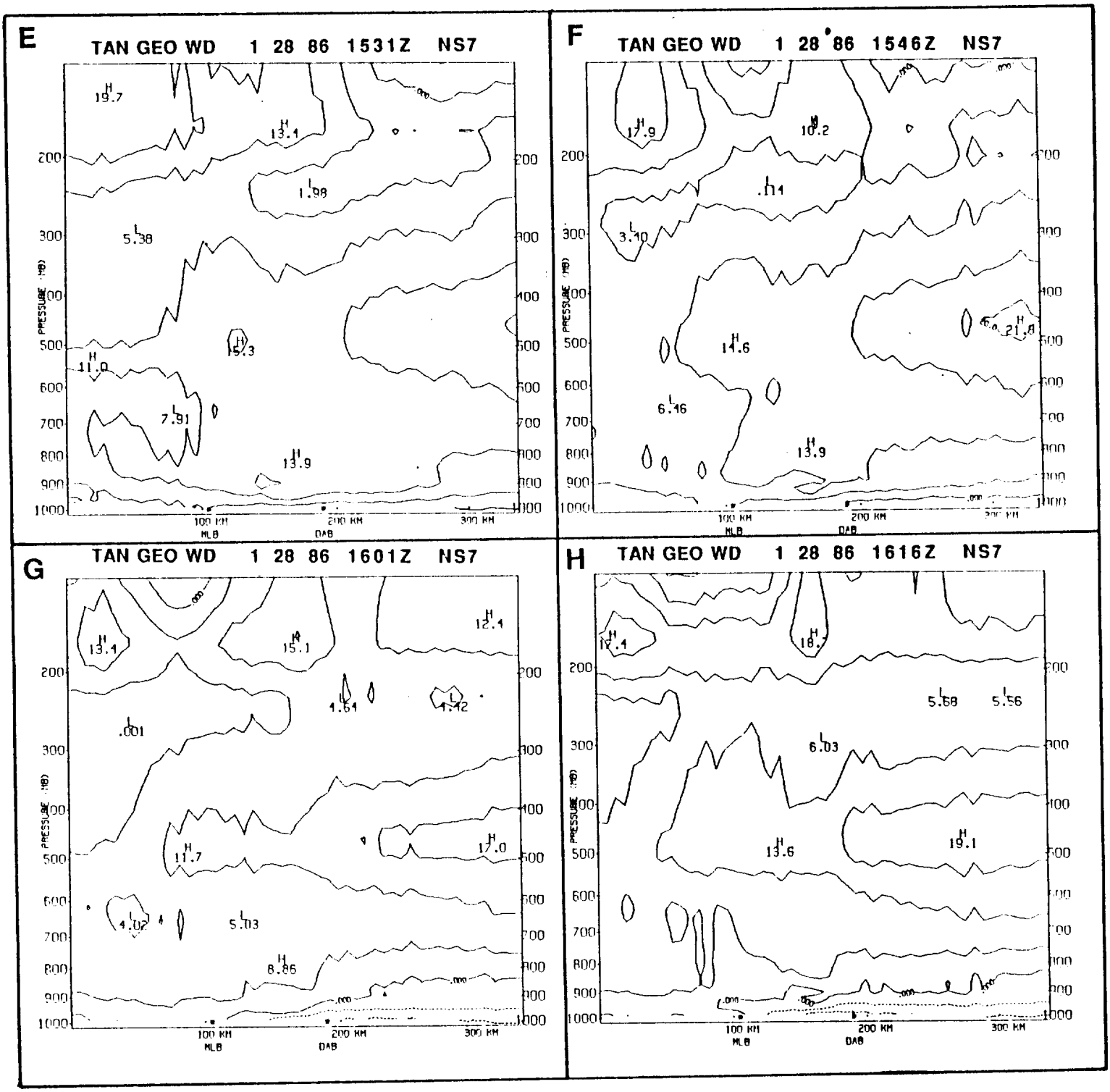

FIGURE 5 continued

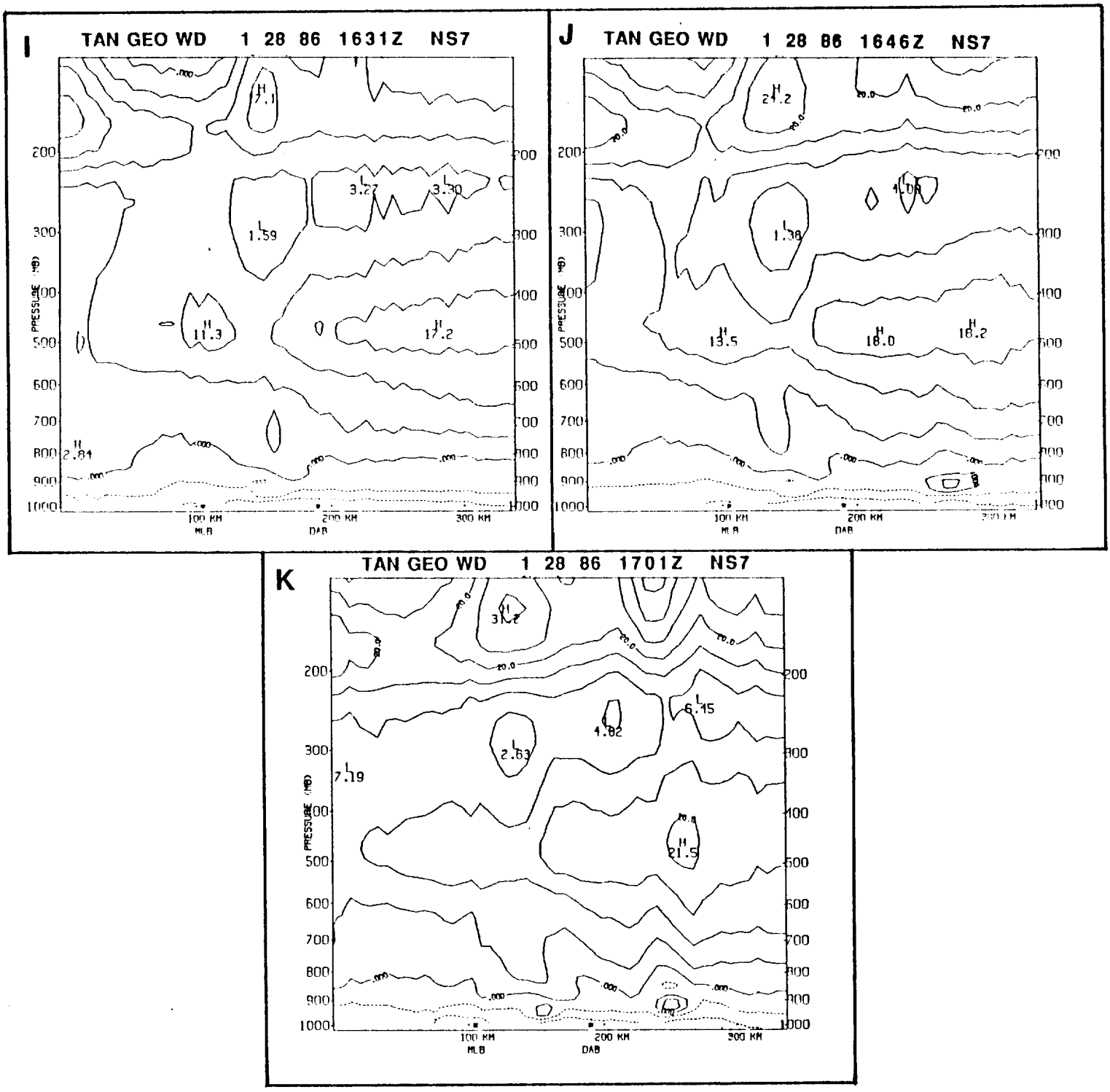

FIGURE 5 continued

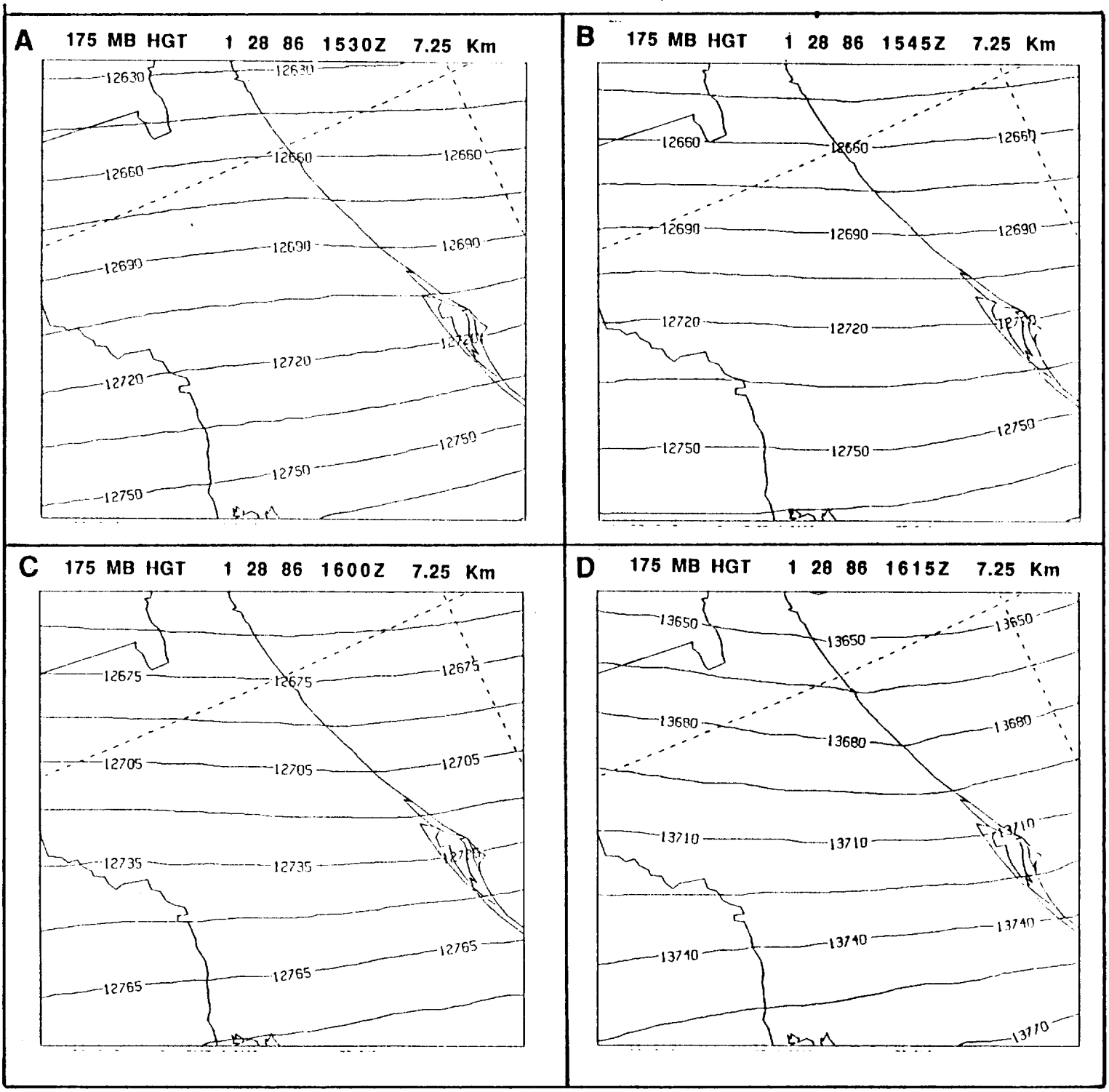
A
175 MB HGT 1 28 86 1530Z 7.25 Km
12630
12660
12690
12720
12750
B
175 MB HGT 1 28 86 1545Z 7.25 Km
12660
12690
12720
12750
C
175 MB HGT 1 28 86 1600Z 7.25 Km
12675
12705
12735
12765
D
175 MB HGT 1 28 86 1615Z 7.25 Km
13650
13680
13710
13740
13770

FIGURE 6

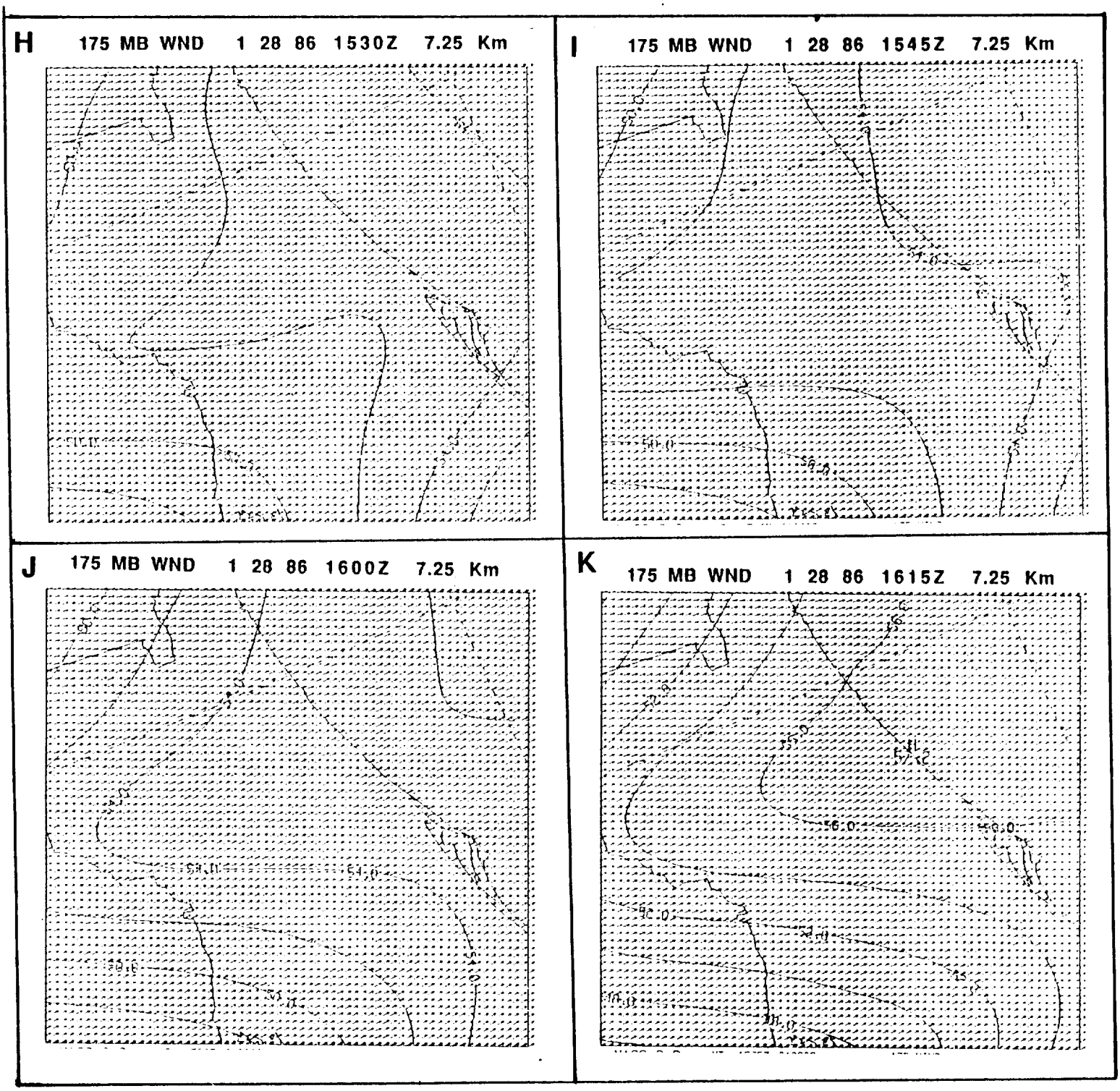

FIGURE 6 continued

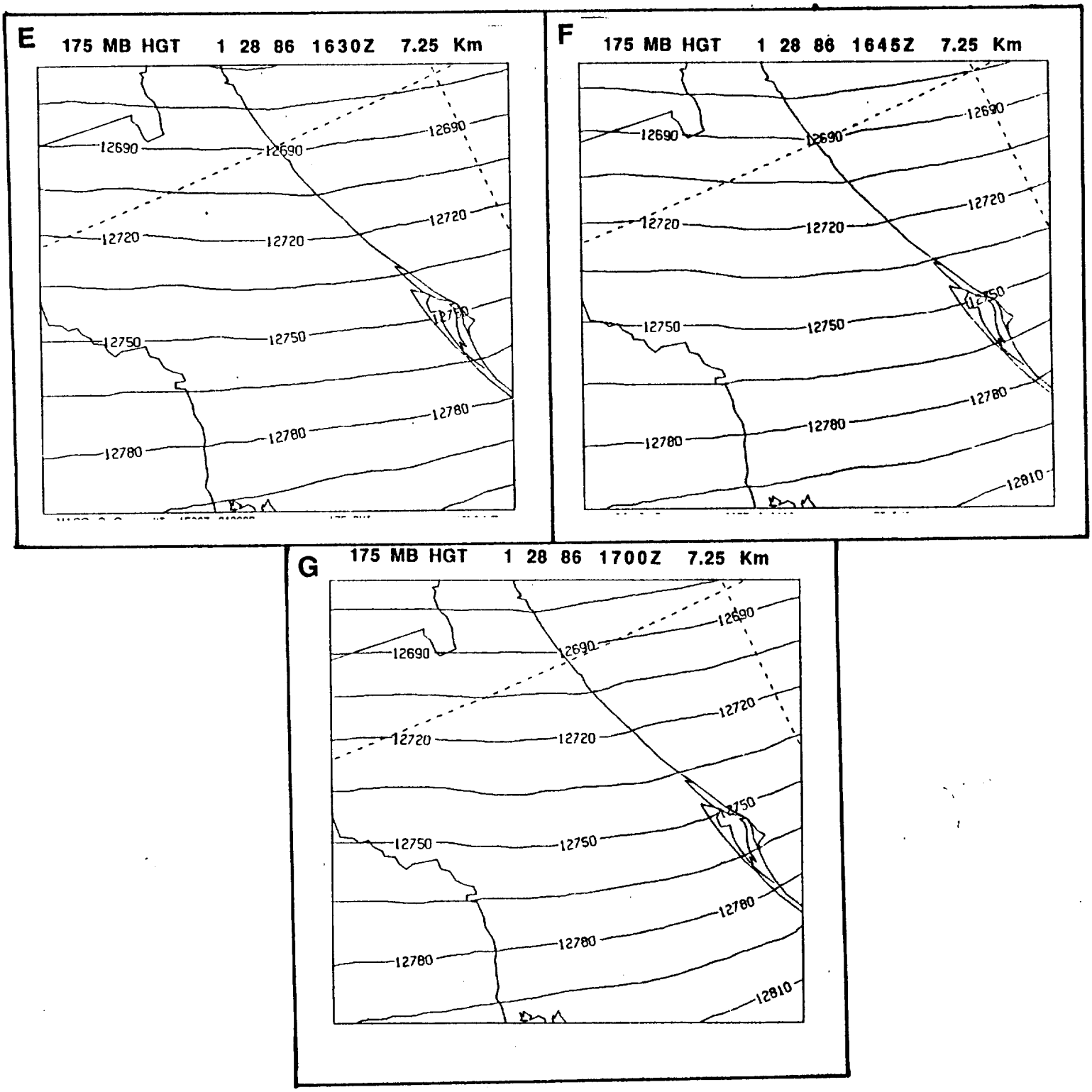

FIGURE 6 continued

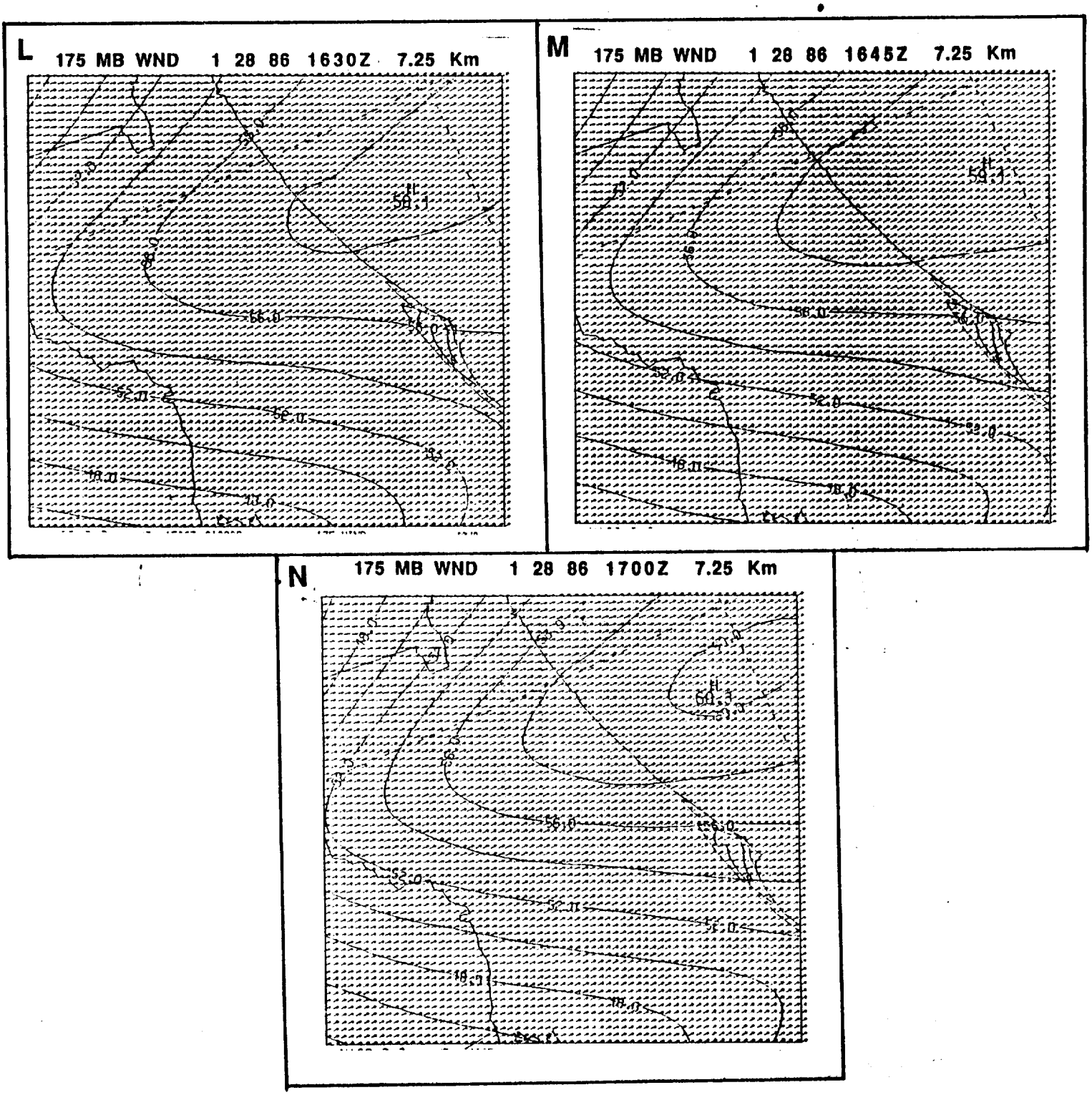

FIGURE 6 continued

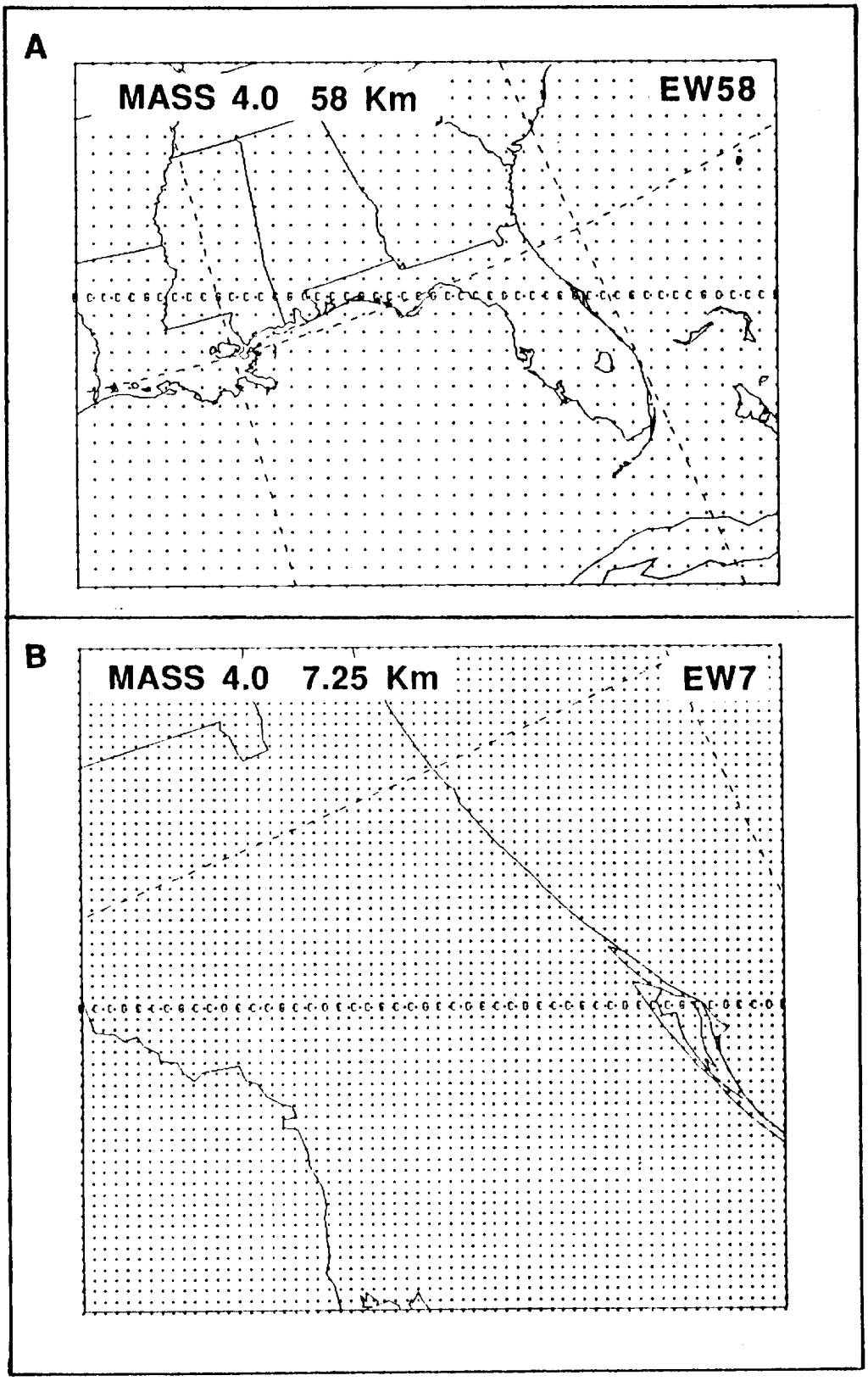

FIGURE 7

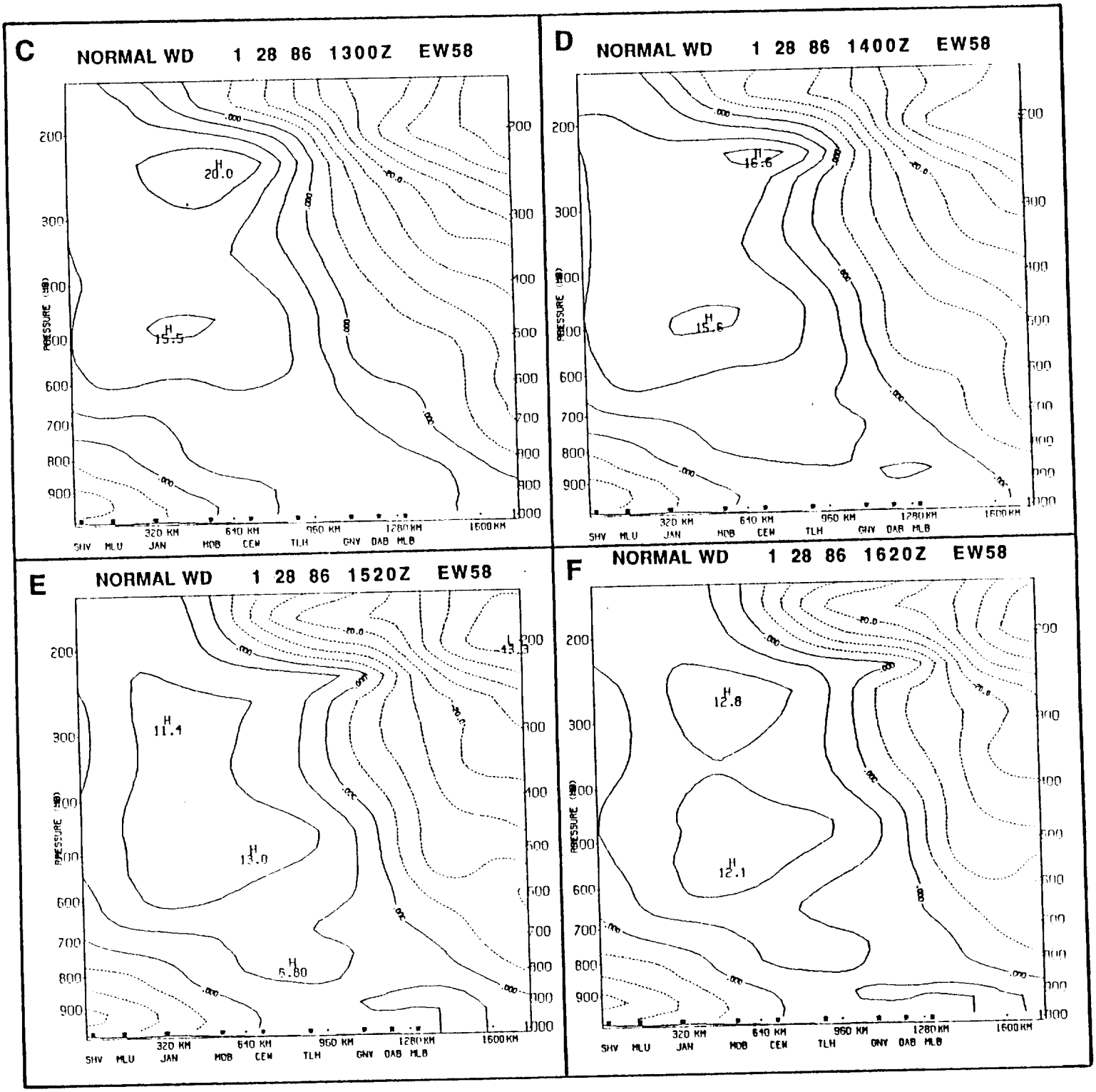

FIGURE 7 continued

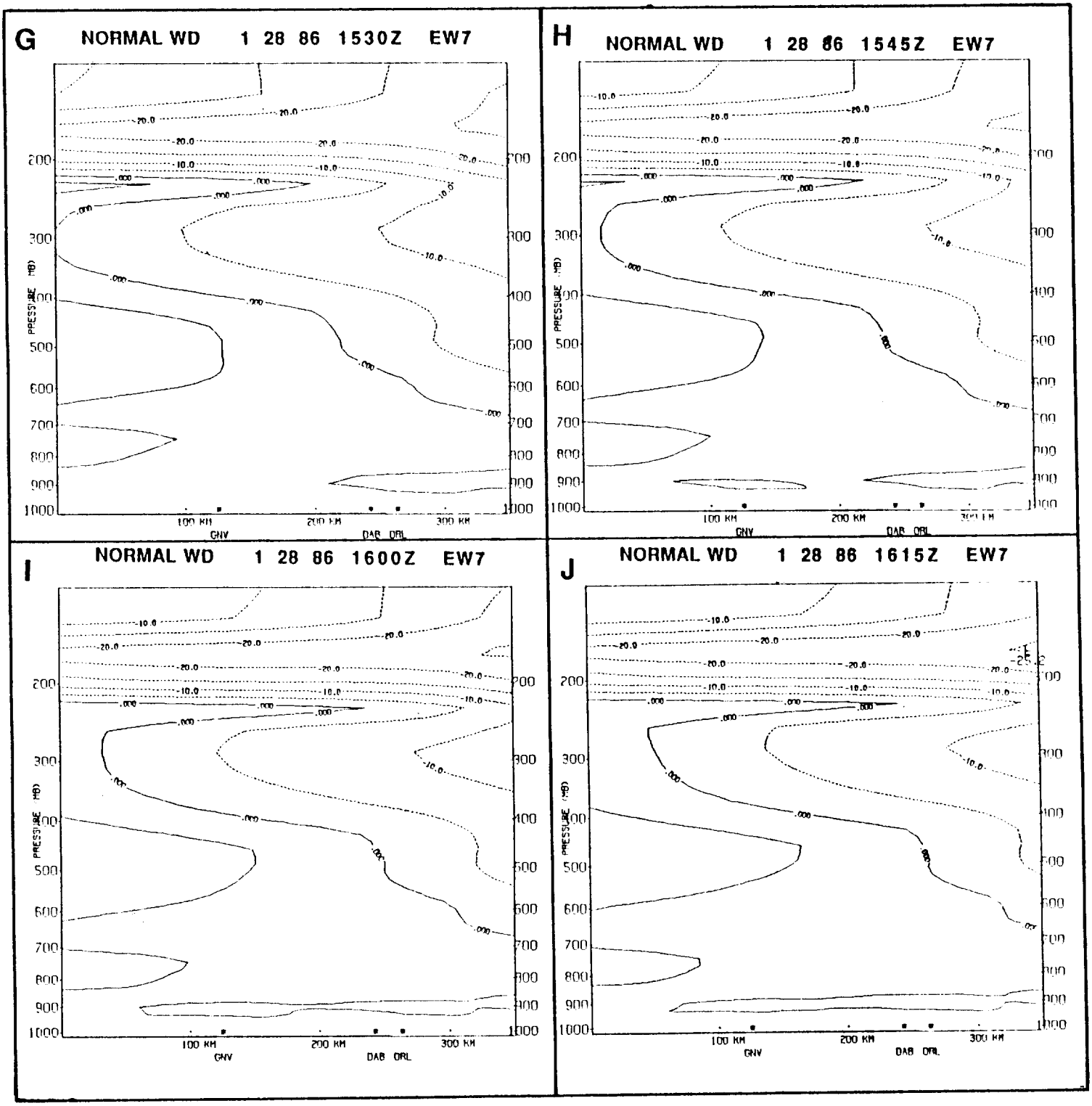

FIGURE 7 continued

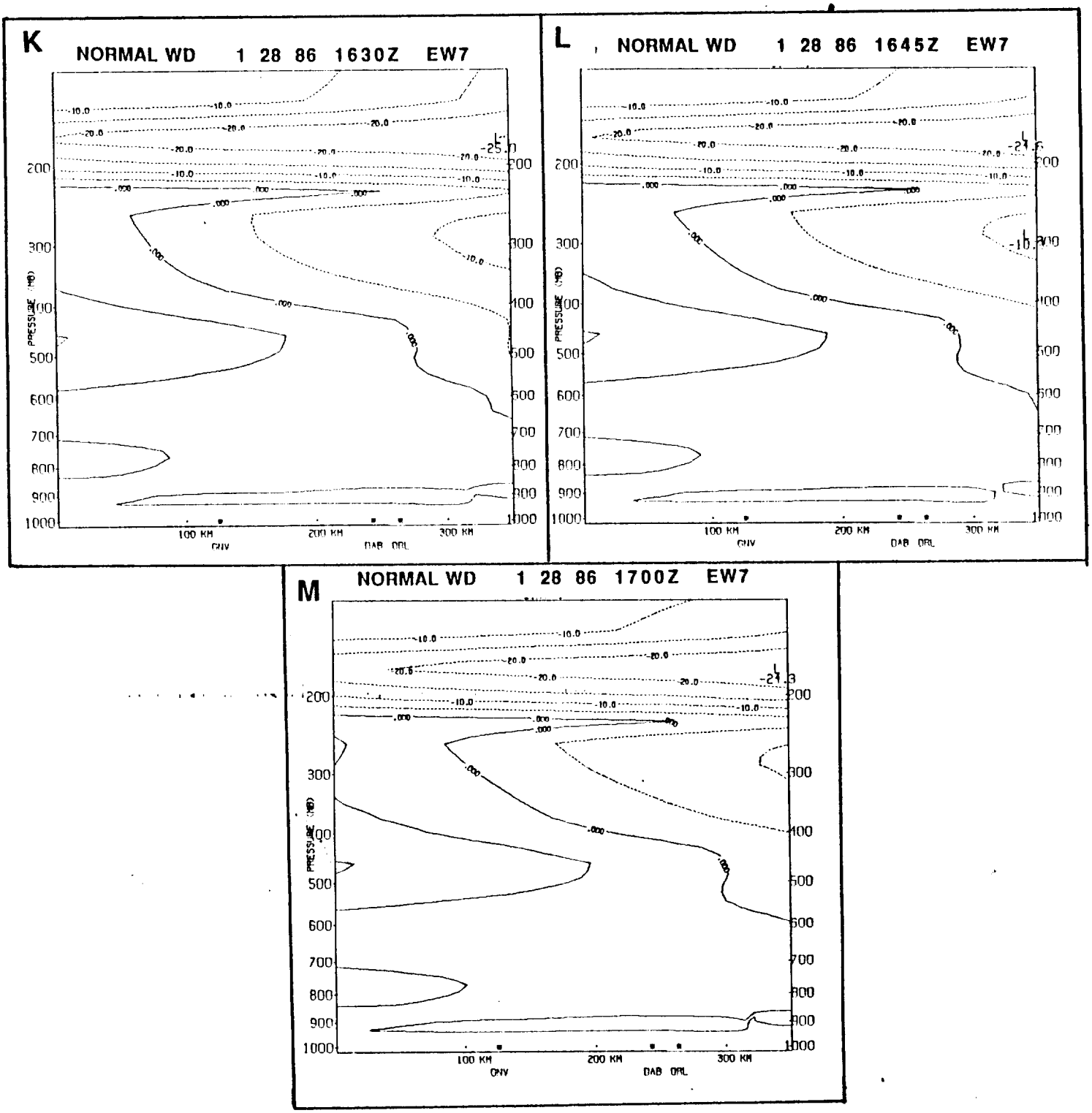

FIGURE 7 continued

MASS 4.0 58 Km BACKWARD TRAJECTORIES

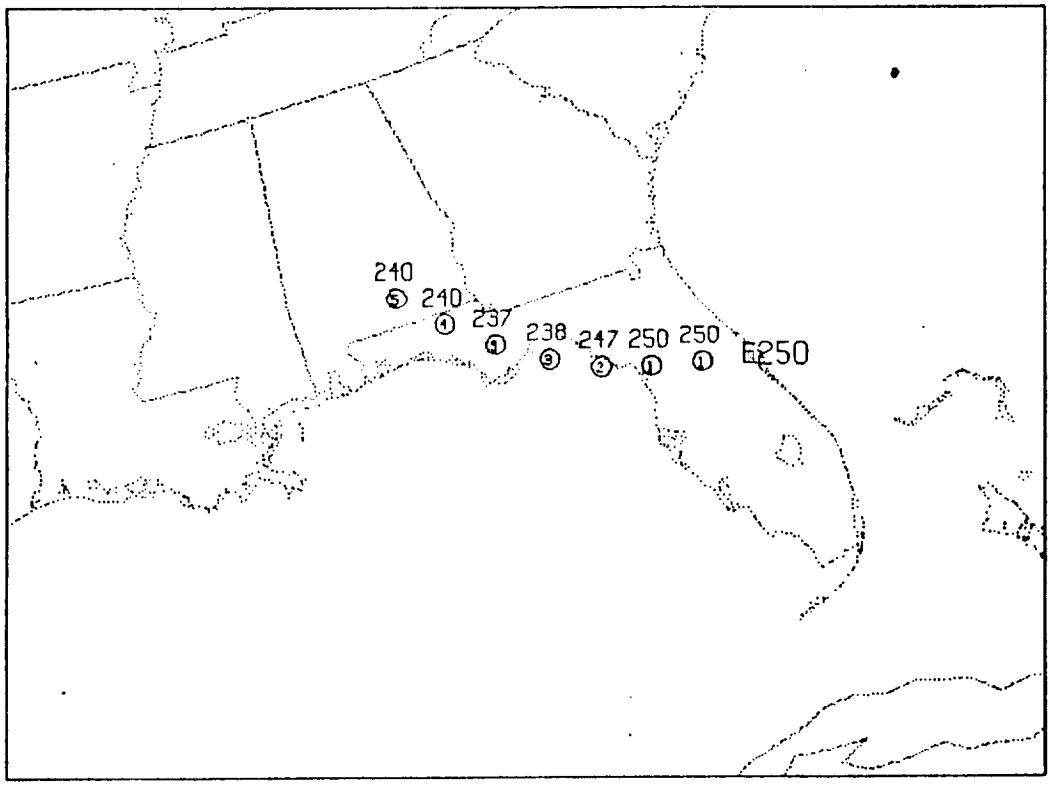

A

DATA FOR BACKWARD TRAJECTORY NUMBER: 6 ZERO HOUR = 1640 1 28 86

TIME (HRS)	PRESSURE (MB)	TEMPERATURE (K)	THETA (K)	MIXING RATIO (G/KG)	RH (%)	U-COMP (M/S)	V-COMP (M/S)	TOTAL WIND (M/S)	SIGDOT (1/S)
1640	250.	219.5	326.4	.0	17.	34.9	7.7	35.7	.2486E-05
1600	250.	219.5	326.2	.0	17.	34.5	4.6	34.8	-.2037E-06
1520	250.	219.5	326.3	.0	17.	34.0	2.0	34.1	.3667E-07
1440	247.	218.7	326.5	.0	18.	34.8	-2.1	34.9	.3449E-05
1400	238.	215.9	325.4	.0	26.	36.4	-7.9	37.2	.3156E-05
1320	237.	215.7	325.5	.0	26.	36.0	-12.2	38.0	-.9174E-06
1240	240.	216.8	326.2	.0	23.	34.3	-15.9	37.8	-.1653E-05
1200	240.	217.0	326.4	.0	22.	33.9	-20.1	39.4	.5582E-06

FIGURE 8

MASS 4.0 58 Km BACKWARD TRAJECTORIES

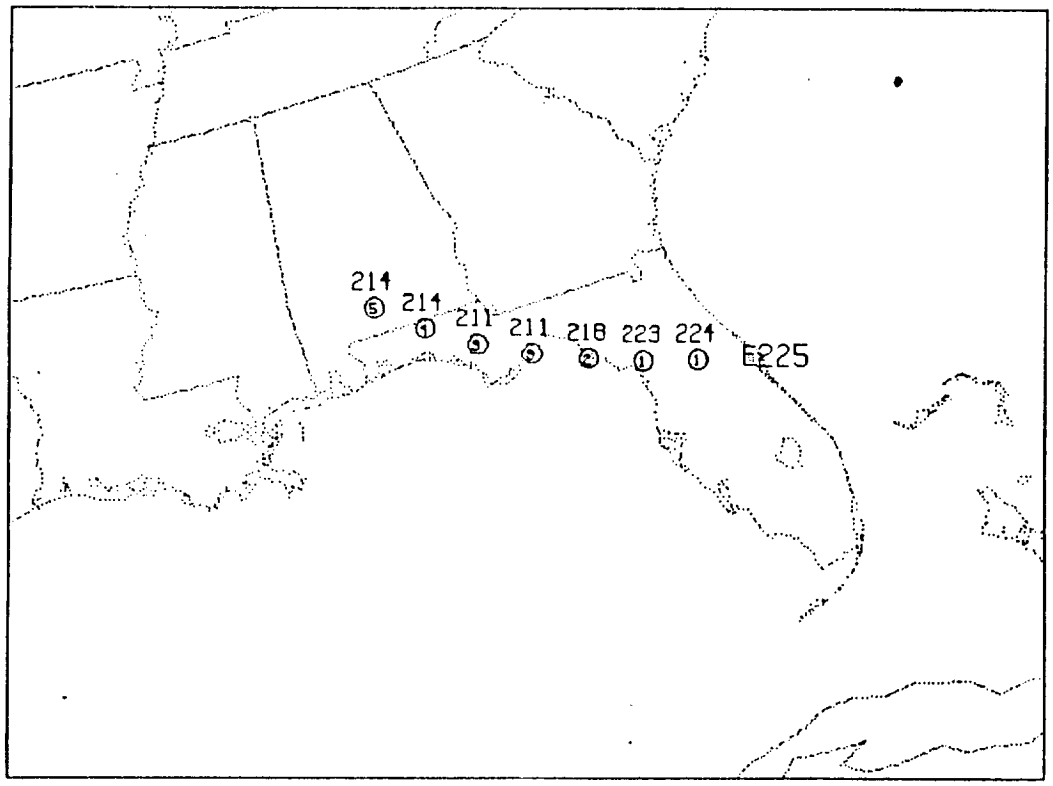

B

DATA FOR BACKWARD TRAJECTORY NUMBER: 7 ZERO HOUR = 1640 1 28 86

TIME (HRS)	PRESSURE (MB)	TEMPERATURE (K)	THETA (K)	MIXING RATIO (G/KG)	RH (%)	U-COMP (M/S)	V-COMP (M/S)	TOTAL WIND (M/S)	SIGDOT (1/S)
1640	225.	217.9	333.9	.0	18.	37.7	4.9	38.0	.8360E-06
1600	224.	217.6	334.0	.0	19.	37.7	2.5	37.8	.3783E-06
1520	223.	217.3	334.0	.0	20.	37.5	-0.2	37.5	.6649E-06
1440	218.	216.2	334.3	.0	22.	38.3	-2.7	38.4	.3574E-05
1400	211.	214.2	334.4	.0	29.	38.3	-4.4	38.6	.2020E-05
1320	211.	214.4	334.4	.0	28.	37.0	-8.1	37.9	-.1031E-05
1240	214.	214.9	334.0	.0	26.	35.6	-12.4	37.7	-.1669E-05
1200	214.	214.6	333.5	.0	27.	35.3	-16.5	39.0	.7883E-06

FIGURE 8 continued

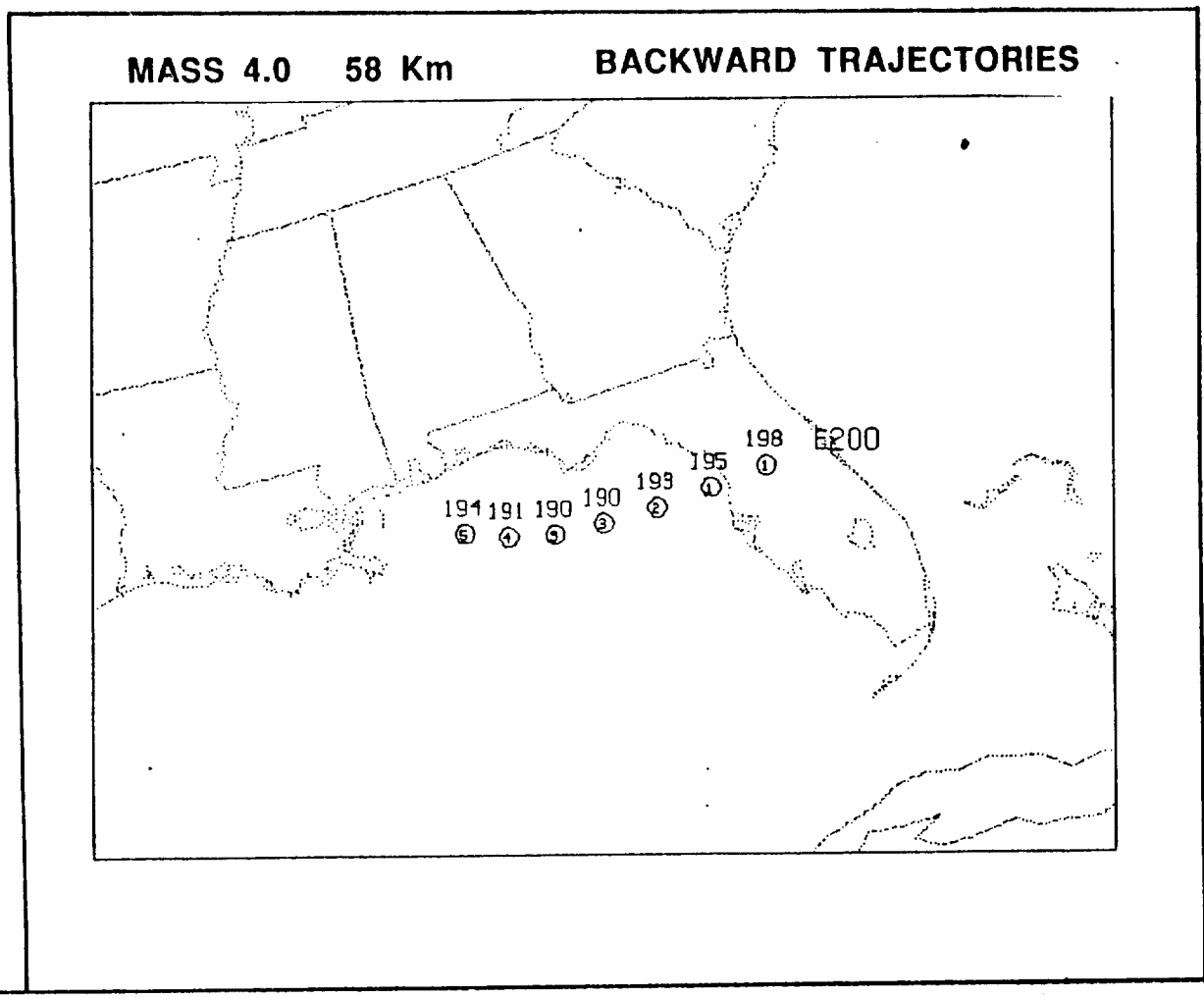

C

DATA FOR BACKWARD TRAJECTORY NUMBER: 8 ZERO HOUR = 1640 1 28 86

TIME (HRS)	PRESSURE (MB)	TEMPERATURE (K)	THETA (K)	MIXING RATIO (G/KG)	RH (%)	U-COMP (M/S)	V-COMP (M/S)	TOTAL WIND (M/S)	SIGDOT (1/S)
1640	200.	220.5	349.5	.0	12.	41.1	19.8	45.6	.1016E-05
1600	198.	219.6	349.2	.0	13.	39.6	16.5	42.9	.1162E-05
1520	195.	218.8	349.2	.0	14.	37.4	14.4	40.1	.9745E-06
1440	193.	217.9	349.0	.0	15.	37.1	12.5	39.1	.1139E-05
1400	190.	217.1	348.8	.0	18.	35.8	9.5	37.0	.1217E-05
1320	190.	216.5	348.3	.0	19.	32.9	5.0	33.3	-.3446E-06
1240	191.	217.2	348.5	.0	17.	30.8	-0.8	30.8	-.1372E-05
1200	194.	218.5	349.0	.0	15.	30.9	-4.1	31.2	-.1080E-05

FIGURE 8 continued

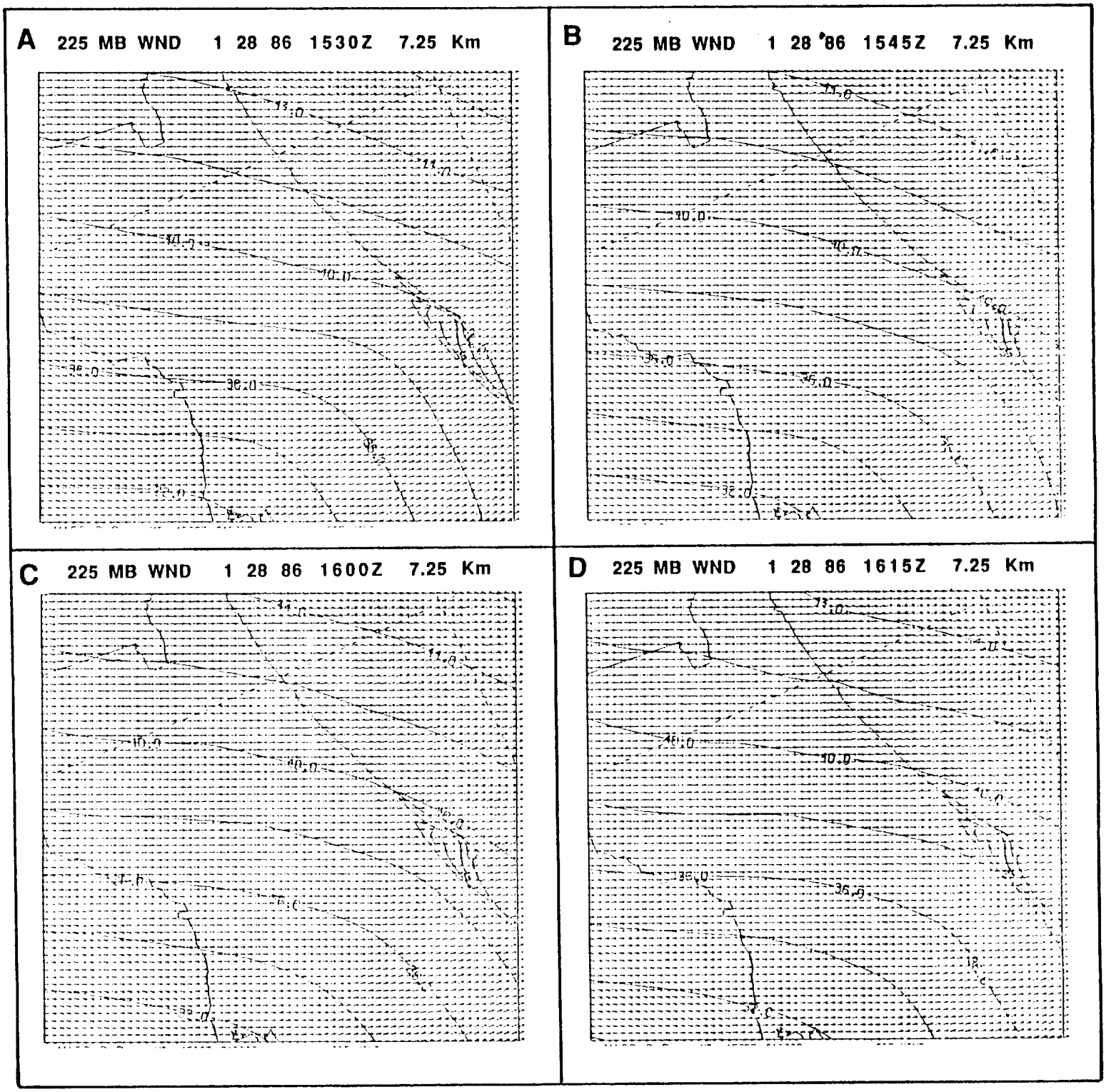

FIGURE 9

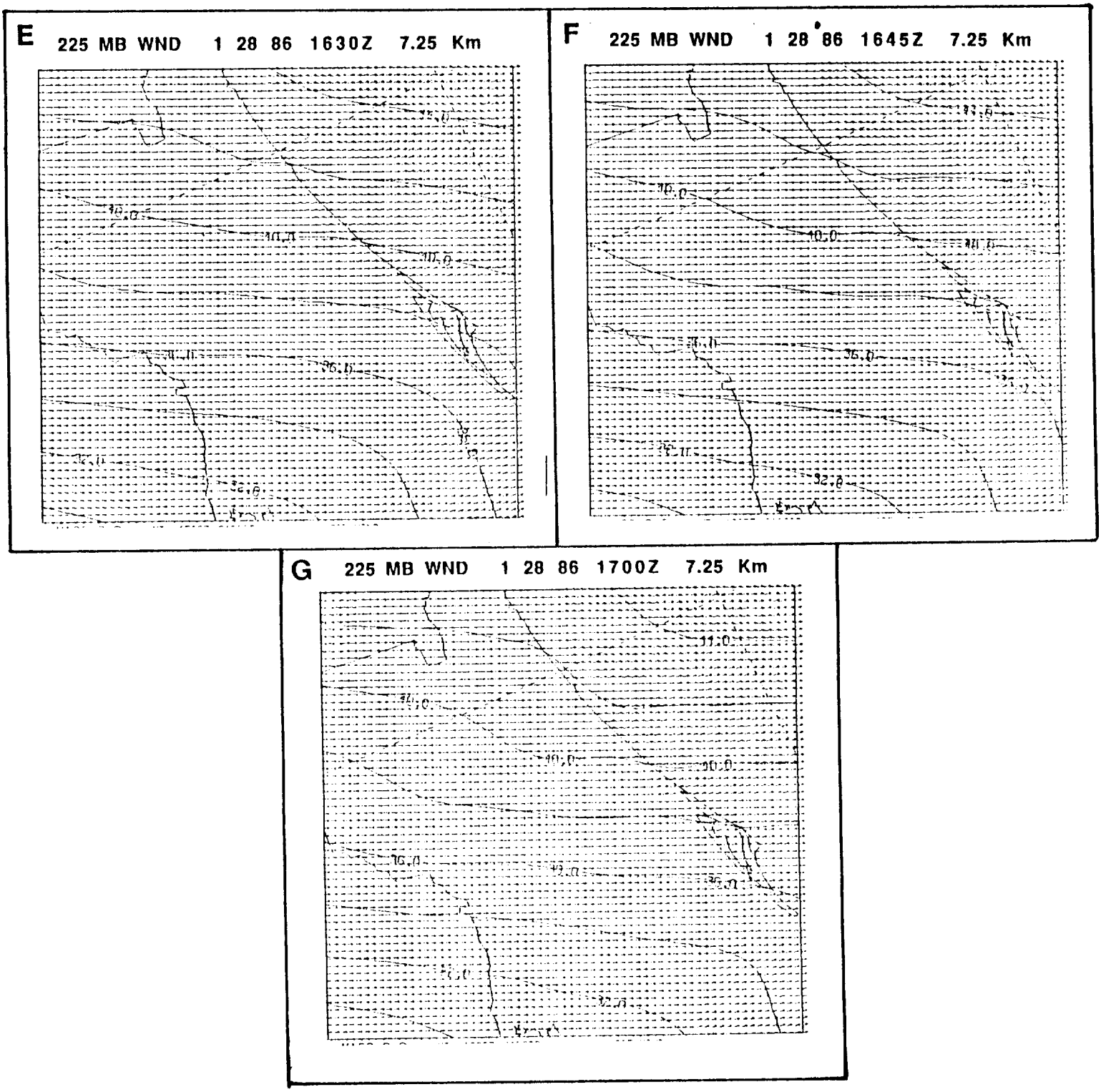

FIGURE 9 continued

MASS 4.0 7.25 Km BACKWARD TRAJECTORIES

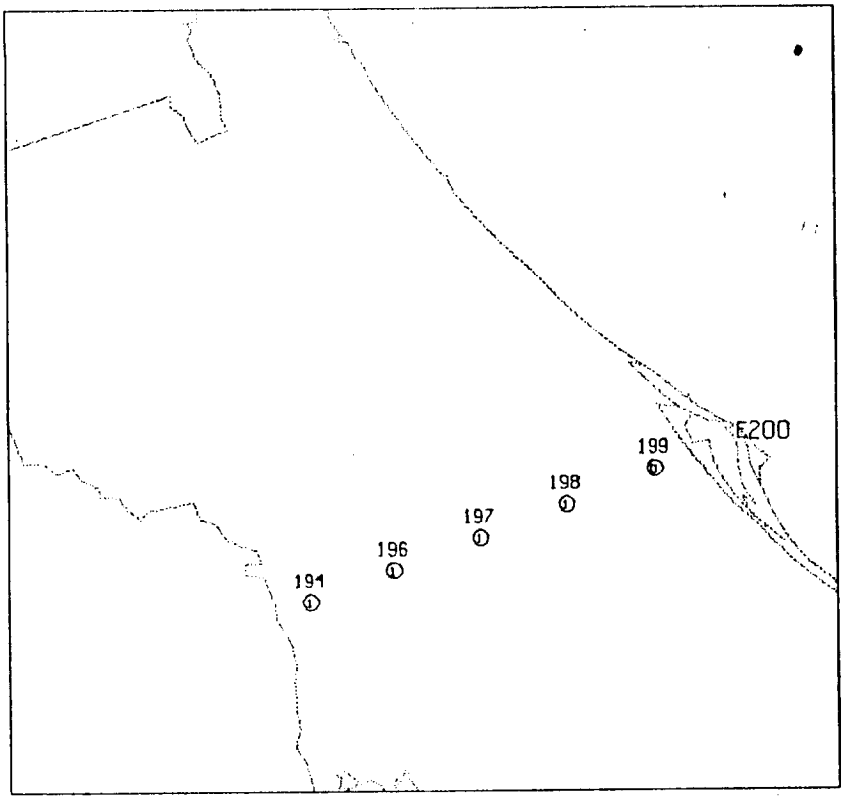

A

DATA FOR BACKWARD TRAJECTORY NUMBER: 8 ZERO HOUR = 1645 1 28 86

TIME (HRS)	PRESSURE (MB)	TEMPERATURE (K)	THETA (K)	MIXING RATIO (G/KG)	RH (%)	U-COMP (M/S)	V-COMP (M/S)	TOTAL WIND (M/S)	SIGDOT (1/S)
1645	200.	220.3	349.1	.0	12.	41.3	17.7	44.9	.1936E-05
1630	199.	219.8	349.0	.0	13.	41.0	17.1	44.4	.6978E-06
1615	198.	219.7	349.1	.0	13.	40.2	16.1	43.3	.9151E-06
1600	197.	219.3	349.1	.0	14.	39.6	15.2	42.4	.1274E-05
1545	196.	218.9	349.0	.0	14.	38.7	14.8	41.4	.1687E-05
1530	194.	218.5	349.0	.0	15.	38.1	14.6	40.8	.1359E-05

FIGURE 10

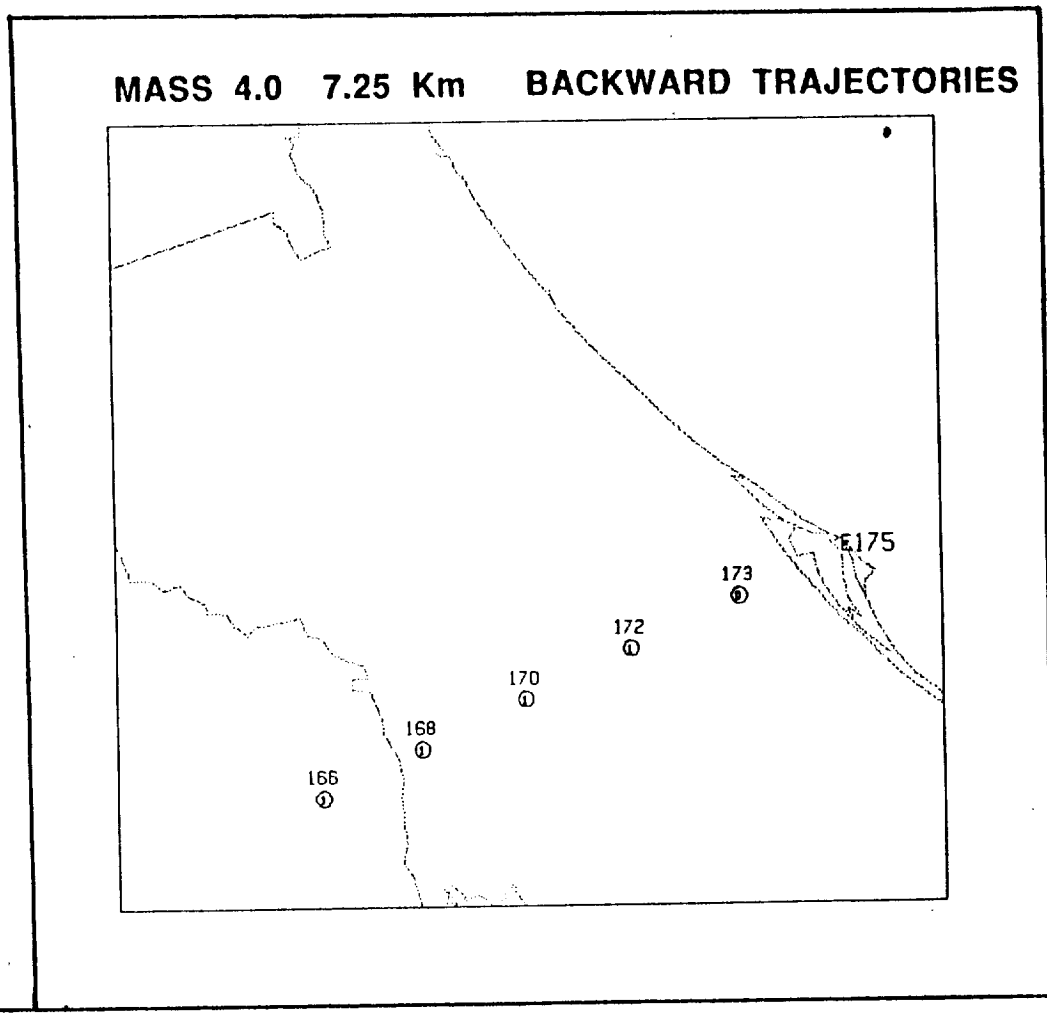

B

DATA FOR BACKWARD TRAJECTORY NUMBER: 9 ZERO HOUR = 1645 1 28 86

TIME (HRS)	PRESSURE (MB)	TEMPERATURE (K)	THETA (K)	MIXING RATIO (G/KG)	RH (%)	U-COMP (M/S)	V-COMP (M/S)	TOTAL WIND (M/S)	SIGDOT (1/S)
1645	175.	218.0	358.9	.0	14.	50.6	24.2	56.1	.2175E-05
1630	173.	217.5	358.9	.0	15.	50.4	24.3	56.0	.8848E-06
1615	172.	217.2	359.1	.0	16.	49.6	24.0	55.1	.2332E-05
1600	170.	216.5	359.0	.0	17.	48.2	23.0	53.4	.2427E-05
1545	168.	215.7	359.0	.0	19.	46.5	22.7	51.7	.2425E-05
1530	166.	215.0	359.1	.0	20.	45.1	22.3	50.3	.2219E-05

FIGURE 10 continued

MASS 4.0 7.25 Km BACKWARD TRAJECTORIES

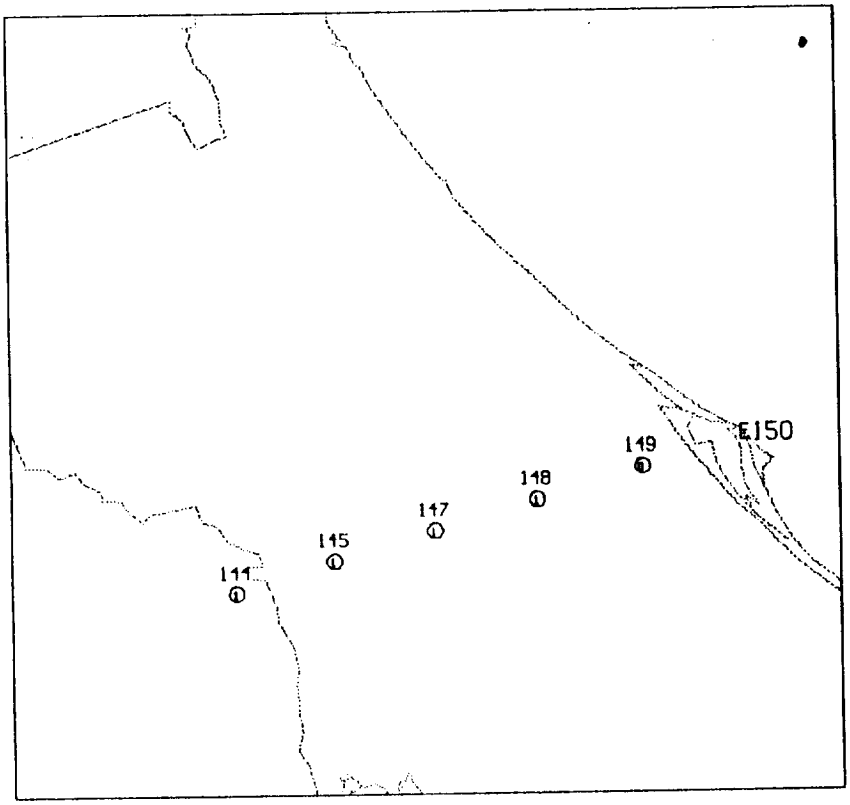

C

DATA FOR BACKWARD TRAJECTORY NUMBER: 10 ZERO HOUR = 1645 1 28 86

TIME (HRS)	PRESSURE (MB)	TEMPERATURE (K)	THETA (K)	MIXING RATIO (G/KG)	RH (%)	U-COMP (M/S)	V-COMP (M/S)	TOTAL WIND (M/S)	SIGDOT (1/S)
1645	150.	214.6	369.2	.0	19.	48.1	15.9	50.7	.1595E-05
1630	149.	214.1	369.2	.0	21.	48.1	15.5	50.5	.7580E-06
1615	148.	213.8	369.2	.0	21.	47.4	14.7	49.6	.1493E-05
1600	147.	213.3	369.2	.0	23.	46.7	14.1	48.8	.1472E-05
1545	145.	212.7	369.3	.0	24.	45.6	14.3	47.8	.1672E-05
1530	144.	212.1	369.3	.0	26.	44.8	14.8	47.2	.1563E-05

FIGURE 10 continued

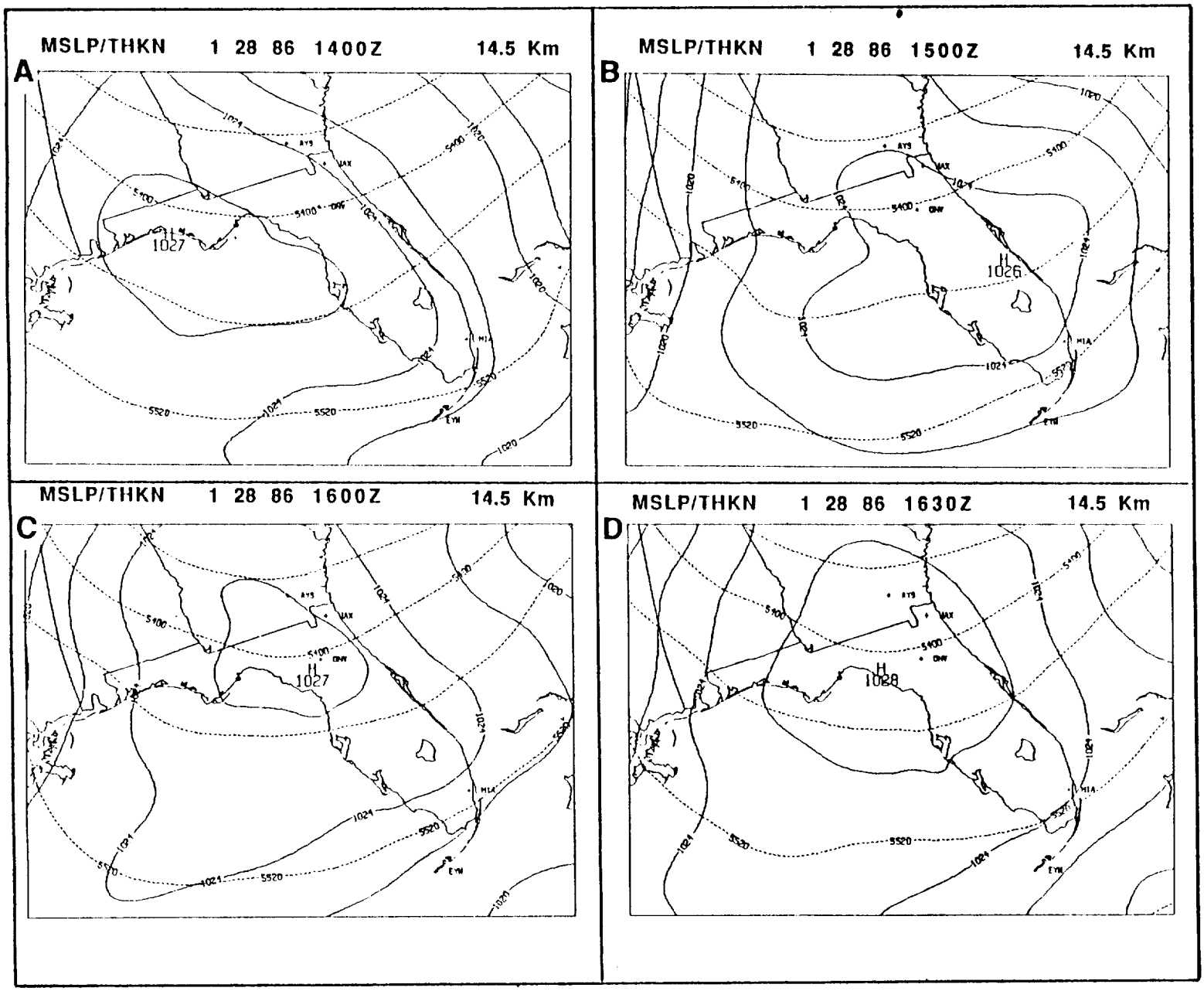
MSLP/THKN 1 28 86 1400Z 14.5 Km
A
1027
5400
5520
1024
1020
MSLP/THKN 1 28 86 1500Z 14.5 Km
B
1026
5400
5520
1024
1020
MSLP/THKN 1 28 86 1600Z 14.5 Km
C
1027
5400
5520
1024
1020
MSLP/THKN 1 28 86 1630Z 14.5 Km
D
1028
5400
5520
1024

FIGURE 11

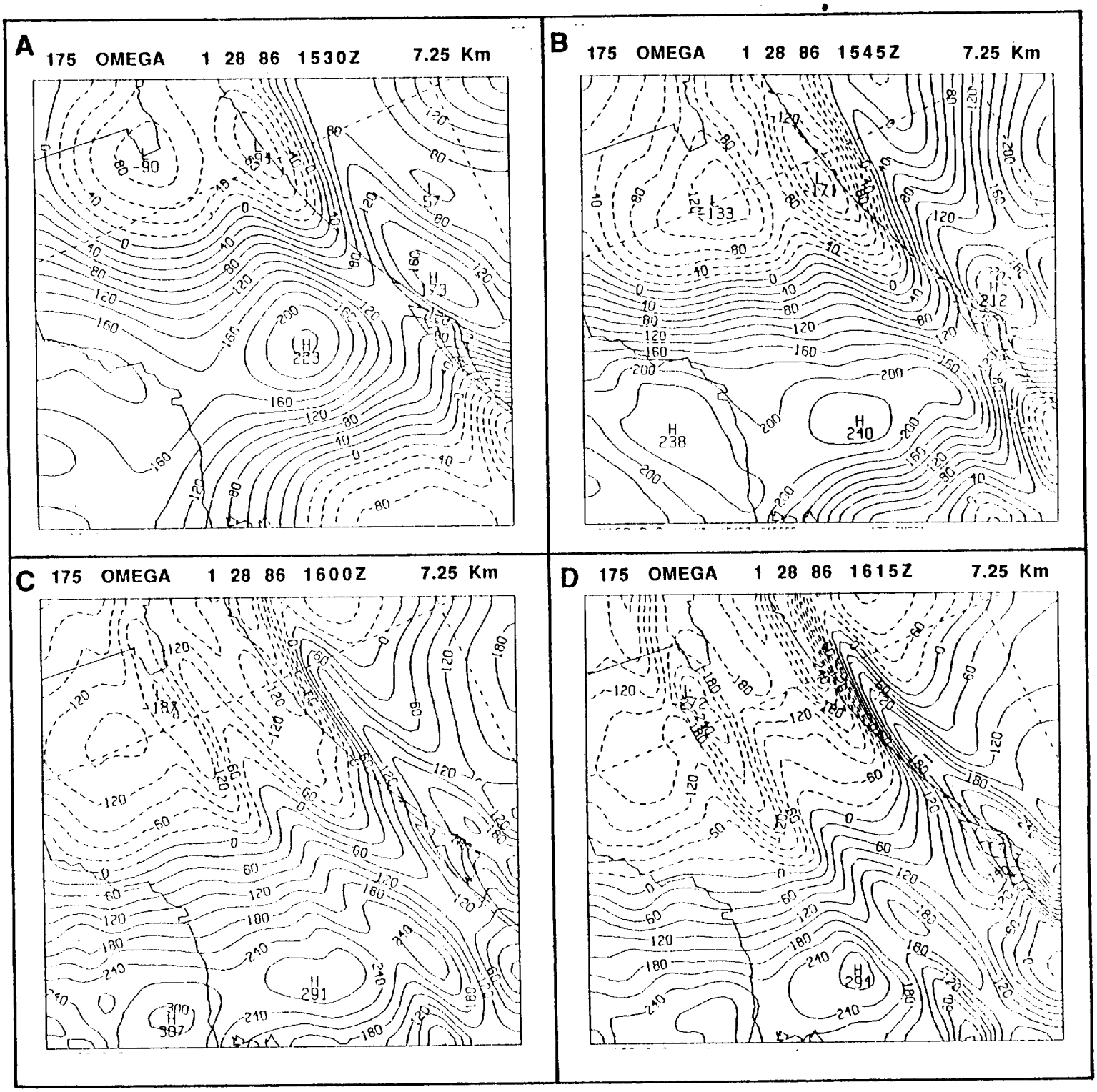
A
175 OMEGA 1 28 86 1530Z 7.25 Km
B
175 OMEGA 1 28 86 1545Z 7.25 Km
C
175 OMEGA 1 28 86 1600Z 7.25 Km
D
175 OMEGA 1 28 86 1615Z 7.25 Km

FIGURE 12

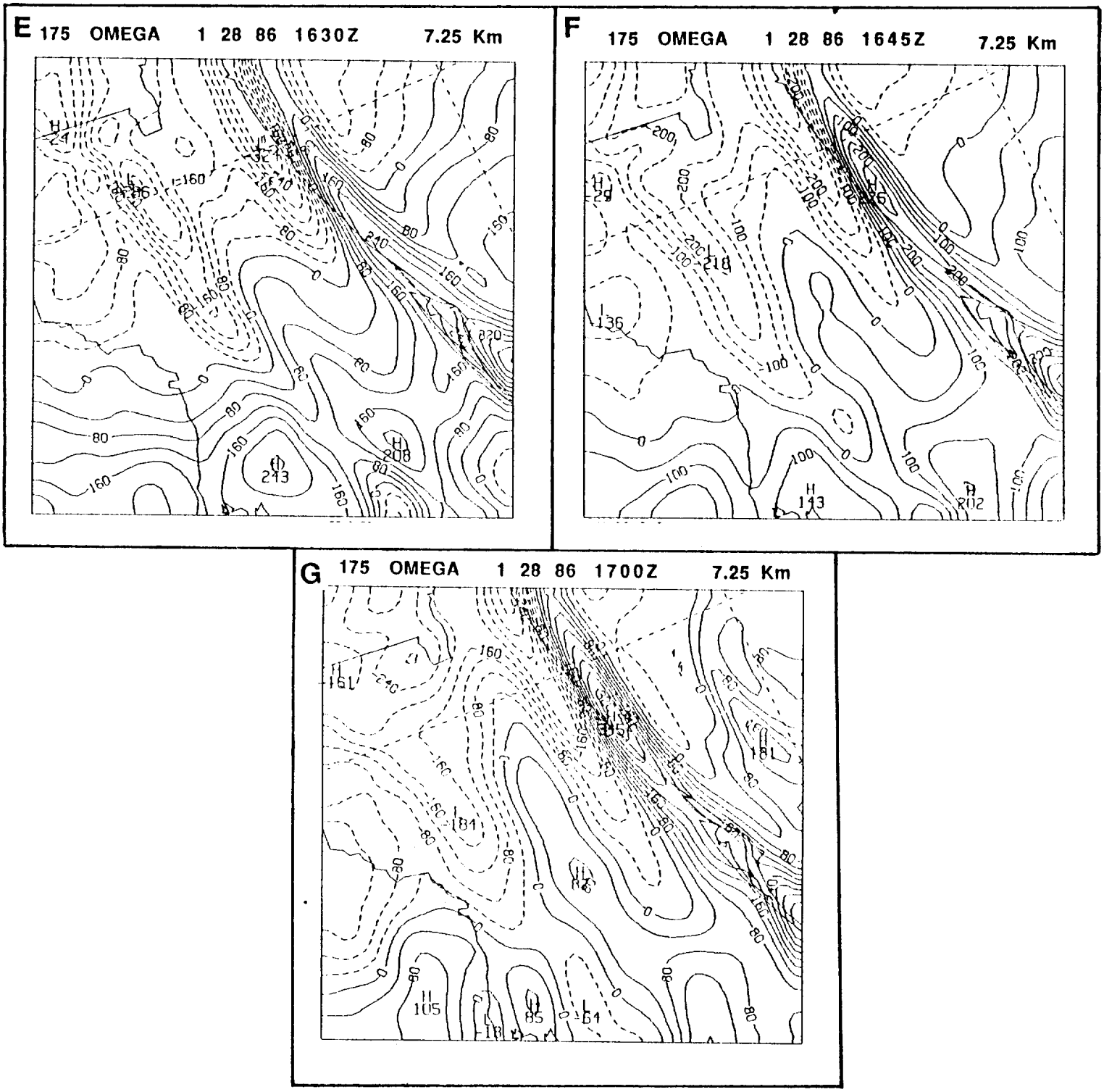

FIGURE 12 continued

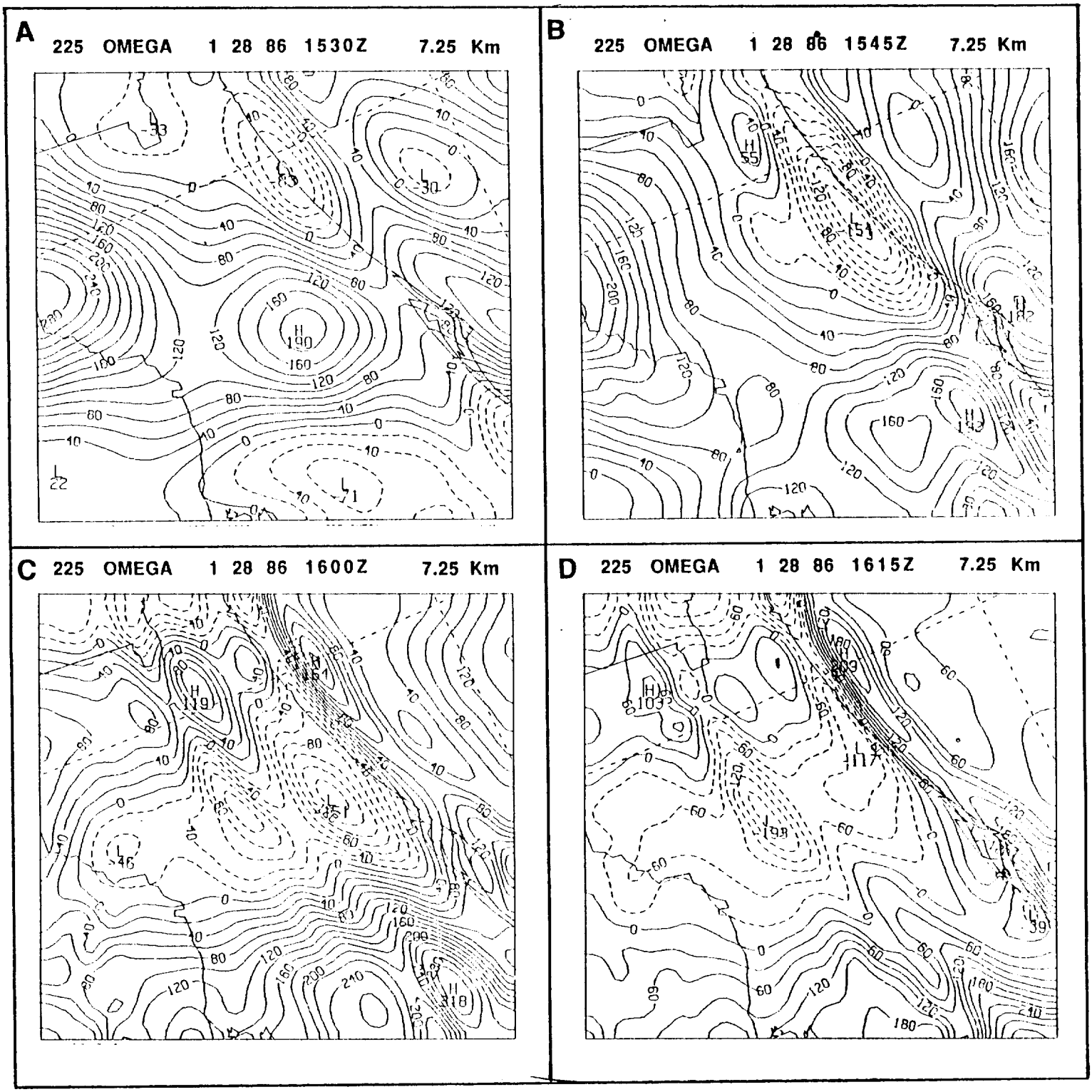
A
225 OMEGA 1 28 86 1530Z 7.25 Km
B
225 OMEGA 1 28 86 1545Z 7.25 Km
C
225 OMEGA 1 28 86 1600Z 7.25 Km
D
225 OMEGA 1 28 86 1615Z 7.25 Km

FIGURE 13

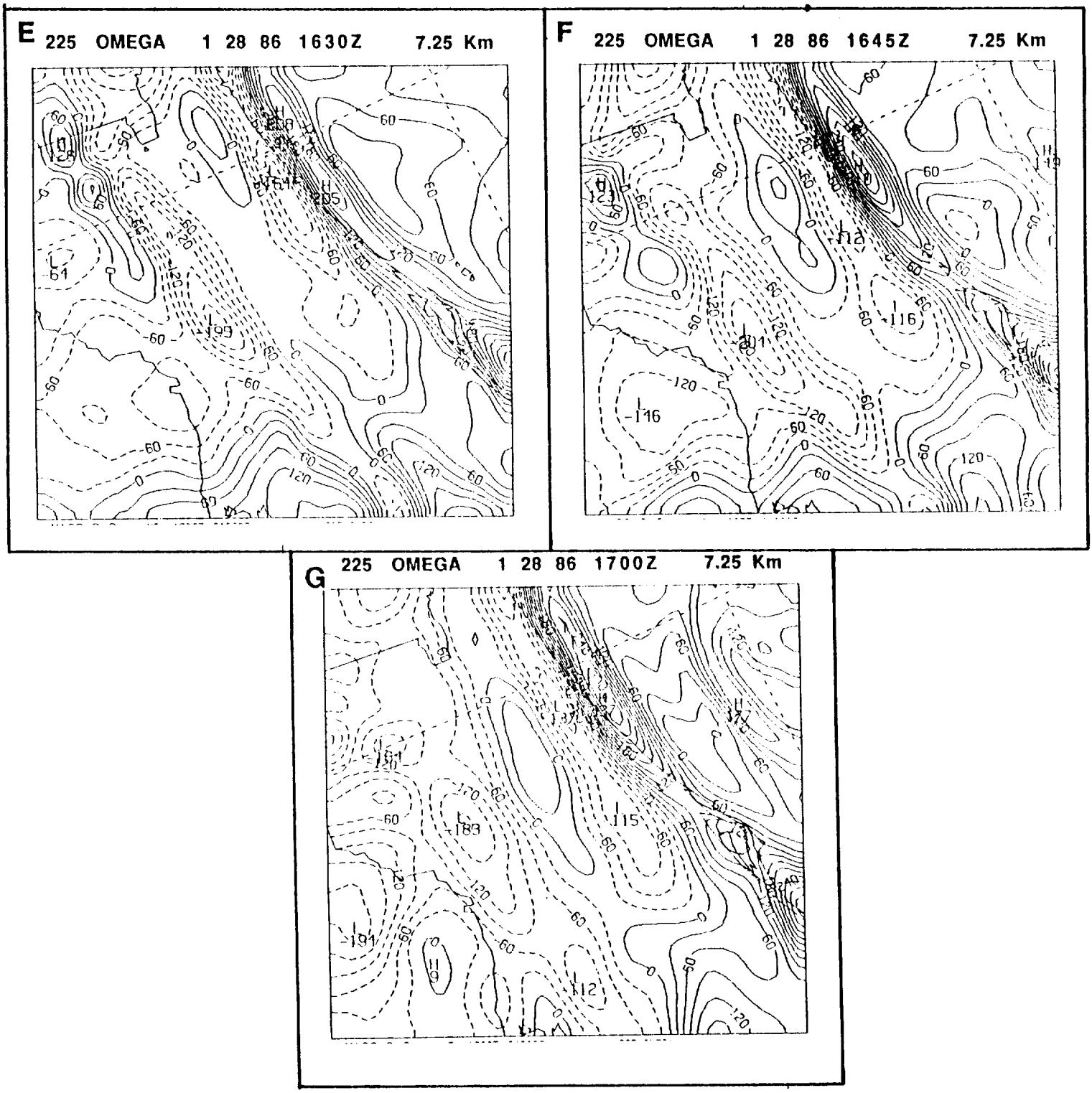

FIGURE 13 continued

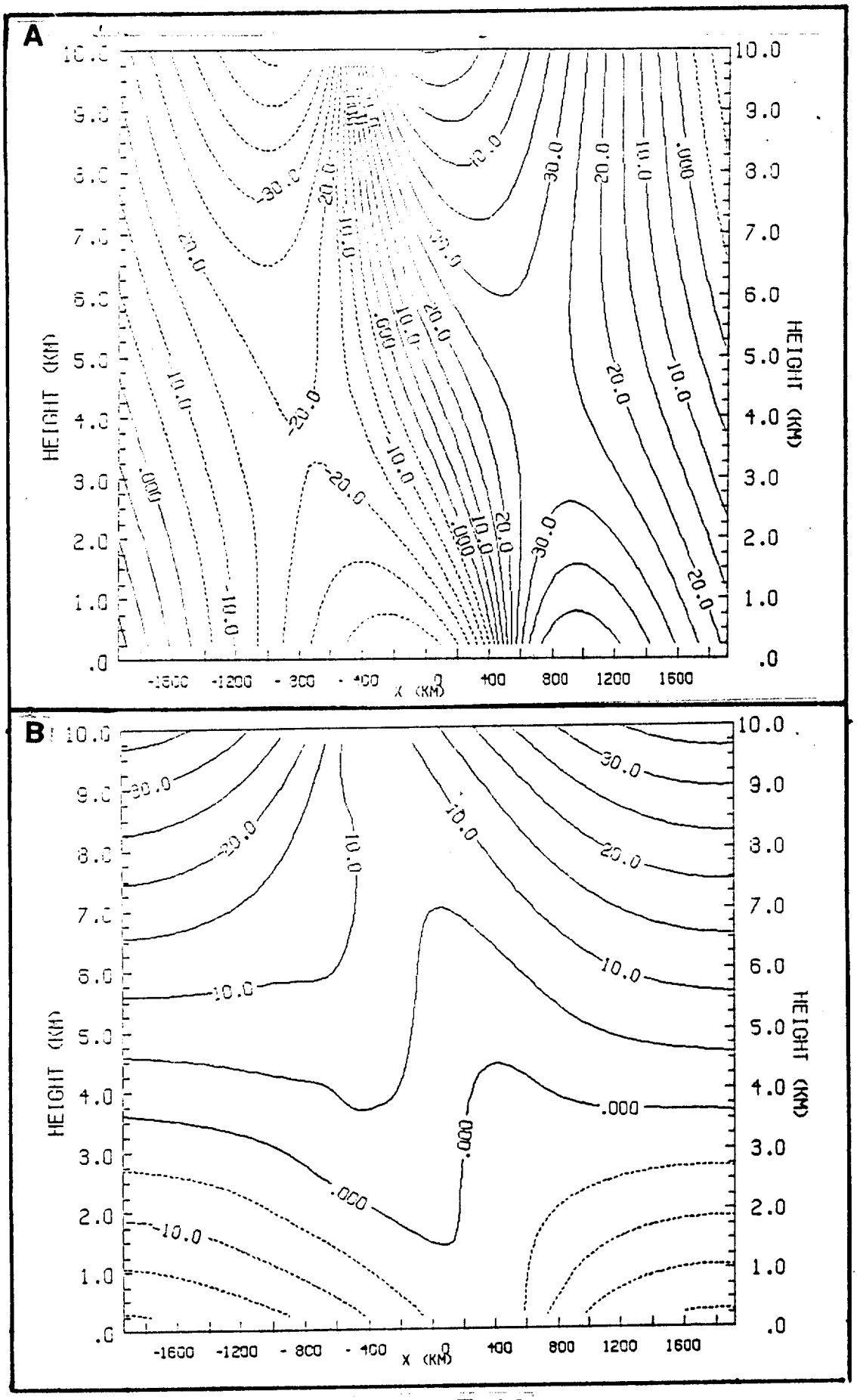

FIGURE 14

ORIGINAL PAGE IS
OF POOR QUALITY

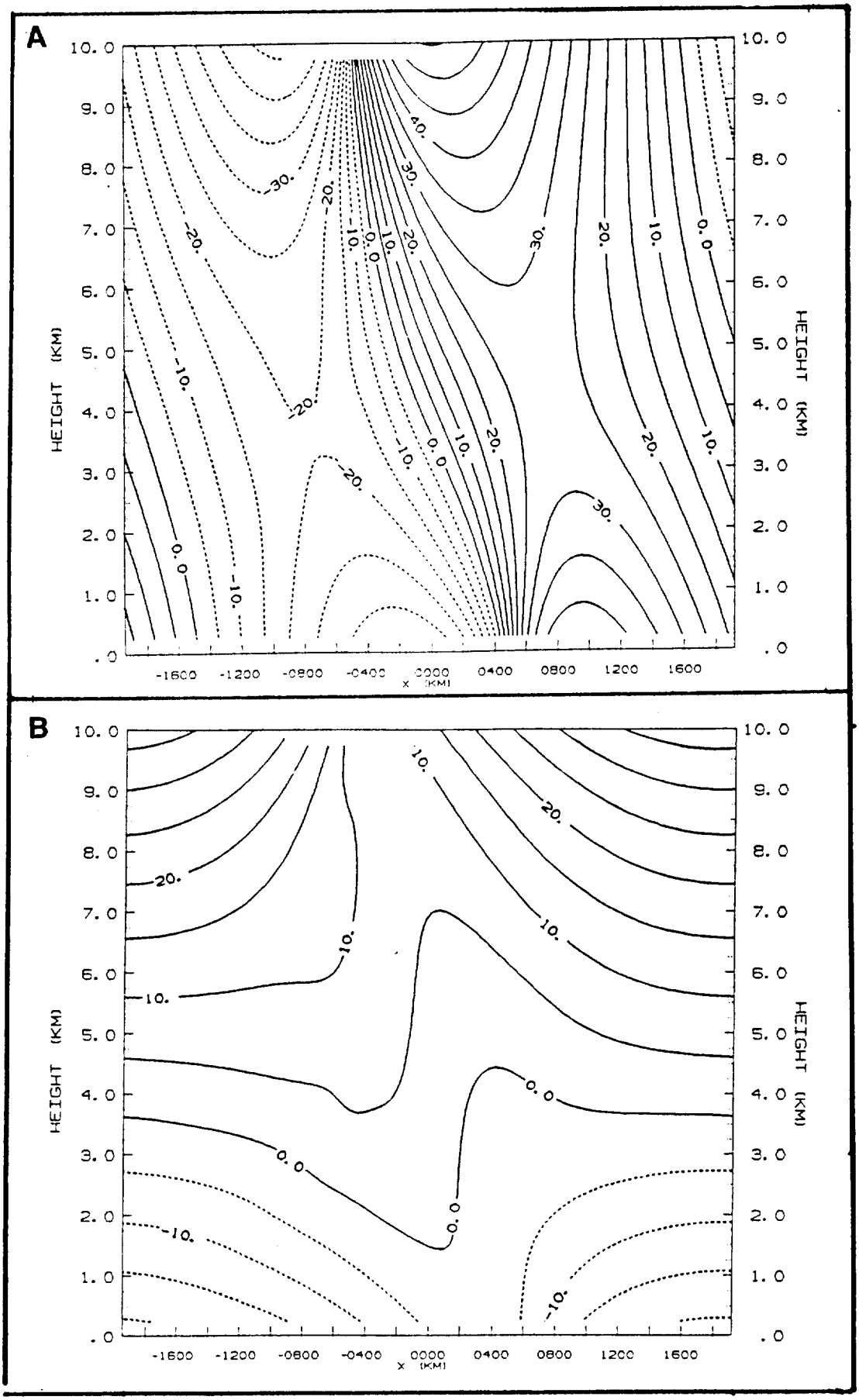
A
B
HEIGHT (KM)
HEIGHT (KM)
10.0
9.0
8.0
7.0
6.0
5.0
4.0
3.0
2.0
1.0
.0
-1600
-1200
-0800
-0400
0000
0400
0800
1200
1600
X (KM)
40.
30.
20.
10.
0.0
-10.
-20.
-30.

FIGURE 15

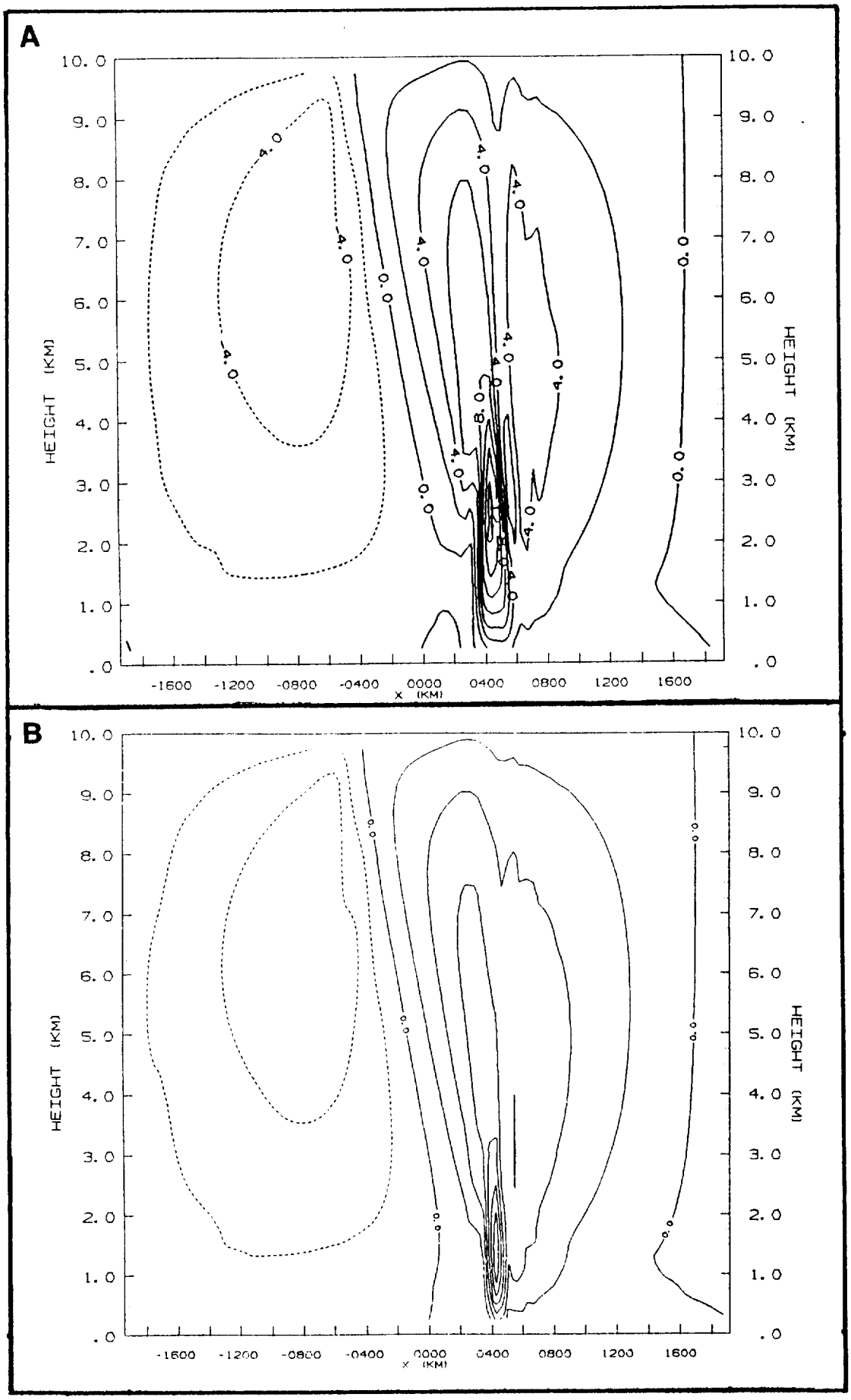
A
B
HEIGHT (KM)
X (KM)
10.0
9.0
8.0
7.0
6.0
5.0
4.0
3.0
2.0
1.0
.0
-1600
-1200
-0800
-0400
0000
0400
0800
1200
1600
4.0
0.0

FIGURE 16

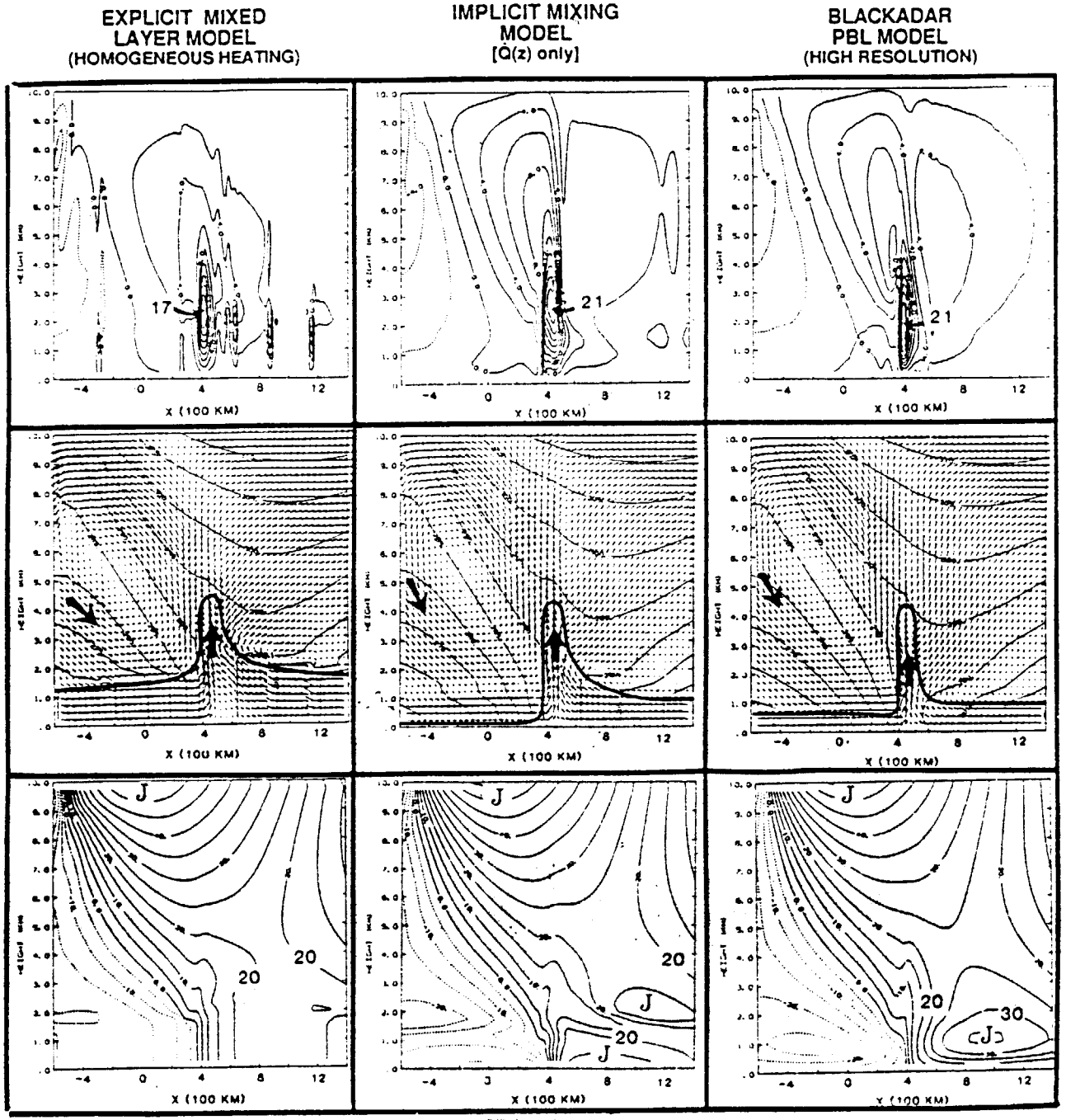

FIGURE 17

ORIGINAL PAGE IS
OF POOR QUALITY

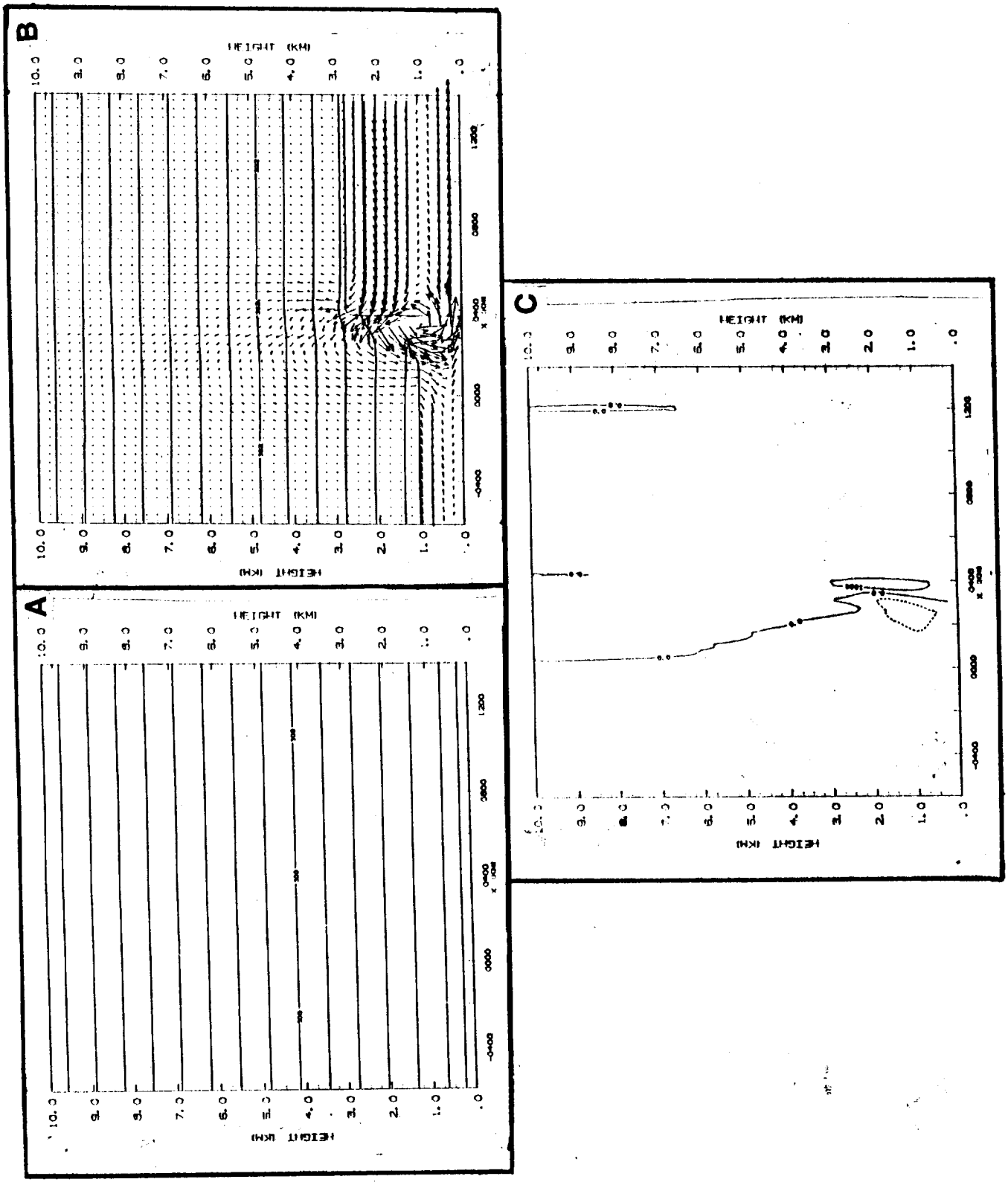

FIGURE 18

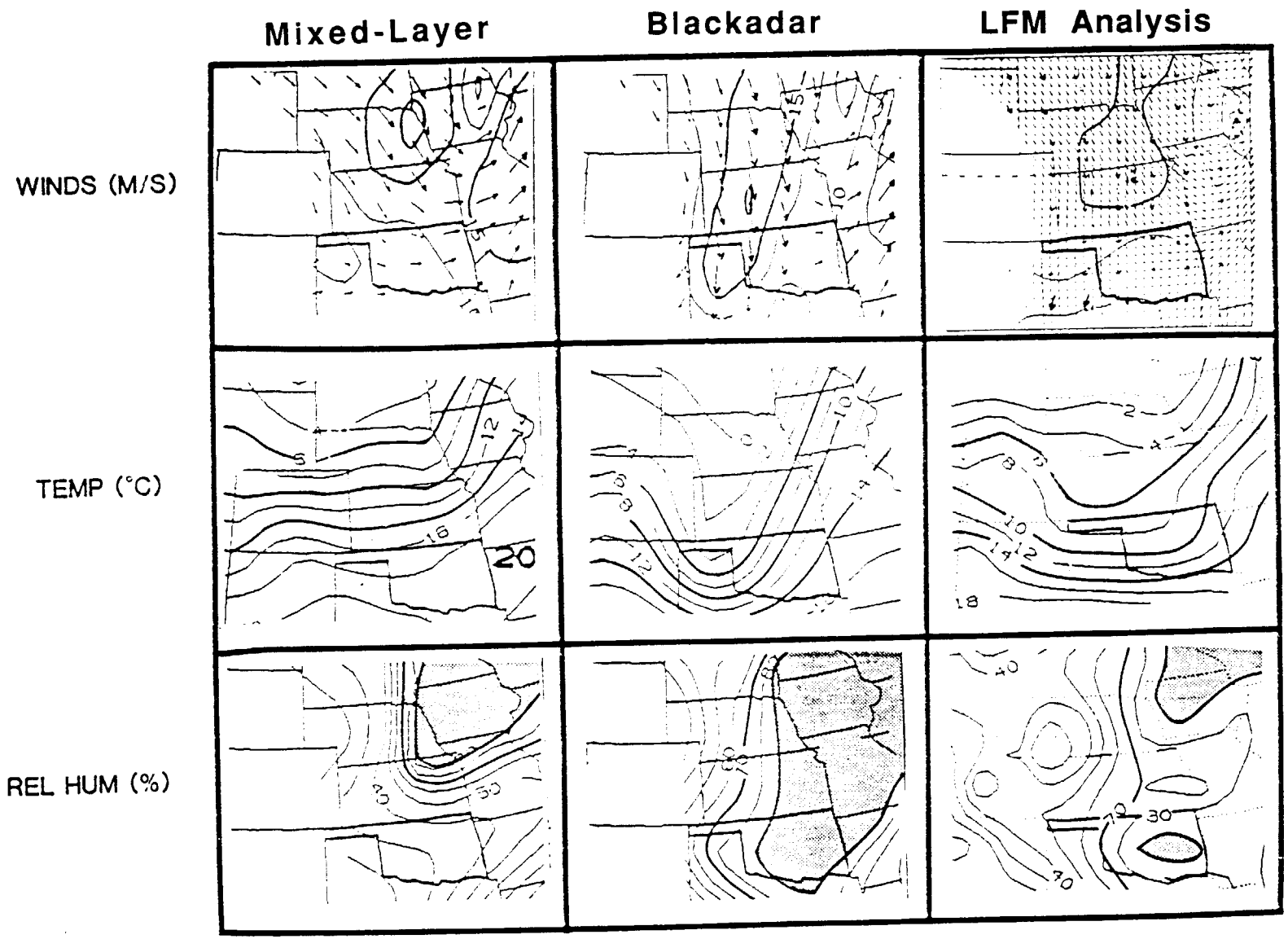
Mixed-Layer
Blackadar
LFM Analysis
WINDS (M/S)
TEMP (°C)
REL HUM (%)
20
18
30
40

FIGURE 19

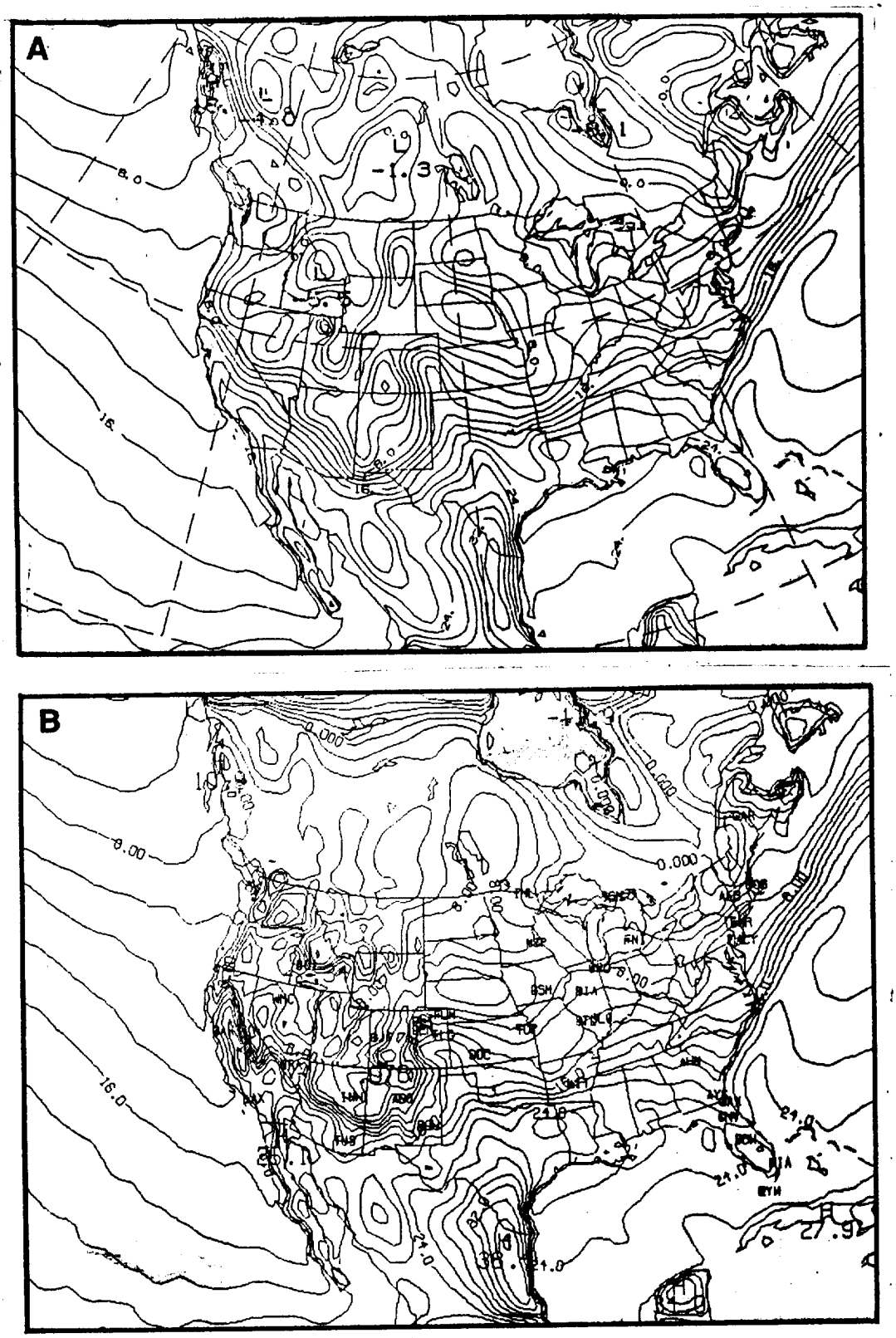

FIGURE 20

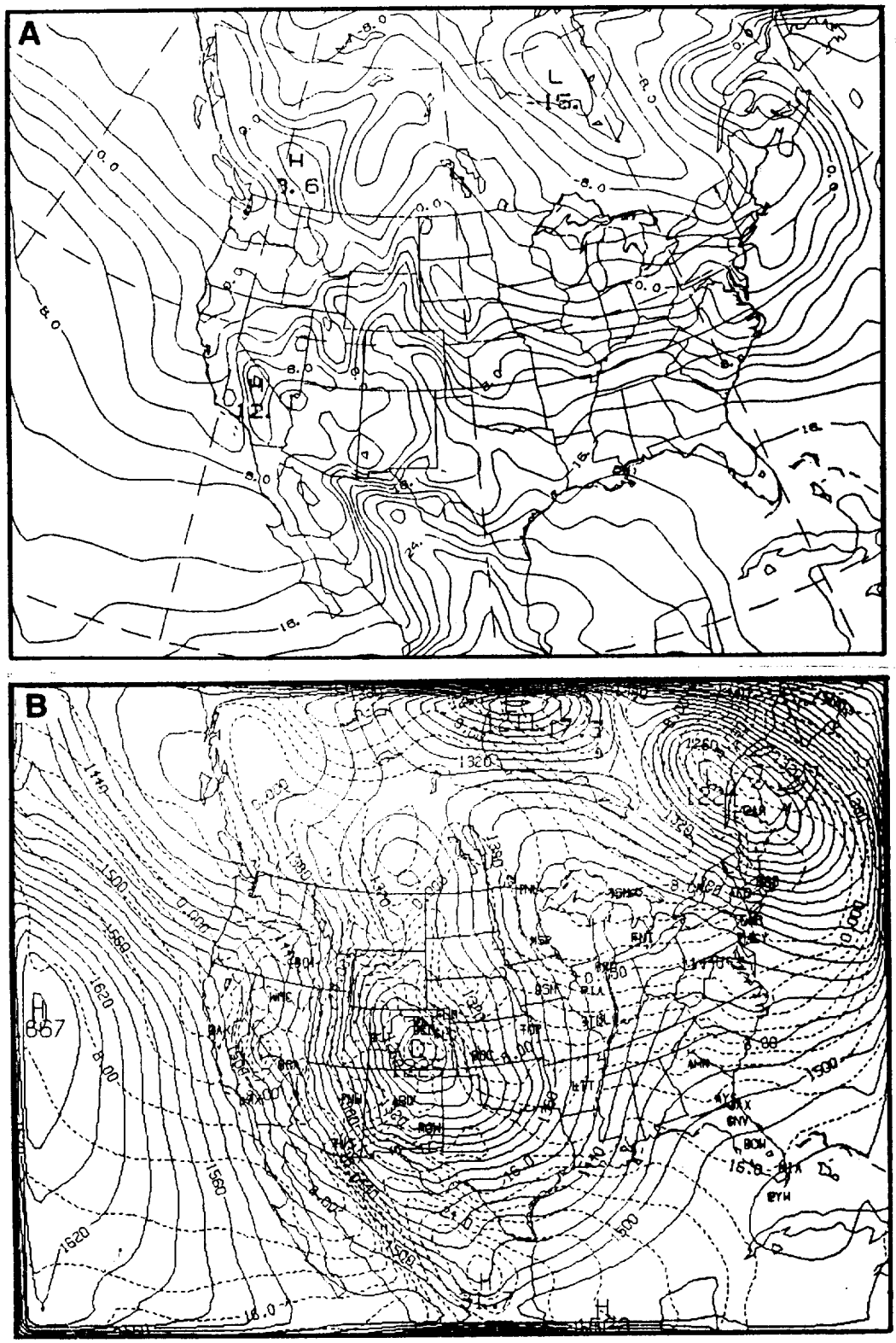

FIGURE 21

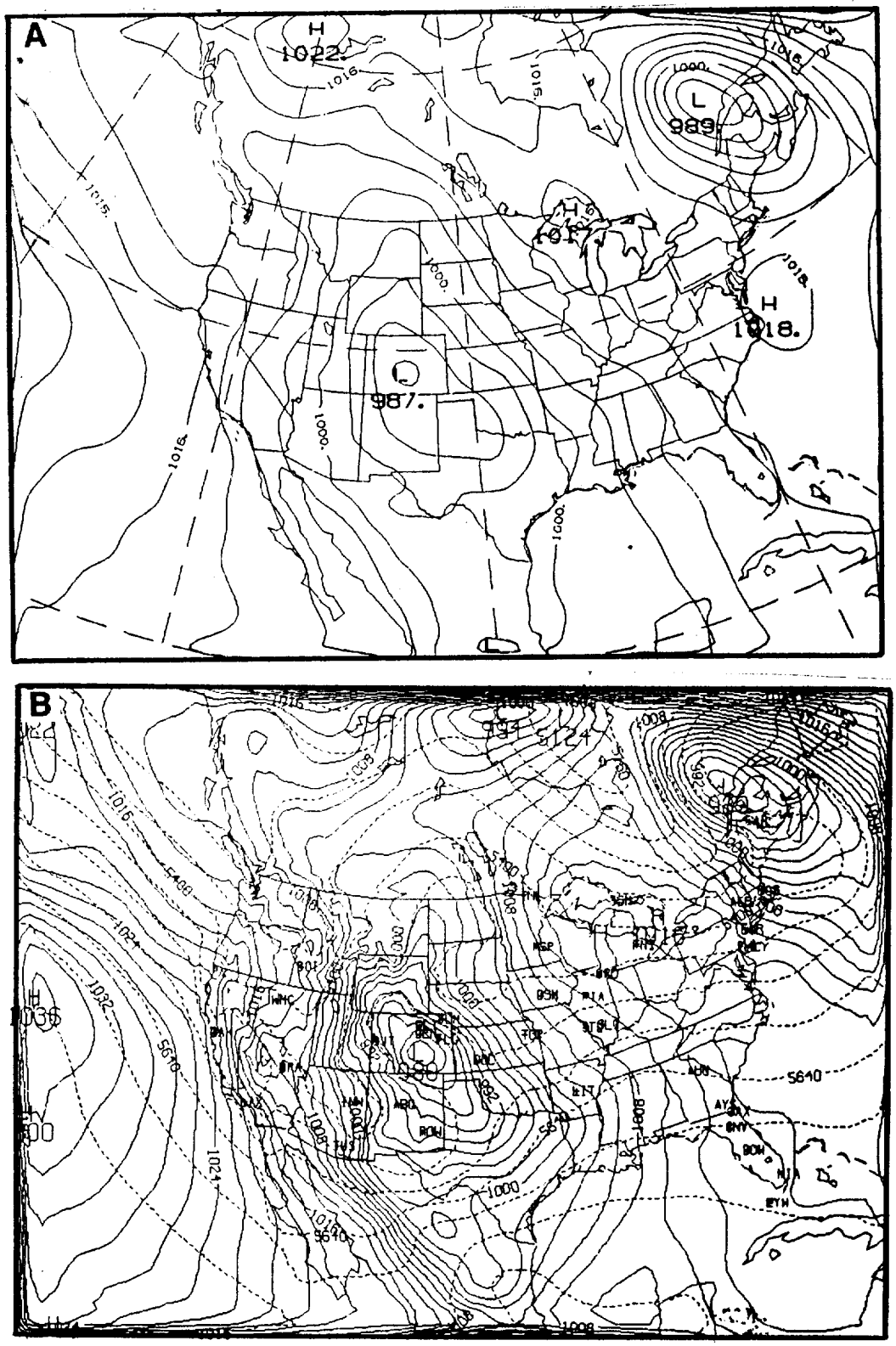

FIGURE 22

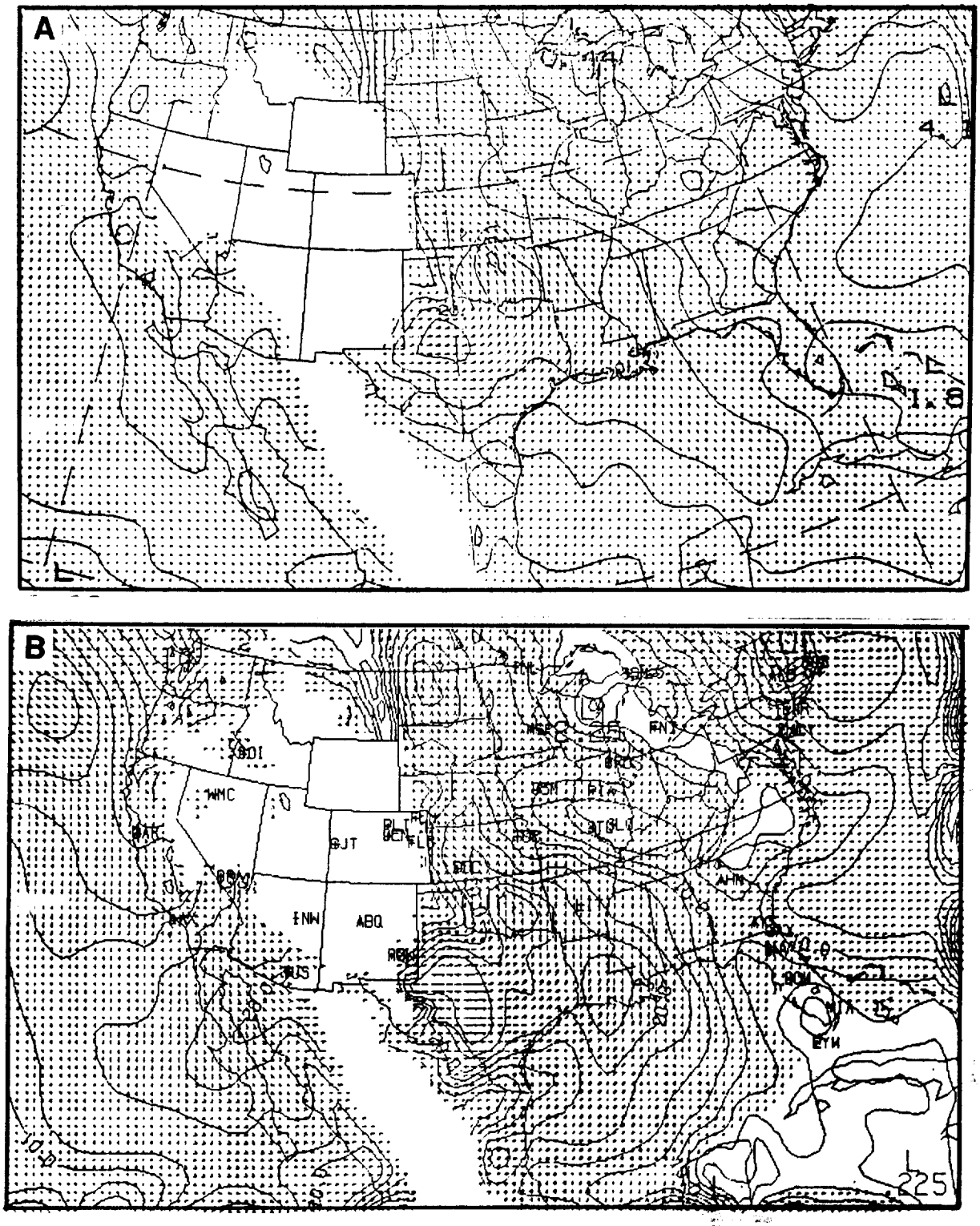

FIGURE 23

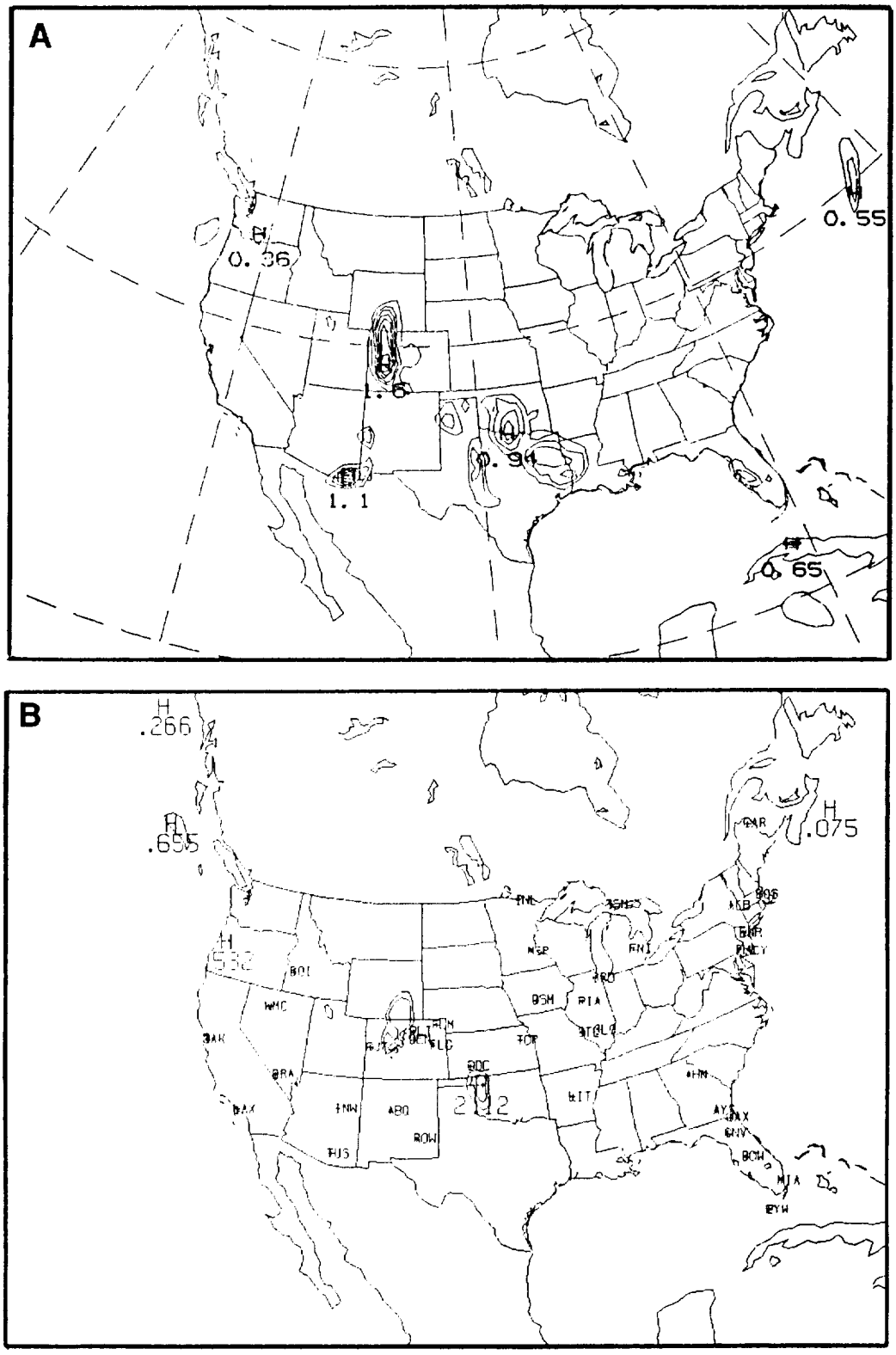

FIGURE 24

NASA
National Aeronautics and Space Administration

Report Documentation Pa

1. Report No.	2. Government Accession No.

4. Title and Subtitle

Development of High Resolution Simulations of the Atmospheric Environment Using the MASS Model

7. Author(s)

Michael L. Kaplan, John W. Zack, and
V. Mohan Karyampudi

9. Performing Organization Name and Address

MESO, Inc.
28 Research Drive
Hampton, VA 23666-1325

12. Sponsoring Agency Name and Address

NASA Goddard Space Flight Center
Goddard Laboratory for Atmospheres
Greenbelt, MD 20771

15. Supplementary Notes

16. Abstract

Numerical simulations were performed with a very h
of the MASS model (Version 4.0) in an effort to diagnose the
stability structure during the Shuttle Challenger disaster wh
These meso-beta scale simulations reveal that the strongest
concentrated in the 200-150 mb layer at 1630 GMT, i.e., at
These simulated vertical shears were the result of two primai
juxtaposition of both of these processes produced a shallow (
vertical wind shear, and hence, low Richardson number valu
Comparisons with the Cape Canaveral (XMR) rawinsonde indicates that the high resolution MASS 4.0 simulation more closely emulated nature than did previous simulations of the same event with the GMASS model.

17. Key Words (Suggested by Author(s))	18. Distribution Statement
Windshear, Turbulence, Model, MASS, Challenger, Shuttle, Numerical	Unclassified - Unlimited

19. Security Classif. (of this report)	20. Security Classif. (of this page)	21. No. of pages	22. Price
Unclassified	Unclassified	79	A01